4.12 Physics and Chemistry of Deep Continental Crust Recycling

C-TA Lee, Rice University, Houston, TX, USA

4.12.1 Introduction

Continental crust, bound vertically by the surface and (traditionally) the Moho and laterally by the extent of the continental shelves, is the most prominent manifestation of silicate differentiation of the Earth. This differentiation is imparted by the solid–liquid segregation on a planet with sufficient gravity. Liquids are generated by partial melting, which is caused by decompression in the upwelling legs of solid-state mantle convection or by volatile flux melting in subduction zones. Owing to their low densities, liquids rise upward to form basaltic crust, which makes up most of the seafloor on Earth and the crusts of other rocky planets. Generating Earth's continental crust, on the other hand, is not so straightforward. Because up to half of Earth's highly incompatible trace elements are stored in the continental crust and the present upper mantle appears to be depleted in these same elements, it is widely thought that the continental crust originally derives from melting of the mantle (Hofmann, 1988). However, compositional models all indicate that the continental crust is too Si-rich and Mg-poor to have derived directly from melting of the ultramafic mantle, motivating the hypothesis that formation of felsic continents requires at least one additional stage of differentiation (Hawkesworth and Kemp, 2006; Kelemen, 1995; Rudnick and Fountain, 1995; Taylor and McLennan, 1985, 1995), wherein (1) primary liquids crystallize and segregate mafic minerals, leaving behind a felsic residual liquid or (2) the basaltic crust is remelted to generate felsic liquids and a residual mafic residue. These mafic cumulates or residues, owing to their high densities, founder or subduct into the convecting mantle, driving the remaining crust toward Si-rich compositions (Arndt and Goldstein, 1989; DeBari and Sleep, 1991; Herzberg et al., 1983; Kay and Kay, 1988; Lee et al., 2007; Rudnick, 1995).

Continental crust is also distinct because it is thicker than oceanic crust. Because of its intrinsically lower compositional density (felsic vs. mafic) and its greater thickness, continental crust is, regardless of its age, positively buoyant with respect to

the mantle and thus more difficult to subduct than oceanic crust. This positive buoyancy tends to isolate continental crust from mantle convection. While oceanic crust volume is roughly balanced by production at mantle upwellings (oceanic spreading centers) and destruction at downwellings (subduction zones), the resistance of continents to subduction makes them thermal insulators. Thus, the thermal history of Earth depends on the evolution of continental crust volume through time (Lenardic et al., 2005). The growth of continents may also have implications for long-term sea-level fluctuations, the evolution of life, and long-term climate change through influences on Earth's albedo (Rosing et al., 2006, 2010).

There is still no consensus on the net continental crust growth curves. Some models suggest that the current volume is at steady state with respect to production and destruction and that most of the volume was formed in the Archean (Armstrong, 1991; Bowring and Housh, 1995). In other models, production outweighs destruction, and continents are thought to have grown progressively, albeit episodically (Albarède, 1998; Bennett et al., 1993; Bowring and Housh, 1995; Hawkesworth and Kemp, 2006; Jacobsen and Wasserburg, 1979; Schubert and Reymer, 1985). Processes that control the volume of continents include the formation or tectonic accretion of juvenile crust and 'tectonic erosion' of the overriding continental plate during ocean–continent subduction (Clift et al., 2009; Von Huene and Scholl, 1991). Processes that control thickness include magmatic inflation/underplating, advective removal of the lower crust, and weathering (physical and chemical weathering) of continental surfaces, the last process transporting sediments to the ocean, after which they are either subducted or 'reaccreted' onto the margins of continents in the form of accretionary prisms (Clift et al., 2009; Plank, 2005). It is important to note that tectonic accretion and tectonic erosion are not directly associated with chemical differentiation because no partial melting takes place in these processes. Removal of lower continental crust (LCC), however, is intimately linked to chemical differentiation as the lower crust itself may be the product of deep-level crystal accumulation and liquid segregation. Weathering can also lead to compositional differentiation of the crust via preferential leaching of soluble elements into seawater, followed by precipitation in marine sediments or hydrothermally altered oceanic crust (Albarède and Michard, 1986; Lee et al., 2008; Shen et al., 2009).

Exploring all these processes simultaneously is intractable. Here, we focus only on the convective removal of LCC and lithospheric mantle because this is one of the most important processes that drive the composition of the crust toward felsic compositions. We use 'convective removal' as a catch-all term to describe any sinking process driven by density instabilities related to thermal or compositional anomalies. Delamination, deblobbing (Peter Molnar, personal communication), detachment, downwelling, dripping, etc., are all types of convective removal (**Figure 1**). Much debate has occurred over which of

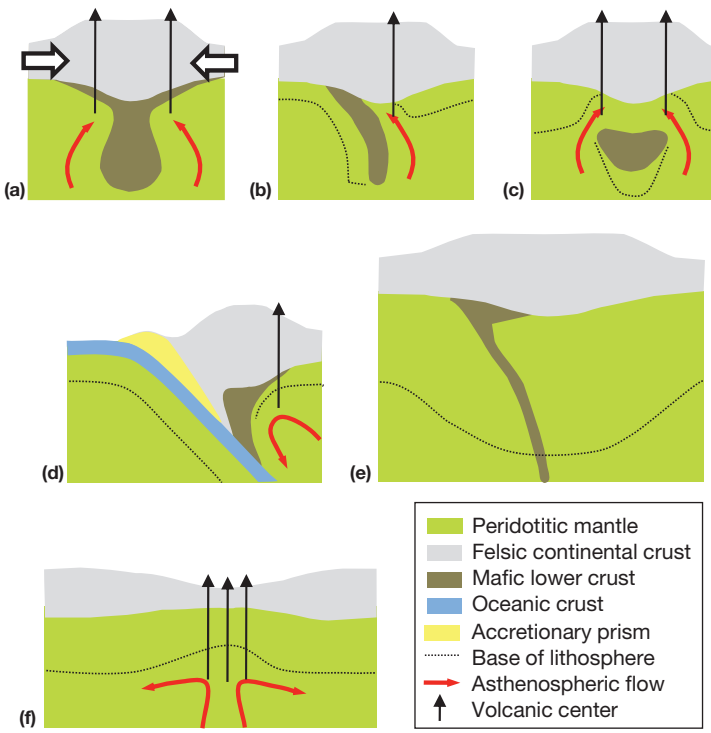

Figure 1 Cartoons of lower crustal foundering scenarios. (a) Growth of a Rayleigh–Taylor-type instability. (b) Peeling or delamination of densified (e.g., pyroxenitic) mafic lower crustal layer initiated at an intracrustal weak zone. (c) Mechanical detachment or delamination of pyroxenitic lower crust initiated at an intracrustal weak zone. (d) Subduction-erosion of basal lithosphere or lower crust. (e) Viscous drainage of a dipping layer of pyroxenitic crust after continental lithosphere has already stabilized. (f) Active or passive extension of continental lithosphere. Red arrows represent asthenospheric mantle flow. Vertical black arrows represent predicted regions of magmatism. Lithosphere is defined as a rheological boundary layer controlled by an increase in viscosity due to temperature decrease in the thermal boundary layer.

these mechanisms operate. However, some aspects of the debate are premature: the first-order issue of when and where these processes operate has yet to be resolved. Furthermore, many of these terms imply very specific mechanisms of convective removal, but they are often used too casually to be effective in communication. These terms are hence defined below. We use the term 'foundering' when no specific mechanism is implied.

A distinction, however, must be made between foundering from other convective processes, such as subduction of oceanic lithosphere. Subduction is related to plate tectonics and is a manifestation of large-scale mantle convection, wherein the dominant length scale of advective heat and mass transfer is the entire mantle. Subduction involves long-lived and focused downwellings of the cold, and hence the dense, upper thermal boundary layer represented by the oceanic lithosphere. Lower crustal (or deep lithospheric) recycling is a local process associated with the growth of small-scale density instabilities at the base of a chemical or thermal boundary layer. In particular, the behavior of these small-scale instabilities is independent of whole-mantle convection. Below, the basic physics of small-scale convective removal is reviewed with the goal of developing intuition. Case studies where foundering of lithospheric mantle and lower crust has been proposed are also discussed.

The final goal of this review is to estimate elemental mass fluxes associated with lithospheric foundering, specifically that of the lower crust, because crustal recycling has direct implications for the compositional evolution of the continents as well as the formation of fertile major-element heterogeneities in the mantle. From a petrogenetic and geochemical point of view, the building blocks of continental crust are of primary interest. We refer to these building blocks as 'crustal material.' Any partial melt of the mantle is considered as potential 'crustal material' for the simple reason that liquids segregate from the mantle and rise toward the surface. The mantle is implicitly taken here to represent a peridotite-dominated system. It follows that all subsequent differentiates (residual liquids, cumulates, and restites) of these liquids are themselves potential crust-building material, and it is the mass exchange of these products between the crust and the mantle that ultimately modulates the composition and growth of the continents. The interface between the crust and mantle is traditionally taken to be the Moho, a transition from the low seismic velocities characteristic of felsic rocks to the high velocities of peridotites. However, from a petrogenetic point of view, such a definition is too restrictive because the transformation of plagioclase-bearing rocks to garnet- and pyroxene-bearing rocks with increasing pressure is also manifested in a distinct velocity jump. Furthermore, early magmatic differentiates are represented by mafic cumulates and restites, whose seismic velocities are also similar to those of peridotites. Thus, many rocks, considered here to be part of the crust, will lie beneath the Moho (Figure 2). When it is necessary to constrain mass fluxes, we will discard the Moho as the conventional definition of the crust–mantle boundary. Here, the crust–mantle boundary is defined by a compositional transition, which may be gradational, between a largely peridotite-dominated system (mantle) and a system dominated by differentiates of magmas (Figure 2).

4.12.2 Physics of Lower Crustal Recycling

While geochemical mass-balance considerations strongly suggest that lower crustal recycling occurs, finding direct evidence for such a process is difficult because the hypothetical mafic component is generally missing. It is thus important to understand the physics of lower crustal recycling. What conditions are necessary for recycling so that we can determine when, where, and how recycling operates? What geologic phenomena are indicative of ongoing or past lower crustal recycling?

Deep crustal or lithospheric recycling may be relevant to a number of geologic processes that occur far inboard of plate margins. Examples include epirogenic uplift (e.g., the Colorado Plateau in southwestern United States and the Hangay Dome in Mongolia, both far from plate boundaries) as well as the magmatism and enhanced surface heat flow often associated with these anomalous uplifts. Bird (1979) may have been the first to highlight that these nonplate tectonic geologic phenomena may result from the growth of small-scale density instabilities. He argued that cold and, hence, negatively buoyant lithospheric mantle would be unstable and could potentially founder back into the mantle, coining the term 'delamination' to describe the scenario in which such lithosphere detaches along a lower crustal weak zone and peels away (**Figure 1(b)**). He showed that 'delamination' once initiated, is faster than thermal diffusion timescales. Consequently, the return flow of hot, asthenospheric mantle during 'delamination' of the cold lithosphere would be manifested in the form of uplift and magmatism. The strong link between postorogenic uplift and magmatism to 'delamination' was later suggested by Kay and Kay (1988, 1993) on the basis of geological observations in the Andes and elsewhere. There is, however, no consensus on the exact nature of lower crustal or deep lithosphere recycling. A number of other investigators have suggested that density instabilities grow by viscous downwelling (Rayleigh–Taylor instabilities) rather than by delamination, and hybrid models have also been proposed (Conrad and Molnar, 1997; Houseman and Molnar, 1997; Houseman et al., 1981; Jull and Kelemen, 2001; Le Pourhiet et al., 2006; Molnar et al., 1998; Schott and Schmeling, 1998). All these models differ from subduction in that the characteristic length scale of the instability is defined locally by the geometry of the density stratification rather than by the whole mantle.

4.12.2.1 Density Anomalies and Buoyancy Driving Forces

4.12.2.1.1 Thermal buoyancy

All recycling mechanisms are ultimately driven by convection, wherein buoyancy forces generated by density anomalies exceed viscous resisting forces. In thermal convection, advection is driven by buoyancies associated with thermal contraction. In particular, the upper thermal boundary layer on Earth is cold and hence denser than the underlying mantle. The temperature contrast between the boundary layer and the mantle can be enhanced by rapid tectonic thickening, which displaces cold geotherms into the hot mantle. The resulting density contrast between the cold boundary layer and the hot ambient mantle is given by $\Delta\rho/\rho = -\alpha\Delta T$, where $\Delta\rho/\rho$ is the relative density contrast, α is the thermal expansion coefficient

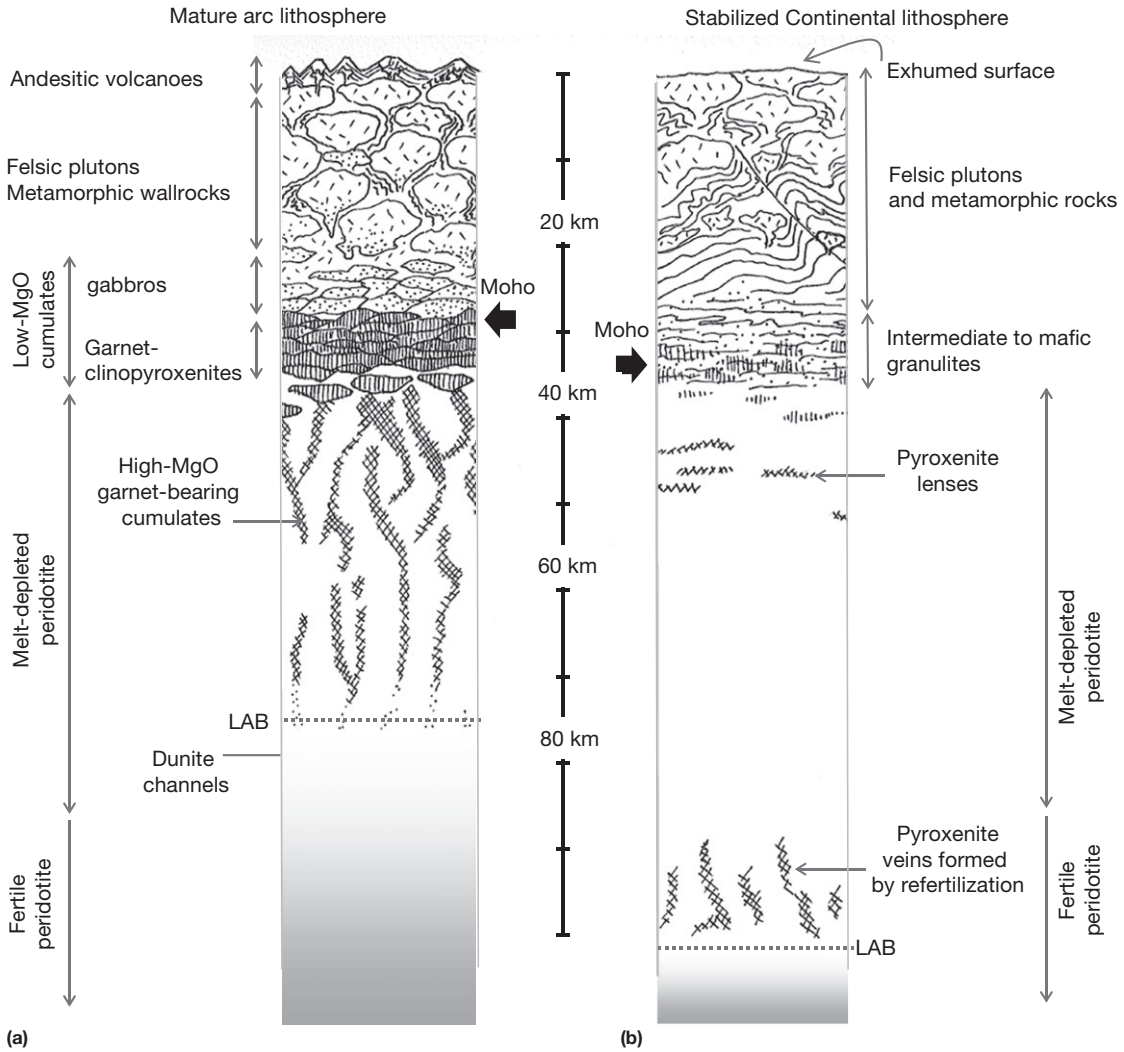

Figure 2 Continental lithospheric sections (a) before removal of pyroxenitic lower crust and (b) after removal and stabilization of continental lithosphere. Preremoval section is synthesized from tilted crustal sections or xenoliths in the Sierra Nevada, Talkeetna, and Kohistan arcs (Dhuime et al., 2007, 2009; Ducea, 2002; Ducea and Saleeby, 1996, 1998b; Greene et al., 2006; Jagoutz, 2010; Jagoutz et al., 2009; Kelemen et al., 2003; Lee et al., 2001a, 2006; Saleeby et al., 2003). Moho corresponds to a seismic discontinuity, reflecting (a) plagioclase to garnet + pyroxene phase change or (b) a transition from intermediate/mafic compositions to ultramafic (peridotite). The base of petrologic crust is deeper than the Moho, but exhibits a continuous gradation rather than a sharp discontinuity. LAB refers to the lithosphere–asthenosphere boundary, which is a rheologic boundary (controlled by an increase in viscosity within the thermal boundary layer), but may also correspond to a transition between melt-depleted peridotites in the lithosphere and fertile peridotites in the asthenosphere. Pyroxenite veins at the base of the continental lithosphere in (b) represent magmatic intrusions in the form of dikes, veins, and sills. Pyroxenites are defined as high MgO or low MgO if their MgO contents are $>$ and $<$14 wt% MgO, respectively (see **Figures 3** and **4**).

($\sim 3 \times 10^{-5}\,^{\circ}C^{-1}$), and ΔT is the temperature contrast between the boundary layer and the surrounding mantle. A temperature contrast of 500 °C, which is relatively large, yields a 1.5% density anomaly.

4.12.2.1.2 Compositional buoyancies from garnet-pyroxenites

Compositional density anomalies are imposed by the presence of dense mineral phases, such as pyroxene and garnet. Here, we refer to garnet- and pyroxene-rich rocks as garnet-pyroxenites. This term encompasses a wide range of bulk compositions and mineral assemblages (Horodyskyj et al., 2007). These rocks are often erroneously referred to in the literature as 'eclogites' but, strictly speaking, the term 'eclogite' is reserved for rocks containing garnet and omphacite (clinopyroxenes with >20% jadeite component) as the dominant phases (Coleman et al., 1965). Garnet-pyroxenites containing orthopyroxene or jadeite-poor clinopyroxene therefore are not true eclogites. True eclogites can be found in exhumed terranes or accretionary prisms associated with tectonic convergence, and their protoliths are often related, but not restricted, to mid-ocean ridge basalts (MORBs; see **Chapter 4.13**) that have undergone hydrothermal alteration (and Na enrichment; see **Chapter 4.16**). In order to avoid confusion, we use the term

'garnet-pyroxenite' as a general term to describe any rock in which garnet and pyroxene are the dominant phases, including eclogites. The term 'eclogite' is reserved for a specific subset of garnet-pyroxenites.

Garnet-pyroxenites are found in the deep roots of continental and some island arcs, but unlike true eclogites, these rocks are cumulates and restites associated with deep magmatic differentiation (Jagoutz, 2010; Jagoutz et al., 2009; Lee et al., 2006, 2007; Rodriguez-Vargas et al., 2005; Weber et al., 2002; **Figures 2** and **3**). Garnet-pyroxenites are also found within the continental lithospheric mantle (Barth et al., 2001, 2002; Beard et al., 1996; Coleman et al., 1965; Esperança et al., 1997; Fung and Haggerty, 1995; Ionov, 2002; Jacob, 2004; Jacob et al., 1994; Kaeser et al., 2009; Liu et al., 2005; Porreca et al., 2006; Pyle and Haggerty, 1998; Schulze, 1989; Selverstone et al., 1999; Smith et al., 2004; Song et al., 2003; Taylor and Neal, 1989; Taylor et al., 2003). These continental pyroxenites could represent subducted oceanic crust, cumulates, restites, melt-rock reaction products, or frozen magmas. The petrogenetic origin of some of these pyroxenites are discussed later.

Pyroxenite density is controlled by the proportions of garnet and clinopyroxene as well as bulk Fe content (**Figures 3** and **4**). Garnet-rich pyroxenites can be up to 10% denser than peridotite (**Figure 4**; Behn and Kelemen, 2003, 2006; Horodyskyj et al., 2007; Lee et al., 2006). This density contrast is far higher than that imparted by thermal contraction; thus the presence of garnet-pyroxenites will strongly influence the buoyancy of the crust or lithospheric mantle. The mode of clinopyroxene and garnet is controlled by metamorphic phase changes associated with increases in pressure (and, to a lesser extent, with decreases in temperature). For example, feldspar is a low-density phase stable at low pressures (<1–1.5 GPa), but when subjected to higher pressures, it reacts to form garnet and clinopyroxene (and some quartz). The effect of pressure on mineral modes (at constant temperature) is shown in **Figure 5** using the different bulk compositions of garnet-pyroxenites shown in **Table 1** (phase equilibria were calculated by Gibbs free energy minimization using the Theriak-Domino software; De Capitani and Petrakakis, 2010). These bulk compositions include average MORB (Arevalo and McDonough, 2010), average LCC (Rudnick and Fountain, 1995), and high- and low-MgO pyroxenites from continental arcs (Lee et al., 2006, 2007). The highest densities occur when feldspar has completely reacted to form garnet and pyroxene ('eclogitization'), which occurs between ~1 and 1.7 GPa (~30–50 km), depending on bulk composition and temperature (**Figures 5** and **6**). In particular, complete reaction of plagioclase to garnet occurs at ~1.5–1.7 GPa (45–50 km) for MORB and LCC at reasonably

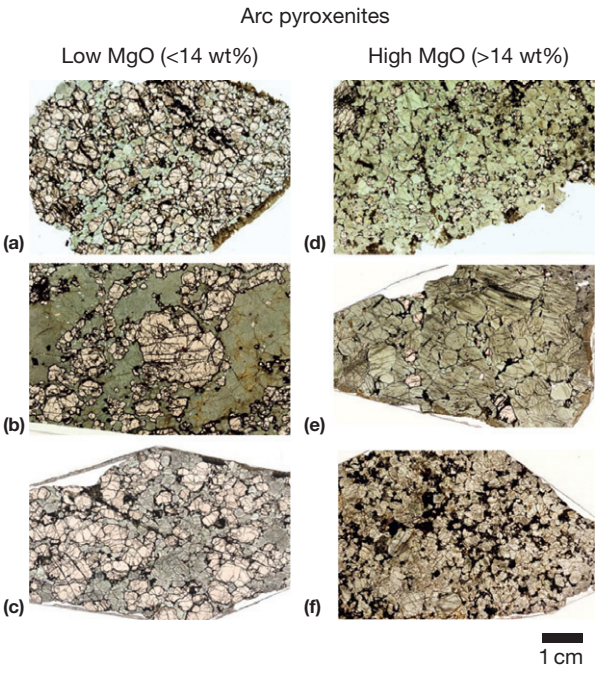

Figure 3 Examples of garnet- and pyroxene-rich rocks from lower continental crust (LCC) and lithospheric mantle. (a–c) Garnet-rich low MgO (<14 wt% MgO) pyroxenites and (d–f) garnet-poor high-MgO (>14 wt% MgO) pyroxenites. These examples are from xenolith specimens in Miocene alkali basalts erupted through the Cretaceous Sierra Nevada continental arc in California. Dull green minerals are clinopyroxene. Pale pink minerals are garnet. Pale brown minerals in (f) are orthopyroxene. Most of the opaque (black) regions represent garnet breakdown products (e.g., kelyphites) due to decompression or reaction with fluids from the host lava.

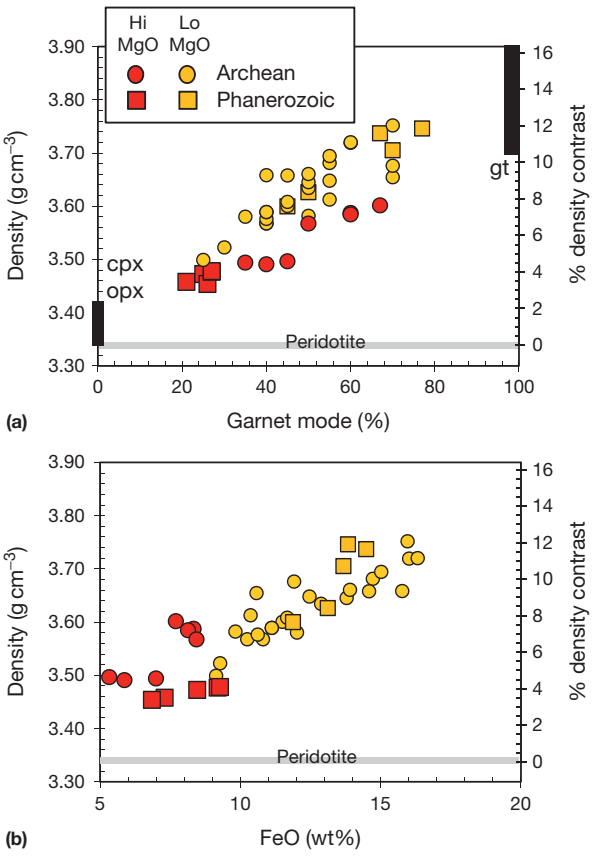

Figure 4 Densities at 1 atm and 25 °C for Phanerozoic and Archean natural garnet-pyroxenites as a function of (a) garnet mode and (b) FeO. Calculations were made for Cretaceous Sierran garnet-pyroxenites and kimberlite-hosted garnet-pyroxenite xenoliths from the Archean West African Craton (Fung and Haggerty, 1995; Horodyskyj et al., 2007). Relative (%) density contrast with pyrolite peridotite is shown on right-hand vertical axes; cpx, clinopyroxene; opx, orthopyroxene; gt, garnet.

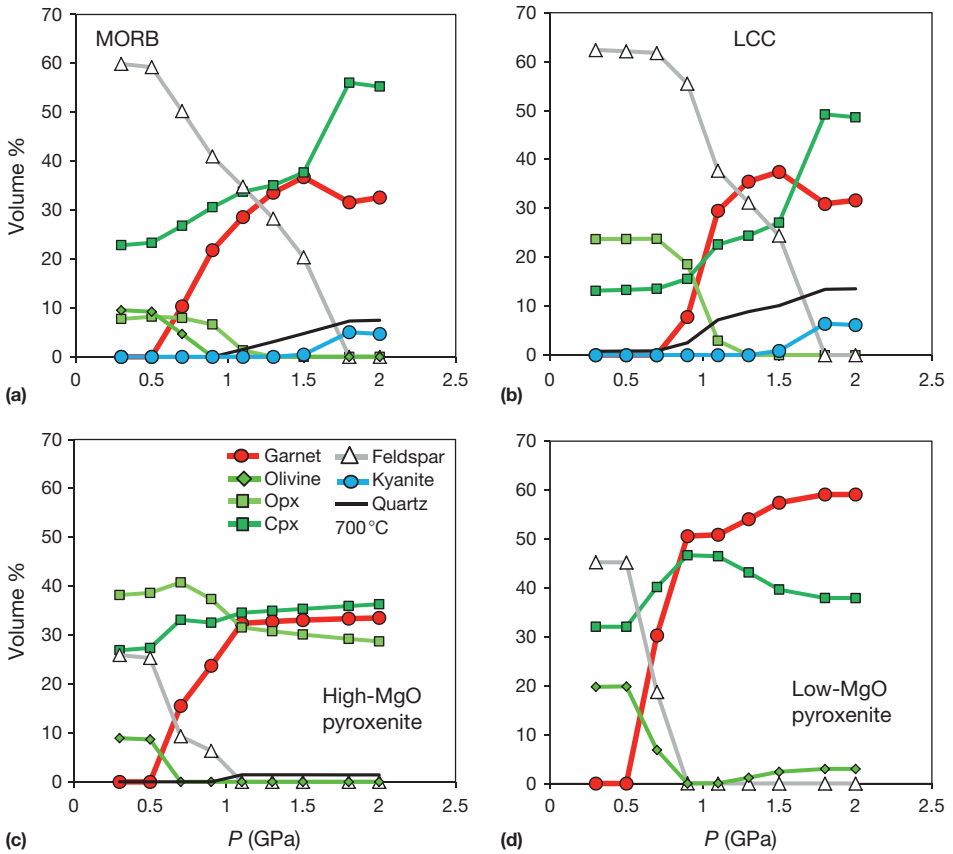

Figure 5 Mineral modes (in volume %) as a function of pressure at constant temperature (700 °C) for different bulk compositions. (a) Average mid-ocean ridge basalt (MORB; Arevalo and McDonough, 2010). (b) Average LCC (Rudnick and Fountain, 1995). (c) Sierra Nevada high-MgO. (d) Low-MgO garnet-pyroxenites (see **Table 1**). Mineral key is shown in (c). Small amounts of spinel are not shown. Calculations were done using the Theriak-Domino software (De Capitani and Petrakakis, 2010) using the thermodynamic database of Holland and Powell (1998).

lower crustal temperatures (~700 °C), but for arc pyroxenites this conversion is complete at lower pressures (1 GPa, ~30 km). Because the feldspar out boundary has a positive *P*–*T* slope (**Figure 6(b)**), hotter geotherms will result in a deeper 'eclogite' transition. Finally, because absolute densities are controlled by the mineral assemblage, bulk density is also controlled by bulk composition (**Figures 5** and **6**). MORBs, LCC, and high-MgO pyroxenites are quartz normative, and therefore their high-pressure mineral assemblage is characterized by intermediate garnet proportions (30–40%) and quartz. By contrast, low-MgO arc pyroxenites are characterized by low bulk SiO_2, which makes these rocks Si-undersaturated and garnet rich (>50%). These are the densest types of garnet-pyroxenites.

Although the objective here is to review lower crustal recycling, it is important to keep in mind that the stability of dense lower crust will also depend on the buoyancy of the underlying lithospheric mantle. A thick and cold lithospheric mantle will add to the negative buoyancy of the mafic lower crust. However, in many cases, especially in Archean cratons, the continental lithospheric mantle is composed of melt-depleted peridotite residues (e.g., atomic Mg/(Mg+Fe) values up to 0.92 compared to 0.89 for that of the fertile asthenospheric mantle; see **Chapter 3.6**), which are intrinsically less dense than the fertile peridotites that make up the ambient asthenospheric mantle. Melt-depletion effects on the density of peridotite residues can impart 1–2% of positive buoyancy, and are thus of the right magnitude to counteract thermal contraction, resulting in isopycnic or neutral density conditions (Jordan, 1978; Kelly et al., 2003; Lee, 2003; Schutt and Lesher, 2006). By contrast, refertilization of the lithospheric mantle via infiltration of basaltic melts (Griffin et al., 2003; Ionov et al., 2005; Le Roux et al., 2007; Lee and Rudnick, 1999; Simon et al., 2003, 2007) increases compositional density (essentially by adding more garnet-pyroxenite component into the lithospheric mantle), aiding destabilization.

4.12.2.1.3 Isostasy and lateral pressure gradients

The importance of density in driving convective instabilities is best demonstrated by considering the effect on horizontal pressure gradients (deviatoric stresses) (Molnar and Lyon-Caen, 1988; Molnar et al., 1993). Consider a model two-layered continent in isostatic equilibrium with respect to the oceanic mantle, which, for simplicity, is assumed to be homogeneously represented by peridotite. The top layer of the continent is made of felsic upper crust with density ρ_c and the bottom layer is made of mafic lower crust $\rho_x > \rho_c$. The mantle peridotite is assumed to be denser than the felsic crust but less dense than the mafic lower crust, that is, $\rho_c < \rho_m < \rho_x$. Lithostatic pressure is defined by $P(z) = \int_0^z \rho(z) g \, dz$, where z is zero at the surface (**Figure 7**). Because of their different density

Table 1 Compositions of crustal end members

	Primitive mantle (McDonough and Sun, 1995)	*MORB (Arevalo and McDonough, 2010)*	*Primitive intra-oceanic arc basalt (Kelemen et al., 2003)*	*Primitive continental arc basalt (Kelemen et al., 2003)*	*Global continental crust (CC)*			*Sierra Nevada and PRB*			*Kohistan*		*Talkeetna*		
					Global lower CC (Rudnick and Fountain, 1995)	*Global upper CC (Rudnick and Gao, 2003)*	*Global bulk CC (Rudnick and Gao, 2003)*	*High-MgO cumulate (Lee et al., 2007)*	*Low-MgO cumulate (Lee et al., 2007)*	*Eastern PRB (average) (Lee et al., 2007)*	*High-MgO cumulate (Jagoutz, 2010)*	*Low-MgO cumulate (Jagoutz, 2010)*	*High-MgO cumulate (Kelemen et al., 2003)*	*Low-MgO cumulate (Greene et al., 2006)*	*Felsic plutons (average) (Kelemen et al., 2003)*
Mass proportion								0.16	0.50	0.33			0.15	0.61	0.23
SiO_2 (wt%)	45.06	50.64	50.46	51.33	53.4	66.6	60.6	49.2	43.8	65.6	51.6	46.0	50.0	47.1	68.5
TiO_2 (wt%)	0.16	1.13	0.91	0.98	0.82	0.64	0.70	0.54	0.73	0.7	0.2	0.9	0.1	0.6	0.5
Al_2O_3 (wt%)	4.44	15.47	15.72	15.7	16.9	15.4	15.9	8.0	15.6	15.9	3.4	17.2	3.4	19.1	15.2
FeO_T (wt%)	8.03	9.33	8.52	8.72	8.57	5.04	6.7	9.8	13.2	3.9	6.5	11.9	8.3	9.9	4.1
MnO (wt%)	0.13	0.17	0.17	0.17	0.10	0.10	0.10	0.19	0.33	0.11	0.13	0.23	0.17	0.18	0.11
MgO (wt%)	37.81	7.84	9.84	9.48	7.24	2.48	4.7	18.4	10.2	1.6	19.5	4.3	28.0	8.1	1.7
CaO (wt%)	3.54	11.52	11.44	9.93	9.59	3.59	6.4	11.5	14.3	4.3	17.8	11.2	9.9	13.2	4.7
Na_2O (wt%)	0.36	2.71	2.35	2.61	2.65	3.27	3.1	0.82	0.91	3.5	0.12	2.1	0.22	1.5	4.4
K_2O (wt%)	0.03	0.18	0.45	0.88	0.61	2.80	1.8	0.18	0.22	2.5	0.00	0.14	0.02	0.11	0.76
P_2O_5 (wt%)	0.02	0.13	0.15	0.22	0.10	0.15	0.1	0.01	0.26	0.18	0.00	0.04	0.01	0.04	0.13
Total	100	99	100	100	100	100	100	99	100	98	99	94	100	100	100
Mg#	0.89	0.60	0.67	0.66	0.60	0.47	0.56	0.77	0.58	0.42	0.84	0.39	0.86	0.59	0.42
Sc (ppm)	16	36.8	36	33	31	14	21.9	53	43	8.9	58	48	32	44	21.4
V (ppm)	82	250	254	247	196	97	138	276	332	66	261	399	106	321	94
Cr (ppm)	2625	326	576	398	215	92	135	1752	82	26	2721	109	3239	159	6.3
Co (ppm)	105	56	44	41	38	17.3	26.6	44	37						
Ni (ppm)	1960	200	240	159	88	47	59	307	99	9.1	214	43	516	42	4.8
Cu (ppm)	30	70	85	92	26	28	27	71	96	15			44	156	25
Zn (ppm)	55	80	72	81	78	67	72	73	104	68			43	62	48
Ga (ppm)	4	21			13	17.5	16	10	13				4	16	15
Y (ppm)	4.3	30	19	19	16	21	19	12	21	16	3	18	3	9	31
Yb (ppm)	0.44	3	2	2	1.5	1.96	2	1.7	4.1	1.8	0.4	1.9	0.2	0.7	3.1

Mg# = atomic Mg/(Mg + Fe_T), where Fe_T is total Fe; FeO_T represents all Fe as FeO; PRB, Peninsular Ranges Batholith; mass proportions of components estimated from inversion with respect to primitive continental arc basalt; residuals represent the difference.

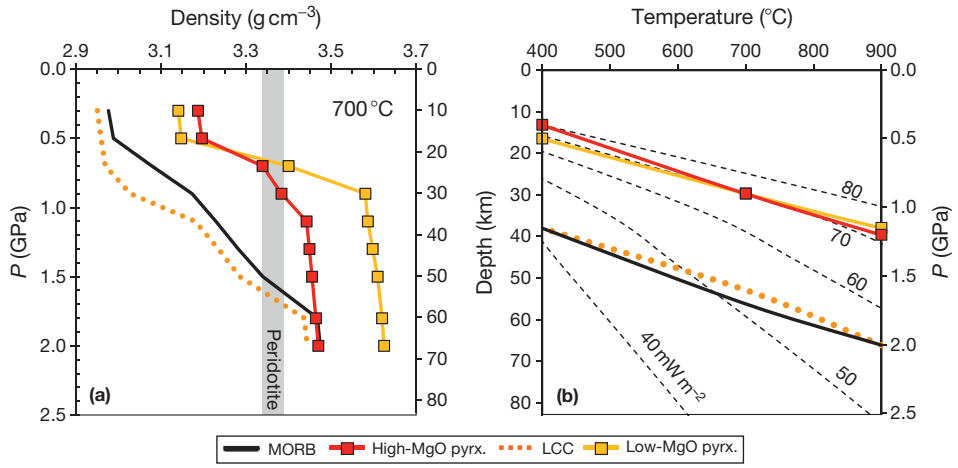

Figure 6 (a) Density versus pressure for the four different bulk compositions shown in **Figure 5** under isothermal (700 °C) conditions. Peridotite (pyrolite) composition is shown for reference. Symbols are shown in the inset. (b) *P–T* diagram showing the feldspar-out curves for the bulk compositions shown in **Figure 5** and (a) of this figure, which is taken to represent full 'eclogitization.' Thin dashed lines represent model steady-state geotherms corresponding to surface heat fluxes of 40, 50, 60, and 80 mW m^{-2} using crustal and lithospheric mantle heat production values given in Rudnick et al. (1998). All other lines are the same as in (a).

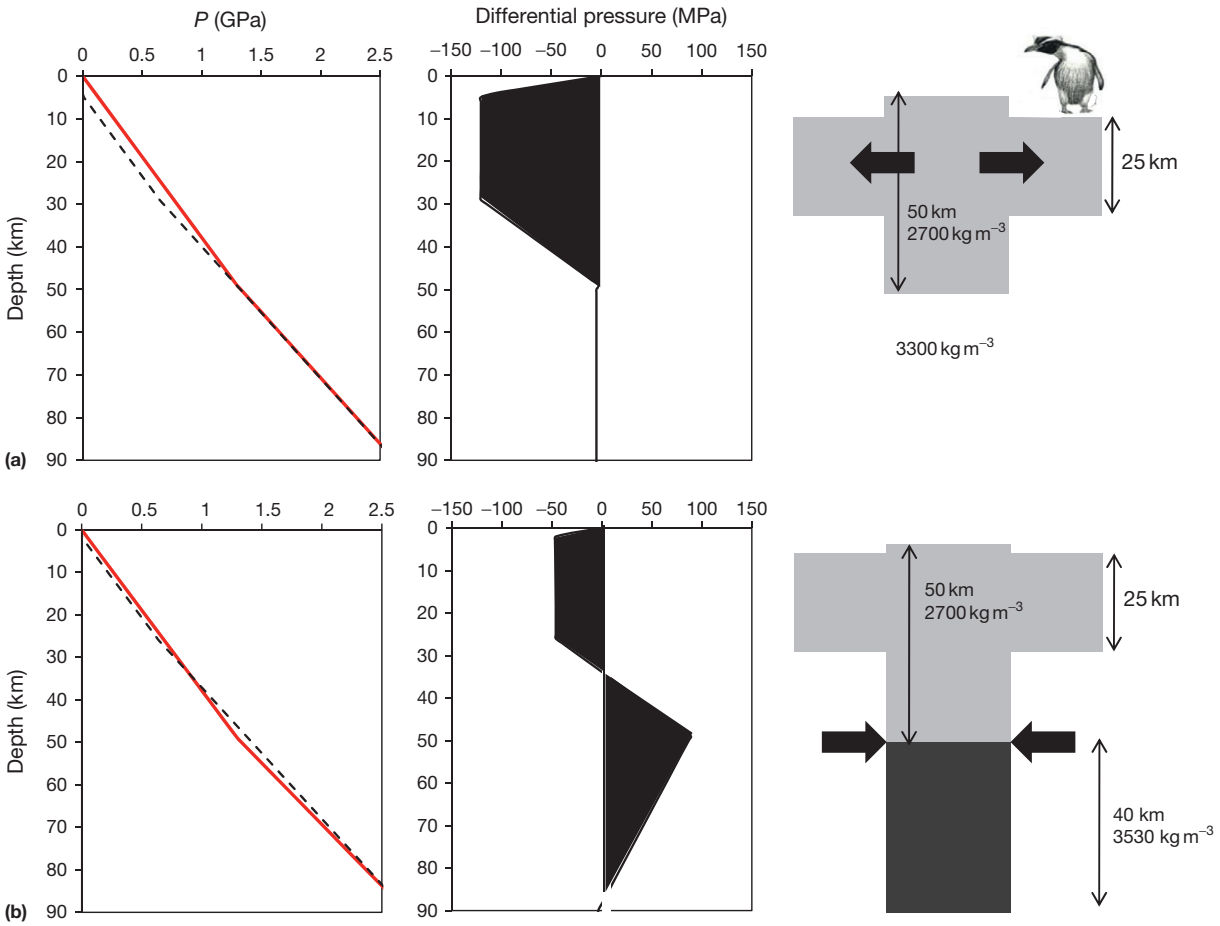

Figure 7 Lithostatic pressures beneath an isostatically compensated continent and surrounding mantle. Density structures are shown on far-right-hand cartoons. (a) Uniform low-density continent. (b) Layered continent with a low-density upper crust and a high-density lower crust. The difference between lithostatic pressures at a given stratum (i.e., the area between the curves in the leftmost panels) is shown in the middle panels (red line represents pressure beneath the continent; black line represents pressure beneath surroundings). Arrows in the rightmost cartoons show the direction of differential horizontal pressure.

structures, lithostatic pressures beneath the continental and oceanic domains differ, converging only at the compensation depth, which is the base of the continental column below which lithostatic pressures beneath the two domains converge. Above the compensation depth, the different lithostatic pressures result in a horizontal pressure gradient between the oceanic and continental domains. These horizontal differences in lithostatic pressure are small (10–100 MPa) compared to the total lithostatic pressure (GPa), but such pressure differences may be sufficient to drive flow. If the entire lithospheric column is positively buoyant, horizontal gradients in lithostatic pressure cause the continent to exert an outward horizontal pressure (**Figure 7(a)**). Thus, mountains and their roots will tend to gravitationally collapse through lateral flow if the viscous resistance of the continents can be overcome. If the felsic crust is underlain by a dense mafic crust, the direction of horizontal pressure gradients becomes more complicated (**Figure 7(b)**). At shallow depths, the continent exerts an outward-directed horizontal pressure as in the above example. However, at greater depths, the surrounding mantle in the oceanic domain exerts a horizontal pressure into the continent. These horizontal pressure gradients cause regions of high topography to gravitationally collapse, but at depth, the inward-directed pressure gradients drive downwelling of the dense lower crust. The highest inward-directed pressures concentrate at the felsic–mafic transition, which coincidentally may also be the location of a rheological weak zone. In summary, the above discussion shows that lateral pressure gradients are a consequence of isostatic equilibrium. These pressure gradients can drive convective thinning of the crust and lithosphere.

4.12.2.2 Mechanisms of Deep Crustal Recycling

4.12.2.2.1 Rayleigh–Taylor-type foundering

The rate at which negatively buoyant lower crust founders into the mantle depends on the magnitude of viscous resisting forces. The standard way of portraying convective removal of a dense layer (for both thermal and compositional buoyancy) is via a Rayleigh–Taylor-type instability, which describes the behavior of a high-density fluid layer above a low-density fluid layer (**Figures 1(a)** and **8**). Small perturbations to the unstable density interface result in the growth of instabilities, which develop slowly but eventually form blobs that ultimately founder into the underlying layer. There are numerous studies that outline the physics and mathematics of the growth of Rayleigh–Taylor instabilities, including the effects of non-Newtonian rheology (Conrad and Molnar, 1997; Houseman and Molnar, 1997; Houseman et al., 1981; Jull and Kelemen, 2001; Molnar et al., 1998; Whitehead, 1986; Whitehead and Luther, 1975). The reader is referred to these papers for details. Here, the physics of foundering is encapsulated at the most rudimentary level in order to develop intuition (cf. Davies, 1999). These solutions are order-of-magnitude approximations and are not meant to describe reality exactly.

Assume a dense, viscous layer of thickness H (representing pyroxenitic lower crust) sandwiched between a rigid upper crust and an inviscid infinite half-space below, which is the mantle (**Figure 8(a)**). The mafic lower crust is cooler than the underlying mantle and, therefore, more viscous than the mantle because viscosity is strongly temperature dependent. For this reason, most of the viscous resistance during initial growth of the instability lies within the mafic lower crust and, therefore, for simplicity it is assumed that the underlying mantle is of much lower viscosity (see Conrad and Molnar, 1997; Jull and Kelemen, 2001). A force balance for a Newtonian fluid (e.g., diffusion creep) yields the relationship:

$$\Delta\rho_x g w \sim \eta_x \dot{\varepsilon} \sim \eta_x \frac{1}{H}\frac{dw}{dt} \qquad [1]$$

where the $\sim$ symbol implies an order-of-magnitude approximation. Because all the viscous resistance is assumed to be in the mafic layer, we take the thickness of this layer H as the characteristic length scale over which shear resistance operates. The first term represents the buoyancy stress, where $\Delta\rho_x$ is the density contrast between the pyroxenitic lower crust and the

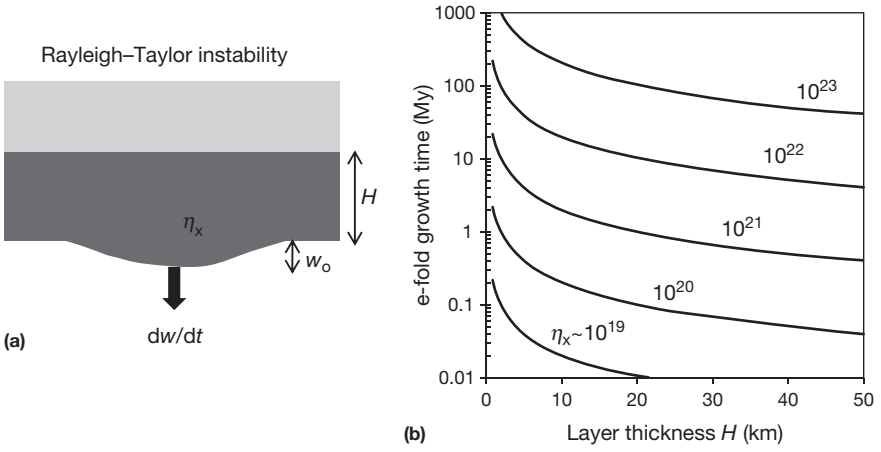

Figure 8 (a) Diagram illustrating a Rayleigh–Taylor instability with a rigid, low-density upper crust and a high-density viscous lower crust. The underlying mantle is assumed to be inviscid so that initially all viscous resistance to negative buoyancy forces are controlled by the dense, viscous lower crust: η_x is the viscosity of the mafic lower crust, H is the thickness of the lower crustal layer, w_o is the initial magnitude of the perturbation to the lower crust–mantle interface, and dw/dt is the growth rate of this perturbation. (b) e-fold growth times in Ma following eqn [3] in the text versus layer thickness H and contoured against the viscosity of the pyroxenitic mafic lower crust η_x in Pa s.

mantle, g is gravity, and w is the thickness of an initial perturbation to the denser layer. The middle term represents viscous resistance, where η_x is the viscosity of the pyroxenitic layer, and $\dot{\varepsilon}$ is the strain rate. The latter can be expressed as the gradient of downward perturbation velocity dw/dt over a characteristic length scale related to the viscous resistance, which is taken to be the thickness H of the layer. Integrating eqn [1] results in an exponential relationship for the growth of the perturbation (this is valid only for small perturbations to the dense layer where H can be considered constant):

$$w = w_o \exp\left(\frac{\gamma \Delta\rho_x g H}{\eta_x} t\right) \quad [2]$$

where γ is a geometric constant. The time for foundering is equivalent to the characteristic e-fold time of instability growth given by

$$t_{crit} \sim \frac{\eta_x}{\Delta\rho_x g H} \quad [3]$$

Equation [2] shows that, once the instability initiates, it grows exponentially (**Figure 8(b)**). Equation [3] shows that foundering occurs quickly if layer viscosity is low and the density anomaly is high. In addition, the thicker the initial layer, the earlier the instability grows. If the layer is too thin, the instability does not grow.

By far the most important parameter controlling growth rates is viscosity because of its strong temperature dependence. These growth rates can be placed into context by considering a few examples. For the sake of simplicity, if the viscosity and the temperature in the asthenospheric mantle is assumed to be 10^{19} Pa s and 1400 °C (1673 K), respectively, which is reasonable for the temperature of the asthenosphere, then the viscosity at temperatures in the lithosphere can be estimated using the following relationship:

$$\frac{\eta(T)}{\eta_{1673\,K}} \sim \exp\left(\frac{E}{R}\left(\frac{1}{T} - \frac{1}{1673\,K}\right)\right) \quad [4]$$

where E is the activation energy, which is between 300 and 500 kJ mol^{-1}. For example, with a 300 kJ mol^{-1} activation energy, viscosities are 10^{20}, 10^{22}, and 10^{24} Pa s at 1200, 1000, and 800 °C, respectively. We can see from eqn [3] that for a ~1–5% density contrast (lower crust of 3330–3450 kg m^{-3} compared to peridotite of 3300 kg m^{-3}) and an initial layer thickness of ~10 km, instability times are <10 Ma for viscosities $<10^{22}$ Pa s, but for viscosities $>10^{22}$ Pa s, corresponding to temperatures <900 °C, the instability times are >100 Ma.

From the simple scalings described above, geologically reasonable growth rates (<100 Ma) are possible only if the layer viscosity is $<\sim10^{21}$ Pa s (**Figure 8(b)**). This becomes particularly limiting if density anomalies are solely driven by temperature because, at timescales >100 Ma, thermal anomalies will diffuse away. The limiting viscosity implies also a limiting temperature. For an activation energy of 300 kJ mol^{-1}, viscosities are too high at temperatures <900 °C to allow a Rayleigh–Taylor instability to develop (at 500 kJ mol^{-1}, temperatures must exceed ~1000 °C). This implies that growth of density instabilities via fluid-like behavior occurs most easily if the dense layer is hot (see Jull and Kelemen, 2001). It similarly follows that a dense pyroxenitic lower crust cannot founder viscously if it is underlain by a cold lithospheric mantle. If, on the other hand, the underlying mantle is hot (>1000 °C) and of low viscosity (asthenosphere), the lower crust can be heated to temperatures high enough to reduce viscous resistance, allowing the layer to founder on a 10-Ma timescale. These temperature constraints can be relaxed by allowing for compositional reduction of viscosity. For example, the addition of water could reduce intrinsic viscosities by 10–100 times (Hirth and Kohlstedt, 1996), in which case foundering could still occur at 800 °C.

Non-Newtonian rheology, wherein strain rate scales with stress following a power-law relationship, $\dot{\varepsilon} \sim \sigma^n$, will result in different types of growth rates. For example, for dislocation creep, where $n \sim 3$, a density perturbation will first grow slowly and then superexponentially rather than exponentially as in the case of Newtonian rheologies ($n = 1$). However, because of the power-law relationship between stress and strain rate for dislocation creep, the onset of superexponential growth varies considerably. If background strain rates are low, such as in the interior of a craton, delay times are long. If, however, background strain rates are high, such as in convergent or extensional margins, the instability may initiate very rapidly, allowing foundering to occur at lower temperatures than possible for temperature-dependent Newtonian fluid. More detailed discussions on non-Newtonian behavior are beyond the scope of this review and the reader is urged to refer to more comprehensive studies in the literature (Conrad and Molnar, 1997; Houseman and Molnar, 1997; Jull and Kelemen, 2001).

4.12.2.2.2 Wholesale delamination or detachment

In the previous section, it was shown that, if the dense lower crust is cold, viscous resisting forces internal to the layer are high, preventing the entire layer from foundering. However, deformation can be accommodated if there is a low-viscosity layer just above the dense layer. Because felsic rocks are intrinsically weaker than mafic (and ultramafic) materials, a low-viscosity layer should form within the felsic crust, provided the thickness of the felsic crust is large enough to ensure that its lower part behaves in a ductile manner (**Figure 9**; Kohlstedt et al., 1995; Ranalli and Murphy, 1987; Tsenn and Carter, 1987). If sinking of the mafic lower crust can be accommodated along a weak decoupling zone, such a process allows for wholesale removal of the dense layer, unlike the growth of Rayleigh–Taylor instabilities, which results in convective thinning of the base of the dense layer. The scenarios described in this section are referred to here as delamination or detachment to distinguish them from Rayleigh–Taylor-type instabilities (**Figures 1(a)–1(c)** and **8**). Below, a simplified view of delamination is provided. More detailed presentations can be found elsewhere (Bird, 1979; Jull and Kelemen, 2001; Le Pourhiet et al., 2006; Morency and Doin, 2004; Schott and Schmeling, 1998).

The rate at which the dense pyroxenitic lower crust detaches can again be approximated by assuming a force balance between the negative buoyancy forces acting on the high-density lower crust and viscous resisting forces. To first order, we can assume that all of the viscous resistance is initially controlled by viscous dissipation within the thin low-viscosity layer (**Figure 10(a)**) (after detachment, the viscous resistance of the underlying mantle becomes more important). We assume

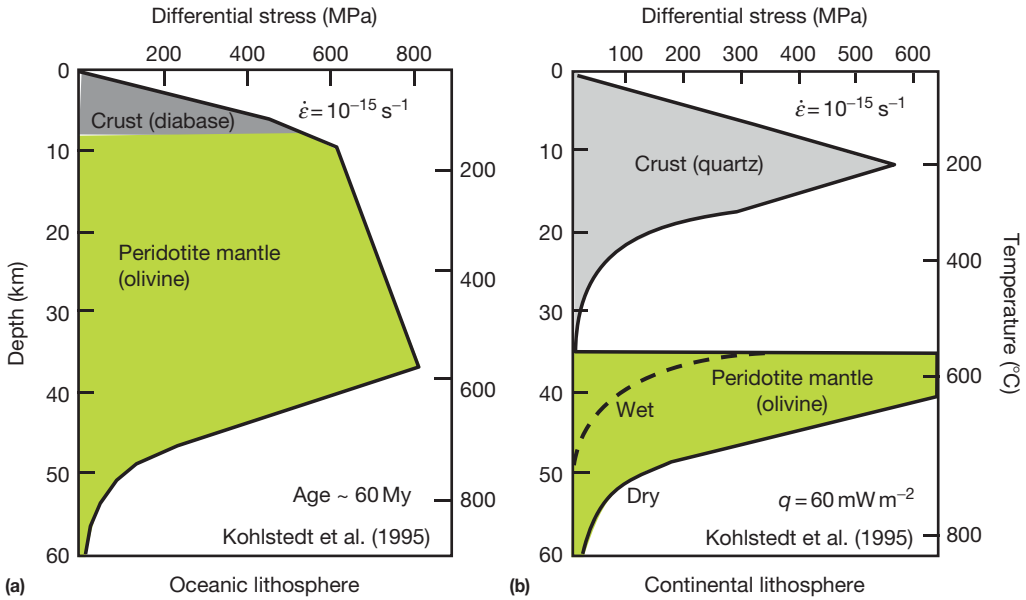

Figure 9 Effective strength profiles for a 60-Ma-old oceanic lithosphere and continental lithosphere with a 60 mW m^{-2} surface heat flux (both corresponding to a lithosphere thickness of ~60 km) from Kohlstedt et al. (1995). Strength profiles are determined from Byerlee's Law, brittle–ductile transition models, and power-law rheologies for wet and dry olivine and quartz, assuming a background strain rate of $\dot{\varepsilon} = 10^{-15}\ s^{-1}$. Note that, because dry olivine is intrinsically stronger than quartz and basaltic oceanic crust (diabase rheology), thick crust in continental environments results in a weak lower crustal zone just above the peridotitic mantle. A similar weak rheologic zone would be expected at the interface between felsic and mafic crust in continents (not shown). With permission of John Wiley & Sons.

that flow in the thin gap is laminar and driven by a pressure gradient, which itself is driven by the sinking lower crust. Thus, the force balance at the onset of detachment is given by

$$\Delta\rho g x \sim \eta_w V L / H^2 \qquad [5]$$

where $\Delta\rho$ is the density contrast between the mafic lower crust and the peridotitic mantle, g is gravity, x is the thickness of the pyroxenitic lower crust, η_w is the viscosity within the low-viscosity layer, H is the thickness of the low-viscosity layer, and V is the average lateral velocity of the rheological fluid within the low-viscosity layer. As the pyroxenitic lower crust sinks, a low-pressure region is generated within the low-viscosity layer, which draws more felsic material into the layer. The force balance approximation assumes that H is small so that the velocity field of the low-viscosity material V is horizontal (i.e., a lubrication approximation). Conservation of mass requires that

$$VH = L\frac{dH}{dt} \qquad [6]$$

where L is the horizontal width of the gap and dH/dt is the rate at which the gap thickens in the vertical direction, which is equivalent to the sinking velocity of the mafic lower crust. Rearranging eqn [6], substituting for V in eqn [5], and integrating with respect to H and t yield a formula describing the delamination rate of the pyroxenitic lower crust

$$H(t) \sim \frac{H_o}{\left(1 - \Delta\rho g x H_o^2 t / \eta L^2\right)^{1/2}} \qquad [7]$$

where H_o is the initial gap thickness. The time for initiation of the instability occurs when the denominator of eqn [7] approaches zero, hence

$$t_{crit} \sim \frac{\eta}{\Delta\rho g x}\left(\frac{L}{H_o}\right)^2 \qquad [8]$$

Equation [8] shows that the mafic lower crust detaches early if η is low, H_o is high, thickness of the lower crust x is high, or L is low. Detachment times <10 Ma are again possible only for viscosities in the low-viscosity layer $<10^{22}$ Pa s (**Figure 10(b)**). For a given viscosity, however, early detachment is favored when the aspect ratio of the gap, L/H_o is small. Instability growth times are infinite if H_o is zero, which means that in the absence of a low-viscosity layer, wholesale detachment of the mafic crust is impossible. The approach taken here is a simplified and conservative version of that originally taken by Bird (1979). In the foregoing, the mafic lower crust is rigid, but Bird allowed the lower layer to bend elastically, which facilitates delamination. Readers are referred to Bird's seminal paper for details.

4.12.2.2.3 Critical thickness to which a dense mafic layer can grow magmatically

An advantage of the simplified approach taken above for delamination is that we can also consider the effect of a growing mafic lower crust. This is especially important when considering formation of mafic cumulates and restites aggregating at the base of an active magmatic arc. Because the delamination rate depends on buoyancy forces and hence the thickness of the mafic layer x, there is a critical x below which delamination is slower than the magmatic growth of the mafic lower crust. Assuming a constant magmatic growth rate of mafic lower crust dx/dt, the critical thickness above which delamination will occur is achieved when the magmatic growth time

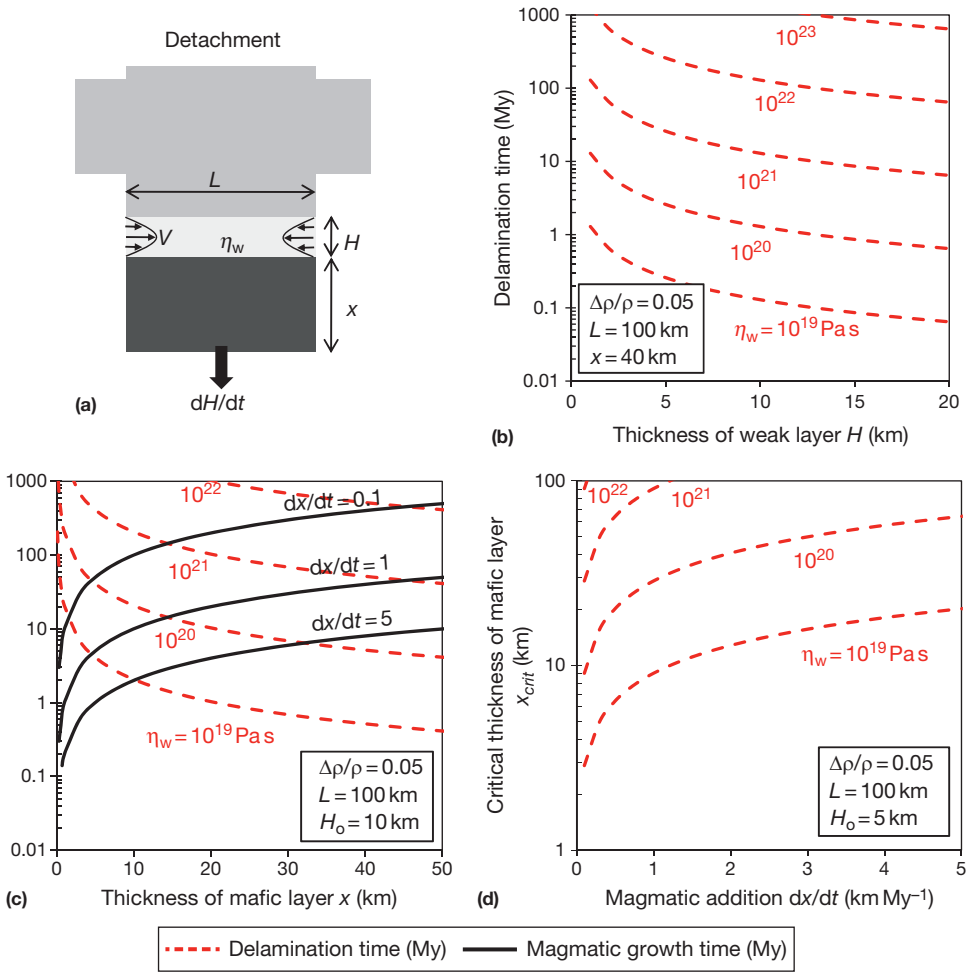

Figure 10 (a) Detachment/delamination of a strong 'eclogitized' lower crust along a weak detachment zone (see **Figure 9**). Felsic lower crust or asthenospheric mantle 'intrudes' into the weak lower crustal zone (low-viscosity layer) as the dense mafic material sinks. Viscous resistance to negative buoyancy occurs primarily within the low-viscosity layer of thickness H. Other symbols are η_w for the viscosity of the low-viscosity layer, L for the horizontal width of the low-viscosity layer, V for the average velocity of flow within the low-viscosity layer, x for the thickness of the mafic lower crust, and dH/dt for the sinking rate of the mafic lower crust. The mafic lower crust is assumed to be perfectly rigid. (b) Delamination time (eqn [8]) versus thickness of weak layer H for different values of η_w in Pa s. Density difference $\Delta\rho/\rho = 0.05$, $L = 100$ km, and $x = 40$ km. (c) Delamination time (red dashed line) and magmatic growth time (black solid line) versus thickness of mafic layer x. Delamination times for different low-viscosity layer viscosities are shown. Initial thickness of low-viscosity layer is assumed to be 10 km ($L = 80$ km). Magmatic growth times for different constant growth rates (in km Ma^{-1}) are shown (dx/dt). Crossover between magmatic growth time and delamination time indicates critical time for delamination; when delamination times exceed magmatic growth time, mafic lower crust continues to grow, but when delamination times are less than magmatic growth time, delamination occurs. (d) Critical thickness of mafic layer for delamination when mafic layer is growing magmatically at a constant rate of dx/dt. This thickness corresponds to that attained at the critical crossover time in (c) ($L = 100$ km, $H_o = 5$ km).

$t_g = x/(dx/dt)$ equals the delamination time t_{crit} (eqn [8]; **Figure 10(c)**). Equating these two times yields a critical thickness x_{crit} of

$$x_{crit} \sim \sqrt{\frac{\eta}{\Delta\rho g}\left(\frac{L}{H_o}\right)^2 \frac{dx}{dt}} \qquad [9]$$

Thus, for a given magmatic growth rate dx/dt, delamination occurs if $x > x_{crit}$. If $x < x_{crit}$, the mafic lower crust can grow magmatically without delaminating (**Figure 10(c)** and **10(d)**). A more detailed numerical treatment of this calculation is given in Behn et al. (2007). However, once dx/dt decreases or approaches zero, such as during a magmatic lull, the system will resume delaminating. For typical arc magmatic production rates (~5 km Ma^{-1}, Annen et al., 2006), critical thicknesses are between 1 and 10 km for viscosities $<10^{20}$ Pa s; for higher viscosities, critical thicknesses can exceed 50 km, explaining how thick mafic roots can develop without immediately foundering.

4.12.2.2.4 Other mechanisms of deep crustal recycling

Other mechanisms of deep crustal recycling include 'viscous drainage' and mechanical or thermal erosion of the lithosphere (**Figure 1(d)–1(f)**). Mechanical erosion can occur if the subducting lithosphere impinges against the overriding plate. For example, 'flat' subduction has been proposed to have removed the lithospheric mantle beneath western North America

(Bird, 1988). Complete removal of the lithospheric mantle would allow lower crustal material to couple to the subducting slab, eventually resulting in its removal. However, the extent to which the continental lithospheric mantle can be removed by such processes is unclear. Geochemical data on peridotite xenoliths and lavas in western North America indicate that at least the shallowest parts of the original continental lithospheric mantle remain (Lee et al., 2001b; Livaccari and Perry, 1993; Luffi et al., 2009; Smith, 2000), implying that direct coupling between lower crust and subducting slab may not have occurred.

A more probable site for direct coupling between a subducting slab and continental crust is in the fore-arc and sub-arc regions, where the asthenospheric mantle wedge is often very thin or absent. While the fore-arc in many trench systems is a place of sedimentary accretion, the truncation of geologic units at the trench has long been suggested as evidence for 'subduction erosion' (Clift et al., 2009; Von Huene and Scholl, 1991). However, because the materials being eroded at the leading edge of the continental plate are likely to be of sedimentary origin, they are not of particular interest in this review because magmatic differentiation is not involved. A more important environment where 'subduction erosion' may lead to mafic lower crustal recycling is in the sub-arc environment (**Figure 1(d)**). When a thick root of mafic cumulates develops, such as beneath the Cretaceous Sierra Nevada Batholith in California (Ducea and Saleeby, 1998b), the asthenospheric mantle wedge could become pinched out, leading to coupling between the subducting slab and the mafic root. All of the above processes involving slab coupling may also be sites of fluxing of slab-derived fluids (English et al., 2003), which could result in significant weakening of the overriding plate (Humphreys et al., 2003; Li et al., 2008; Smith et al., 2004; Xu, 2001) and thereby enhance lower crustal recycling.

In viscous drainage, dipping layers of pyroxenites within the lithospheric mantle could be expected to 'drain' in a channel-like instability (**Figure 1(e)**). These dipping layers could form during the imbrication of the oceanic lithosphere (Helmstaedt and Doig, 1975; Helmstaedt and Schulze, 1989). This mechanism provides one means of removing pyroxenites through cold lithospheric mantle without destroying the lithospheric mantle. The rates of drainage should scale as

$$v \sim \frac{\Delta\rho g h^2 \sin\theta}{\eta} \qquad [10]$$

where h is the channel thickness and θ is the angle of dip. For a viscosity of 10^{22} Pa s, a density contrast of 100 kg m^{-3}, and a channel thickness of 10 km, the minimum amount of time for drainage through a 50-km lithosphere will be ~500 Ma. Thus, unless h is much larger or viscosity much lower, removing pyroxenites within continental lithosphere is difficult. Effects of thermal erosion are discussed below.

4.12.3 The Aftermath of Foundering

4.12.3.1 Topographic Effects of Foundering

One immediate aftermath of foundering dense lower crust (or lithospheric mantle) should be an increase in elevation due to the replacement of a dense layer by asthenospheric mantle, which is hotter and, hence, less dense than the foundered layer (Bird, 1979; Houseman et al., 1981; Kay and Kay, 1993; Platt and England, 1993). This uplift is a consequence of isostatic readjustment and is independent of any dynamic effects, such as topography generated by plate flexure, deviatoric stresses in the asthenosphere, or asthenospheric mantle with anomalously high potential temperatures (**Figure 11**). The elevation h of a crustal column (the lithospheric mantle is ignored here because its contribution is smaller than the crustal effects) relative to its surroundings is given by

$$h = \frac{[(\rho_m - \rho_c)c + (\rho_m - \rho_x)x + (\rho_c - \rho_m)d]}{\rho_m} \qquad [11]$$

where ρ is density (subscripts m, c, and x indicate the mantle, normal crust, and mafic lower crust) and c, x, and d are the thicknesses of the felsic crust, mafic lower crust, and surrounding crust, respectively. Differentiating the above equation shows how h changes as the thickness of the lower crust x changes (**Figure 11**), that is,

$$\frac{dh}{dx} = \frac{\rho_m - \rho_x}{\rho_m} \qquad [12]$$

Thus, if $(\rho_m - \rho_x) < 0$, that is, the mafic lower crust is denser than the mantle, a decrease in the thickness of the lower crust by foundering would result in a net rise in elevation proportional to the relative density contrast between the foundered material and the asthenospheric mantle (obviously, if $(\rho_m - \rho_x) > 0$, elevations would decrease in response to crustal thinning). For a compositionally controlled density contrast of 2–5% (similar to the density contrast between low-MgO pyroxenite and peridotite; **Figure 6**), the predicted elevation response would be 0.02–0.05 km of surface uplift for every 1 km of the mafic lower crust removed. Removing 20 km, for

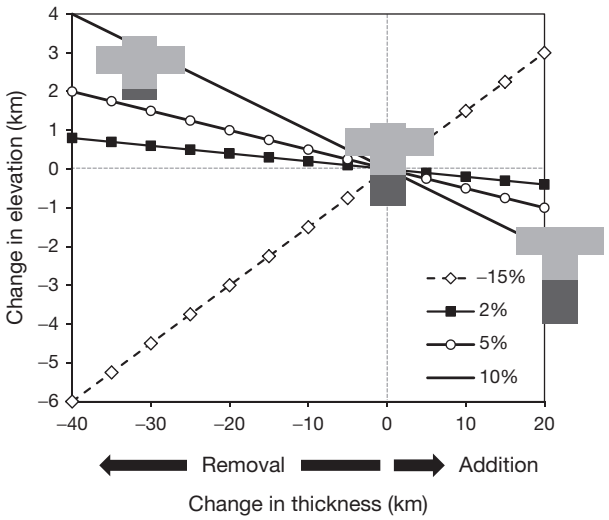

Figure 11 Topographic response to removal of lower crust for different density differences (%) between the lower crust and underlying peridotite of pyrolite composition. Removal of dense lower crust results in an increase in surface elevation. Note that, if the lower crust is buoyant and could be hypothetically removed or thinned, a decrease in elevation would follow.

example, would yield 0.4–1 km of surface uplift. Density contrasts solely associated with temperature are smaller than compositional density anomalies and will result in smaller elevation responses.

Dynamic effects could enhance or suppress isostatic readjustments to topography. For example, if the asthenospheric return flow has a higher mantle potential temperature than ambient asthenosphere, uplift would be enhanced. High vertical deviatoric stresses, supported by active upwelling (such as in a plume), could also enhance uplift. Topography can also be affected during foundering. As the dense layer sinks, regardless of the mechanism, the sinking body will generate dynamic stresses at the base of the overriding lithosphere, depressing the topography. After the dense layer sinks far enough away from the overriding lithosphere, these viscous effects will subside and the lithosphere will relax back to isostatic conditions. It is beyond the scope of this review to discuss dynamic topography quantitatively. However, it is important to understand the conceptual differences between these two types of topographic responses. Fundamentally, the difference between the two is that free-air gravity anomalies will be zero for isostatically compensated topography but nonzero for dynamically controlled topography.

Finally, it is important to note that, although uplift is predicted to immediately follow foundering, subsequent thermal relaxation will likely cause this thinned lithosphere to rethicken by the growth of a rejuvenated thermal boundary layer. The timescales to thermally relax back to the original lithosphere thickness will scale as $t \approx x^2/\kappa$ where x is the thickness of material foundered and κ is the thermal diffusivity ($\sim$30 km^2 Ma^{-1}). For example, for $x \sim$50 km, the relaxation time will be $\sim$80 Ma. Thus, topographic effects associated with foundering are short-lived.

4.12.3.2 Thermal Effects of Foundering and the Generation of Magmatism

4.12.3.2.1 Foundering-induced decompression melting of upwelling asthenosphere

Once foundering initiates, it proceeds rapidly because viscous resistance is no longer controlled by the overriding lithosphere but by the weak asthenosphere. Far-field sinking of foundered material occurs on <10 Ma timescales, which, as discussed above, is shorter than thermal diffusive timescales for the characteristic length scales involved. Consequently, foundering will impose a return flow of hot asthenospheric mantle to fill the newly vacated 'space' (**Figure 12(a)**). This return flow will be characterized by near-adiabatic upwelling. If this upwelling mantle crosses the mantle solidus, partial melting will occur (**Figures 12(a)** and **13**). Impingement of hot asthenosphere against the cold overlying lithosphere should also lead to conductive heating of the former and cooling of the latter, in turn leading to new lithosphere formation by 'underplating' of newly formed melt residues and conductive cooling of ambient asthenospheric mantle; melting of the overlying lithosphere is also possible (**Figure 12(a)**; Bird, 1979; Kay and Kay, 1993; Platt and England, 1993).

The importance of foundering-induced magmatism is underscored by numerous examples of postorogenic magmatism. Many of these magmas are unusual: they tend to be alkalic to ultrapotassic in composition and are often highly enriched in incompatible trace elements (Farmer et al., 2002; Turner et al., 1996, 1999). The concept of foundering-induced magmatism is illustrated in **Figures 12(a)** and **13**. The composition of the magmas will be dictated by the average pressure of melting (P_{ave}), the average melting degree (F_{ave}), and the mantle potential temperature (T_P). Both P_{ave} and F_{ave} of the

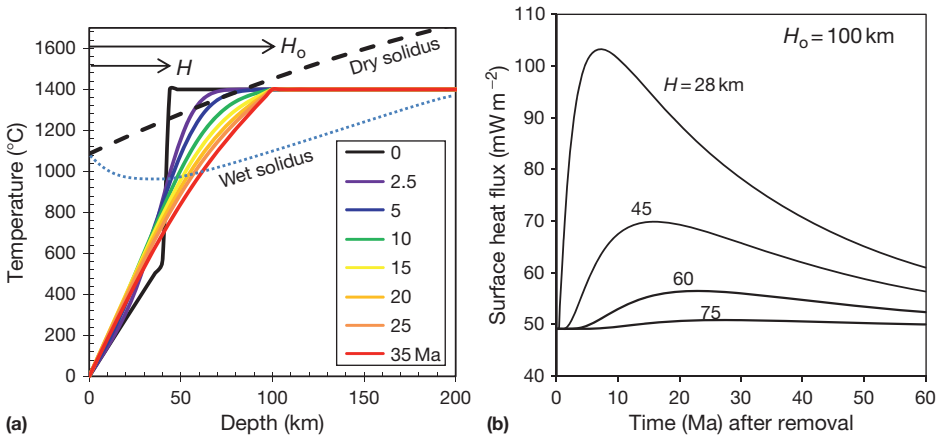

Figure 12 Thermal response to rapid removal of lower crust or lithospheric mantle. (a) Rapid removal results in juxtaposition of hot asthenospheric mantle against cold remaining lithosphere, which heats up the lithosphere and cools the underplated asthenospheric mantle. Colored lines represent finite-difference cooling curves in the temperature–depth space in time intervals given in the inset of (a). Dry and wet peridotite solidi are shown for reference. Decompression of asthenospheric mantle in response to rapid removal of dense lithosphere or lower crust can result in decompression melting. (b) Surface heat flux response after removal of deep lithosphere layer followed by underplating by hot asthenospheric mantle using the output of the thermal models in (a). *X*-axis represents time after removal of denser lower crust or lithosphere. Initial lithosphere thickness H_o is 100 km (T at 0 km is 0 °C and at H_o is 1400 °C). Thickness of lithosphere remaining after removal of lower lithosphere is given by H (T at base of lithosphere is always maintained at 1400 °C). Thermal response is shown for different values of H. Extensive removal of lower lithosphere leaves behind a thin lithosphere and a large thermal anomaly at the surface. Small-scale thinning of the deep lithosphere does not lead to a noticeable change in surface heat flux. Solidi are from Katz et al. (2003).

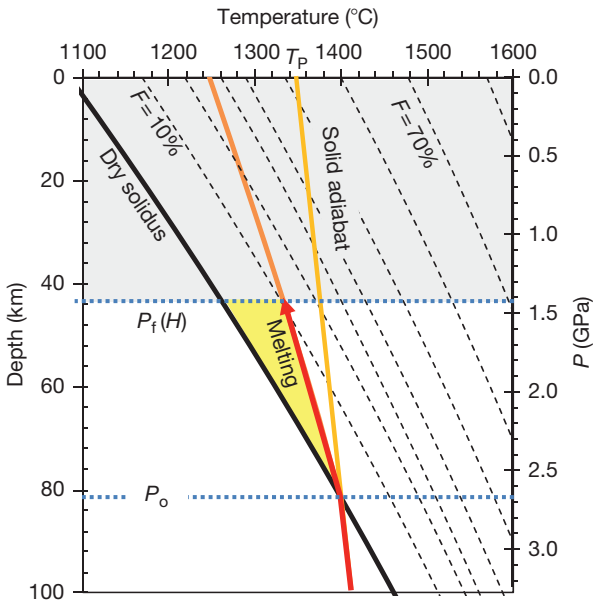

Figure 13 Conceptual diagram showing how solid-state adiabatic decompression in response to crustal or lithospheric foundering leads to decompression melting if solid mantle adiabat crosses the solidus. Initial depth of melting (P_o) is defined by the intersection of the adiabat and the solidus, and should therefore correlate well with mantle potential temperature (T_P). Final depth of melting (P_f) is controlled by lithosphere thickness, which 'caps' further decompression. Note that P_f is equivalent to the remaining lithosphere thickness H in **Figure 12**. The total amount of melt generated (as reflected in the melt fraction F discussed in the text) is dictated by the difference between P_f and P_o. Dashed lines and solidus are taken from Katz et al. (2003) and Hirschmann (2000), and are shown at 10% intervals of F. Melting adiabat is modeled following the approach shown in Katz et al. (2003).

upwelling mantle are controlled by the thickness of the lithospheric lid and the initial pressure of melting (**Figure 13**). The latter corresponds to the intersection of the mantle adiabat with the solidus, and the former corresponds to the thickness of the remaining lithosphere after foundering. Following the approach of Langmuir et al. (1992) and accounting for the latent heat of fusion yields the simple energy balance

$$(P_f - P_o)\left(\frac{dT}{dP_a} - \frac{dT}{dP_s}\right) = F\left(\frac{H_f}{c_P} + \frac{dT}{dF}\right) \qquad [13]$$

where P_f is the final pressure of melting (limited by the lithospheric cap), P_o is the initial pressure of melting, dT/dP_a is the temperature gradient of the solid mantle adiabat ($\sim$10 °C GPa^{-1}), dT/dP_s is the temperature gradient of the mantle solidus ($\sim$120 °C GPa^{-1} for a dry solidus,), F is degree of melting, H_f is the total heat of fusion ($\sim$420 J g^{-1}), and c_P is the isobaric heat capacity ($\sim$1.3 J g^{-1} K^{-1}). For simplicity, melt productivity is assumed to be linear with temperature for a given pressure; that is, dT/dF is assumed to be constant. Equation [13] can be integrated to yield the degree of melting as a function of decompression, that is,

$$\frac{dF}{dP} = \frac{dT/dP_a - dT/dP_s}{H_f/c_P + dT/dF} \qquad [14]$$

More sophisticated approaches, which account for variable dT/dF and the effects of water, are given by Katz et al. (2003) and shown in **Figure 13**.

The nature of foundering-induced magmas will depend largely on the thickness of the remaining lithosphere, which limits the extent of decompression and hence melting (**Figure 13**). If the lithospheric lid is >50 km, foundering-induced magmas will be characterized by high P_{ave} and low F (DePaolo and Daley, 2000; Haase, 1996; Langmuir et al., 1992; Wang et al., 2002). High-P melting also implies high T because of the positive slope of the mantle solidus. Primary magmas derived from partial melting of upwelled peridotitic mantle will therefore be characterized by low SiO_2 (due to high P) and high FeO (due to high T) (cf. Carmichael et al., 1970; Langmuir et al., 1992; Lee et al., 2009). These magmas will also be incompatible-element enriched (e.g., Na, K, light rare earth elements, Ba, Sr, Rb, and Ti) because the enrichment of such elements in a liquid relative to its solid source scales as $1/F$ (Langmuir et al., 1992). For this reason, foundering-induced magmatism may be characterized by alkali basalts, depending on how much of the deep lithosphere or lower crust foundered. Volatile components, such as H_2O and CO_2, also behave almost perfectly incompatibly, and will therefore be enriched in low-F melts, even if the mantle source is not enriched in these components. Melting at higher P_{ave} will also favor melting of components in the mantle that have lower melting points than dry peridotitic mantle. For example, if the mantle contains pyroxenites, such rocks may be chemically overrepresented in the melt because they begin to melt at greater depths than peridotite (Dasgupta et al., 2010; Ito and Mahoney, 2005a,b; Pertermann and Hirschmann, 2003a,b). Similarly, the incompatible element and isotopic compositions of such melts would be expected to reflect small-scale mantle heterogeneities. If, on the other hand, significant lithospheric removal has occurred, leaving a <50-km-thick lid, foundering-induced magmas will be produced by higher degrees of melting and should be tholeiitic basalts (higher SiO_2 and lower alkalis). Such magmas would likely have more homogeneous trace element and isotopic signatures. As the compositions of magmas are influenced by average pressures and temperatures of melting, basaltic magmas can be a useful tool in mapping the spatial and temporal evolution of the lithosphere–asthenosphere boundary (LAB) during and after foundering. These concepts will be dealt with again later.

4.12.3.2.2 Increased surface heat flux and melting of the overlying lithosphere

The incursion of hot asthenospheric mantle after deep lithospheric foundering should also lead to enhanced surface heat flux (equal to the near-surface temperature gradient multiplied by the thermal conductivity of rock). The increase in heat flux (**Figure 13**) depends on the amount of lithosphere remaining after foundering, that is, the thickness of the lithospheric lid, which defines P_f (**Figure 13**). For example, removal of 60 km of lower lithosphere (from an initial thickness of 100 km) increases heat flux by 40–50 mW m^{-2}, whereas removing only 25 km yields no measurable rise in heat flux. Because it takes time for the thermal anomaly at depth to propagate to the surface, the peak in heat flow occurs several Ma after foundering. For a remaining lithosphere thickness of $\sim$25 km, peak

heat flux lags foundering by ~8 Ma. Thermal equilibration of the underplated asthenosphere will eventually cause geotherms, surface heat flux, and topography to subside.

Increased heat flux may produce melting at the base of the crust. This, of course, would occur only if the overriding lithosphere was heated by the underlying hot asthenosphere to temperatures above its solidus. If hot asthenosphere impinges directly onto the base of the felsic crust, such as after wholesale delamination/detachment of lithospheric mantle or mafic lower crust, extensive anatexis would be expected. Such melts would likely be granitic to granodioritic in composition (Bird, 1979; Black and Liegeois, 1993; Mosher et al., 2008; Turner et al., 1999). If only the base of the lithospheric mantle is removed, such as during the growth of Rayleigh–Taylor-type instabilities, melting of the crust and what remains of the lithospheric mantle would be limited.

4.12.3.2.3 Melting of sinking garnet-pyroxenite blob

A second melting scenario is that the foundered material melts as it sinks. Cold, dense material will heat up conductively as it founders into hot asthenosphere. If the melting point of the foundered material is low, such as might be the case for mafic crust or volatile-rich (H_2O and CO_2) lithospheric mantle (cf. Dasgupta and Hirschmann, 2006), melting may occur (Elkins-Tanton, 2007). The extent of such melting will depend on the rate of sinking because the solidus temperature increases with pressure. For example, because a large blob heats up slowly and sinks rapidly, melting will not occur except at the extreme margins of the blob. Only if the blob is small and sinks slowly will it be substantially heated and melted, but because the total volume of the blob is small, the volume of the melts generated would also be small. Thus, although sinking pyroxenite blobs may partially melt, the total amount of such melts is likely to be far less than that generated by decompression melting of the asthenospheric mantle upwelling in response to lithospheric foundering.

4.12.3.3 Similarities with Lithospheric Extension and Thermal Erosion

Many of the geologic phenomena predicted to mark the aftermath of foundering are similar to those expected for active lithospheric extension or rapid thermal erosion of the base of the lithosphere. Rapid lithospheric thinning by extension also results in the replacement of cold (and hence dense) lithospheric mantle with hot asthenosphere (**Figure 1(f)**), leading to sustained high elevations. Lithospheric thinning will also give rise to basaltic magmatism and enhanced surface heat flux. The Basin and Range Province in western North America is a good example where extension-related geologic phenomena are similar to those predicted in the aftermath of foundering. These ambiguities will be highlighted below in the discussion of various cases studies. Lithosphere extension may itself be a natural by-product of deep lithosphere foundering. The important distinguishing feature for the purposes of this review is whether the mafic lower crust sinks and detaches from the lithosphere, or whether it is laterally advected during extension but otherwise remains attached to the continental crust.

4.12.4 Case Studies

It is impossible to summarize all instances where foundering has been suggested. For example, lithospheric foundering has been invoked in Mongolia (Cunningham, 2001), Tibet (Chen and Tseng, 2007; Harrison et al., 1992; Houseman and Molnar, 1997; Turner et al., 1996), the Wallowa Mountains in Oregon (Hales et al., 2005), Papua New Guinea (Cloos et al., 2005), Carpathians (Knapp et al., 2005), Colorado Plateau (Bird, 1979), much of western North America (West et al., 2009), the Transverse Ranges in California (Houseman et al., 2000; Humphreys and Clayton, 1990), the Appalachians (Nelson, 1992), the Grenvillian belt (Mosher et al., 2008), the North China Craton (**Section 4.12.4.4**), the Sierra Nevada in California (**Section 4.12.4.1**), the Andes (**Section 4.12.4.2**), the western Mediterranean (**Section 4.12.4.3**), and on Venus (Elkins-Tanton et al., 2007). It has also been suggested to explain trench-parallel seismic anisotropy beneath arcs (Behn et al., 2007). Most of the evidence for deep crustal/lithosphere foundering is circumstantial, occasionally leading to contrived interpretations, so it is possible that some suggestions of deep foundering, especially deep crustal foundering, will be proven wrong in the future. As noted above, it is difficult to distinguish the aftermath of foundering from the effects of lithospheric extension. Below, the Sierra Nevada, the Andes, the western Mediterranean, and the North China Craton are used as case studies of possible lower crustal or deep lithosphere foundering. The first two cases probably involve composition-driven instabilities associated with the formation of dense, mafic cumulates during arc magmatism. In these instances, foundering has a direct impact on the compositional evolution of the continental crust. The last two cases involve deep lithospheric processes, possibly related to thermally driven density instabilities associated with collisional orogens, where removal of deep lithospheric mantle is implicated. In all cases, the 'stories' are not set in stone; hence, outstanding unresolved problems or debates are highlighted as best as possible.

4.12.4.1 Sierra Nevada, California

The Sierra Nevada, California (**Figure 14**), may be one of the clearest case studies in which mafic lower crust has foundered. The Sierra Nevada's current high elevation is not compensated by a thick crustal root, as evidenced by its shallow Moho (Ducea and Saleeby, 1996; Ruppert et al., 1998; Wernicke et al., 1996). The high topography is thought to be recent (late Miocene to Pliocene) because of the westward tilting of Eocene paleo channels along the western slope of the mountain range (Huber, 1981; Unruh, 1991). Seismic studies show vertically trending high-velocity anomalies beneath the Great Valley and western foothills in the southern part of the Sierras (Boyd et al., 2004; Yang and Forsyth, 2006; Zandt and Carrigan, 1993; Zandt et al., 2004). These observations have been taken as indirect evidence that a thick crustal root was recently removed and the current high elevations are sustained by the return flow of hot asthenospheric mantle. The high-velocity anomalies are interpreted to represent foundering lower crust or deep lithosphere (Jones et al., 2004; Saleeby et al., 2003). Broadly consistent with this interpretation is the

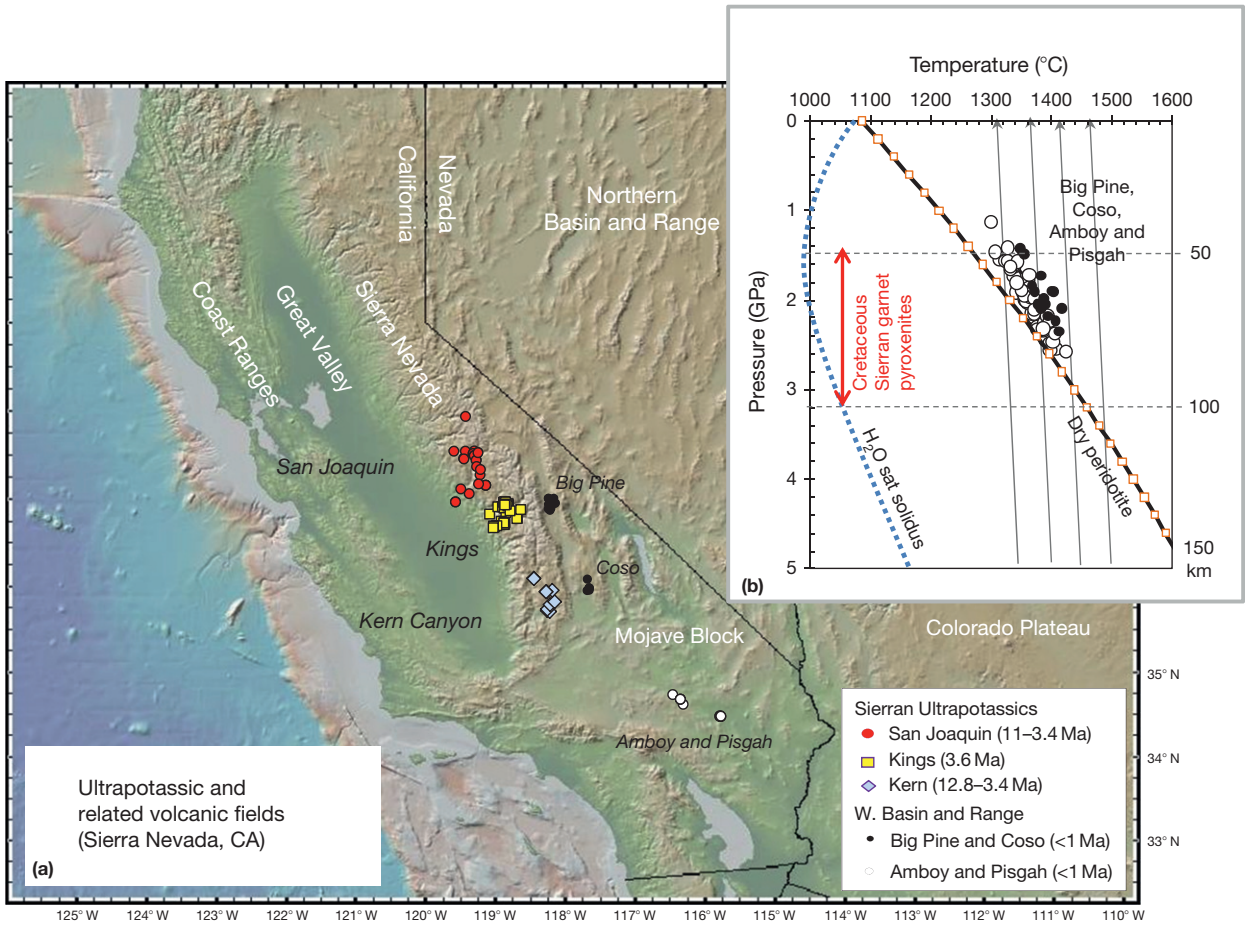

Figure 14 Postdelamination magmatism from the Sierra Nevada, California, USA. (a) Map of the Sierra Nevada region shows locations of Miocene to Pleistocene alkali and ultrapotassic eruptives, some of which host mantle and lower crustal xenoliths. These lavas erupted through the Sierra Nevada Batholith, remnants of a Cretaceous continental magmatic arc. Foundering of mafic lower crust is thought to have occurred beneath the region now denoted by late Cenozoic ultrapotassic volcanism. (b) Inset figure shows the results of thermobarometry applied to those magmas that are undoubtedly derived from a peridotitic mantle source (see **Figure 15**). These are the <1-Ma lavas in the eastern part of the Sierra Nevada (Big Pine and Coso volcanic fields; black circles) and the Mojave block in southern California (Amboy and Pisgah; open circles). *P–T* calculations could not be done on the central Sierran ultrapotassics because they may not derive solely from peridotitic sources (see **Figure 15**). These *P–T* estimates should reflect the temperature and depth of melting within peridotitic mantle and therefore they place constraints on the thickness of the lithosphere. These peridotite-derived magmas come from depths between 50 and 80 km and overlap the depth range over which garnet-pyroxenites were formed in the Cretaceous Sierran arc (see **Figure 2(a)**). This implies that most of the Sierran pyroxenites were removed by 1 Ma. *P–T* calculations use the thermobarometer of Lee et al. (2009) with data from the literature (Beard and Glazner, 1995; Farmer et al., 2002; Feldstein and Lange, 1999; Mordick and Glazner, 2006; Van Kooten, 1980, 1981). Solidi are from Hirschmann (2000) and Katz et al. (2003). Gray lines represent solid mantle adiabats for given mantle potential temperatures.

flare-up of small-volume, low-*F* alkali basalt and ultrapotassic magmas in the Pliocene, which have been argued to represent decompression melts generated just after root foundering (**Figures 14** and **15(a)**; Farmer et al., 2002; Jones et al., 2004; Manley et al., 2000; Van Kooten, 1980, 1981).

The strongest line of evidence for recent removal of the root beneath the high Sierras comes from secular changes in xenolith demographics (Ducea and Saleeby, 1996) and inferred thermal state of the lithosphere. The Cretaceous Sierra Nevada batholith was once underlain by a thick layer of mafic cumulates in the form of garnet-pyroxenites making up the lower crust and parts of the lithospheric mantle (**Figures 2(a)** and **3**; Dodge et al., 1988; Ducea, 2001, 2002; Ducea and Saleeby, 1996, 1998b; Lee et al., 2006, 2007; Mukhopadhyay and Manton, 1994). These cumulates have been shown to be petrogenetically linked to the granodioritic plutons dominating the batholith (Ducea, 2002; Ducea and Saleeby, 1998b; Lee et al., 2006, 2007). The cumulates can be found as xenoliths in late-Miocene (8.3 Ma) alkali basalts, which are associated with the end of subduction and initiation of Basin and Range style lithospheric extension (**Figure 14**). Thermobarometric studies of late Miocene-hosted xenoliths indicate that these cumulates derive from depths up to ~90 km and record equilibration temperatures <800 °C (**Figure 14**; Chin et al., 2012; Ducea and Saleeby, 1996, 1998b; Mukhopadhyay and Manton, 1994). The deeper cumulates are interleaved with spinel and garnet-bearing spinel peridotites, most of which also record temperatures below 800 °C (Ducea and Saleeby, 1996, 1998b;

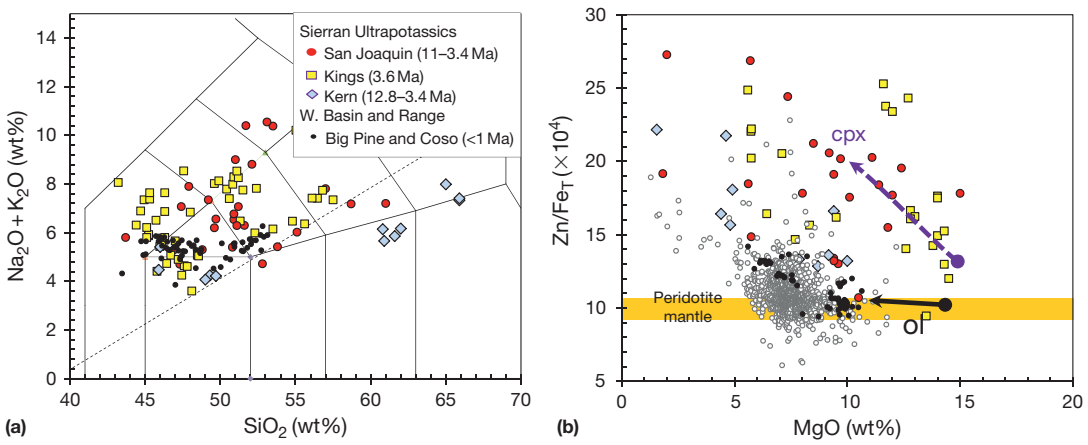

Figure 15 Postdelamination magmas from the Sierra Nevada. (a) Whole-rock compositions of Sierran alkali and ultrapotassic series lavas (Beard and Glazner, 1995; Farmer et al., 2002; Feldstein and Lange, 1999; Mordick and Glazner, 2006; Van Kooten, 1980, 1981) plotted in a standard total alkali versus SiO_2 classification diagram (Le Bas et al., 1986). (b) Whole-rock elemental ratio of Zn/Fe_T (Fe_T = total Fe) versus MgO. MORB data from the Ridge PetDB (www.petdb.org) database are shown for reference. Peridotitic mantle is from Le Roux et al. (2010). For magmas with MgO > 8 wt%, only those with Zn/Fe_T ratios similar to that of peridotitic mantle and primitive MORB derive from a peridotites source. High Zn/Fe_T magmas derive from a garnet-pyroxenite source. Arrows show the effects of olivine (ol) and clinopyroxene (cpx) crystal fractionation.

Lee et al., 2001a). By contrast, Pliocene and younger basaltic magmas in the Sierra Nevada do not contain any garnet-pyroxenite xenoliths. Instead, these basalts contain spinel peridotites equilibrated at temperatures of >1000 °C, which is clear evidence that the cold, pyroxenite-laden root of the Sierras was removed and replaced by asthenospheric mantle between the late Miocene and Pliocene (Ducea and Saleeby, 1996, 1998b; Lee et al., 2001a). Finally, as will be shown later, thermobarometric constraints on the late-Pliocene and younger basaltic magmas suggest that they derived from peridotites melting at depths between 50 and 70 km, further indicating that much of the thick and cold garnet-pyroxenite dominated root has been replaced by hot asthenospheric mantle (**Figure 14**).

The geologic history of the deep Sierran lithosphere can be summarized as follows (see also Saleeby, 2003; Saleeby et al., 2003): A thick, mafic root was generated in the mid- to late Cretaceous as the cumulate complement of the Sierran granitoids. This thick cumulate layer cooled, perhaps by 'refrigeration' imparted by the subducting Farallon plate. In the Miocene, the Pacific–Farallon ridge collided with the North American plate, terminating subduction and resulting in the generation of an ocean–continent transform fault. This resulted in the opening of a 'slabless' asthenospheric window beneath the Sierra Nevada by the late Miocene. Heating from below may have helped to weaken the cold mafic root, prepping it for convective removal. Large-scale removal of the pyroxenite-dominated root appears to have culminated in the Pliocene (~3.5 Ma), resulting in a resurgence in small-volume alkali basaltic magmatism (**Figures 14** and **15**) and surface uplift, which continues even today. Downwelling may still be ongoing in the western and southern Sierras and may be imparting dynamic topography in the form of localized basins in the southern portion of the Great Valley (Saleeby et al., 2003). The removal mechanism of the Sierra mafic root is still far from understood. What is clear is that the negative buoyancy was dominantly compositional. If the interpretations of seismic studies are taken at face value, it would seem that the mafic root is being removed asymmetrically. One possibility is that the root is 'draining' via a Rayleigh–Taylor-type instability toward the west (Boyd et al., 2004; Zandt et al., 2004). Another possibility is that the root is peeling away and propagating westward. This scenario involves wholesale delamination (cf. Bird, 1979), which initiated along a crustal weak zone and is maintained by intrusion of asthenospheric mantle from the Basin and Range extensional province to the east (Le Pourhiet et al., 2006). Yet another possibility is that this high-velocity anomaly represents ancient fragments of Farallon plate rather than actively detaching Sierran arc lithosphere, as recently suggested by Forsyth and Rau (2009) (see also Schmandt and Humphreys, 2011; Wang et al., 2009).

A perplexing question is why root removal occurred so long (~70 Ma) after its formation in the Cretaceous? Given the high densities of garnet-pyroxenites (**Figure 4**), this root should have foundered soon after its formation. A possible explanation is that refrigeration of the root by the Farallon plate made the root too viscous to founder, and only when subduction ended was this constraint removed. This begs the question of whether the Sierran case study is unique. However, some studies suggest that the formation and removal of mafic roots in arc systems may be cyclic. DeCelles et al. (2009) argued that the major fluxes in Sierran arc magmatism are linked to enhanced periods of lithospheric shortening. They suggest that thick layers of mafic cumulates/restites form during this time until a critical thickness is reached and the dense root founders, providing room for a second phase of shortening and magmatism. If correct, these ideas suggest that lithospheric foundering and magmatism may be intimately linked. This is consistent with suggestions by Lee et al. (2000, 2001a), on the basis of the young Os isotopic composition and thermal histories of Sierran peridotite xenoliths, that a major lithospheric removal event accompanied or was the precursor to Cretaceous arc magmatism. In any case, additional xenolith studies in other parts of the Sierra Nevada should be carried out to assess the robustness of the above conclusions.

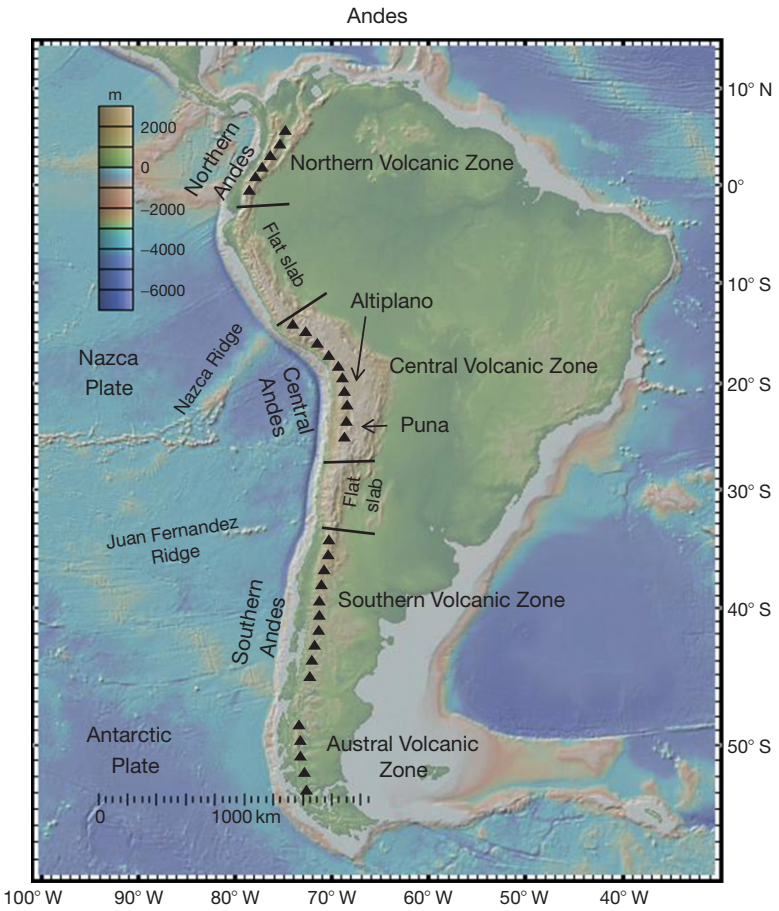

Figure 16 Map of the Andes and the South American continent. Volcanically active segments of the Andean belt are shown schematically with black triangles. These regions are underlain by steeply subducting slabs. Amagmatic segments are shown devoid of black triangles and correspond to regions of flat slab and limited or minimal asthenospheric mantle wedge beneath the Andean chain. Region of highest elevation is the broad Altiplano and Puna regions within the Central Andes. This is the region where foundering of arc lithosphere has been proposed. Map has been modified from Stern (2004) and Kay et al. (2004).

4.12.4.2 The Andes

The Andean mountain chain is an ocean–continent subduction zone with an active continental magmatic arc, presumably the modern analog of the Cretaceous Sierra Nevada continental arc magmatism discussed above (Oncken et al., 2006; Figure 16). Removal of lower crust and lithospheric mantle has been suggested to have recently occurred (Miocene to present) beneath the central Andes (10–30 °S) (Garzione et al., 2008; Kay and Kay, 1993; Kay et al., 1994). This segment of the Andes is dominated by the ~500-km-wide Altiplano–Puna Plateau, which in some places reaches peak elevations of 6 km (Oncken et al., 2006). The Altiplano is flanked to the west by an active magmatic arc (the Central Volcanic Zone of the Western Cordillera) and to the east by fold-and-thrust belts in Paleozoic sediments (Eastern Cordillera). The presence of arc magmatism is consistent with a steeply subducting Nazca plate, which implies the presence of an asthenospheric mantle wedge. By contrast, flat subduction occurs to the north and south of the Central Volcanic Zone and is associated with a lack of arc magmatism. The Central Andes segment also appears to have undergone more significant (300–350 km) shortening of the South American Plate than the northern and southern Andes (Oncken et al., 2006).

Circumstantial evidence for recent removal of lower crust derives mainly from the fact that crustal thickness does not correlate with elevation. In the central Altiplano, the Moho depth as inferred from P-wave to S-wave converted seismic phases is ~70 km, but in the Puna part of the plateau, it is only ~50–55 km (Yuan et al., 2000, 2002), indicating that the high elevations are not supported by a deep crustal root. Seismic tomography and attenuation studies indicate low P-wave velocities and high P-wave attenuation beneath the Puna region, which suggests the presence of hot, asthenospheric mantle rather than a deep, cold crustal root (Schurr et al., 2006). The inferred seismic velocity structure of the crust suggests that most of the crust is felsic (Beck and Zandt, 2002). Late Miocene to Pliocene basaltic lavas in the Altiplano and Puna regions are thought to represent partial melts of the asthenospheric mantle (Carlier et al., 2005; Kay and Kay, 1993; Kay et al., 1994). These observations have been interpreted to indicate that portions of the deep crustal root beneath the Central Andes have recently been removed and replaced by hot asthenospheric mantle

(see Garzione et al., 2008 for review). The mechanism of removal is not known, but numerical models suggest that high-density garnet-pyroxenite lower crust is needed to drive convective removal of the lower crust (Sobolev and Babeyko, 2005). Paleo-elevation studies of pedogenic carbonates in the Altiplano using stable isotopes show that 2.5–3.5 km of uplift occurred between ~6.8 and 10.3 Ma, corresponding to an uplift rate of ~1 km Ma^{-1} (Garzione et al., 2006; Ghosh et al., 2006). Garzione et al. (2006) and Ghosh et al. (2006) used these observations to corroborate the suggestion that uplift most likely resulted from the foundering of a dense garnet-pyroxenite root rather than from crustal shortening because crustal shortening in most of the Central Andes appears to have ended in the last 10 Ma (McQuarrie, 2002). However, crustal shortening probably did not end in the last 10 Ma. Oncken et al. (2006) show that much of the upper crustal shortening appears to have migrated trenchward toward the narrow sub-Andean belt in the last 10 Ma. In addition, Sobolev and Babeyko (2005) show with numerical models that much of the recent uplift, while not accommodated by widespread upper crustal shortening, can be linked to enhanced shortening in the lower crust. These authors argue that the primary driver of high elevations in the central Andes is the westward drift of South America, and not deep crustal foundering alone. Nevertheless, as pointed out by these authors, deep crustal foundering may be critical in weakening the remaining continental lithosphere, allowing shortening to occur. In any case, the similarity of the Andes with the Cretaceous Sierra Nevada batholith suggests that deep garnet-pyroxenite cumulates may also be present beneath the Andes. Garnet-pyroxenite cumulates are known to occur in the lower crust of the northern Andes (as sampled by lower crustal xenoliths, Rodriguez-Vargas et al., 2005; Weber et al., 2002).

4.12.4.3 Alboran Region, Western Mediterranean

A number of geological and geophysical features in the western Mediterranean (the Alboran region; **Figure 17**) suggest a dynamic deep lithosphere, prompting the idea of lithospheric thinning. This region is associated with collision between Africa and Europe, but, paradoxically, much of the region (Alboran Sea) is underlain by thinned lithosphere, indicating that extension may be occurring (Maldonado et al., 1999; Platt and Vissers, 1989). The Rif-Betic mountains define the northern (Spain) and southern (Morocco) flanks of the extended Alboran region and trace an arc of mountains that wraps westward across the Strait of Gilbraltar. The Ronda and Beni Bousera peridotite massifs, exposed in the Rif-Betics, appear to have been exhumed to crustal depths in the late Oligocene–early Miocene. Thermobarometric studies of the massif and surrounding metamorphic aureoles suggest that these massifs were emplaced while they were still at high temperatures (~1000 °C) characteristic of the mantle (Platt and Vissers, 1989; Platt et al., 1998). Exhumation of these massifs is manifested as metamorphic core complexes, which occurred under high thermal gradients. These observations suggest significant extension under the Rif-Betics as well, despite the fact that they are presently at high elevations.

Magmatism in the Alboran region is unusual (**Figure 17**). It spans the lower Oligocene (~35 Ma) to the Pleistocene (0.65 Ma) (Duggen et al., 2003, 2004, 2005; Turner et al., 1999) and appears to be associated with high surface heat flux (Polyak et al., 1996). The spatiotemporal trends of magmatism are more complicated than those expected for a simple plate boundary. From ~35 to 20 Ma, the region was marked by tholeiitic magmatism (Malaga dikes) characterized

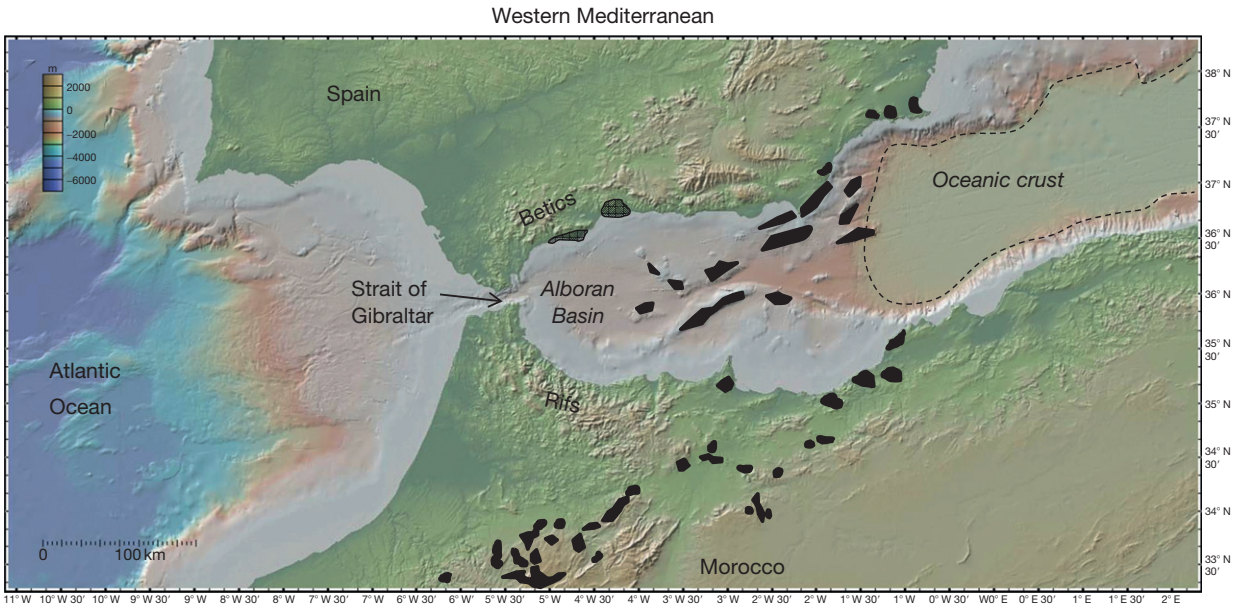

Figure 17 Western Mediterranean region, bounded to the north by the Eurasian continent, to the south by the African continent, and to the west by the Atlantic Ocean. The Alboran Basin represents recently thinned continental crust. To the east lies oceanic crust. The Betic-Rif mountain belt forms an arcuate mountain range that wraps around the Strait of Gibraltar. Black shapes represent Late Cenozoic volcanic fields. Those in the Alboran Basin and southeastern Spain are characterized by calc-alkaline compositions (Duggen et al., 2003). The high elevations of the Betic-Rif mountains and the presence of late Cenozoic volcanism have been interpreted to represent either the aftermath of deep lithospheric foundering or westward rollback of the paleo-Tethyan oceanic lithosphere. Volcanic fields are taken from the literature (Duggen et al., 2003, 2004, 2005; Turner et al., 1999).

by nonradiogenic Sr and radiogenic Nd isotopes and interpreted to derive from mid-ocean ridge-type asthenospheric mantle (Turner et al., 1999). From ~15 to 4 Ma, the region was characterized by tholeiitic, calc-alkaline, and shoshonitic series magmas (basaltic to rhyolitic), characterized by radiogenic Sr and nonradiogenic Nd isotopes and relative enrichments in fluid-mobile trace elements. These features have been interpreted as subduction-related signatures (Duggen et al., 2003, 2004) or crustal contamination (Turner et al., 1999). Cordierite-bearing dacitic magmas, representing partial melts of crustal origin, also occur within this time window. A transition in the composition of magmas occurs at ~6–4 Ma. Alkali basalts, many containing mantle xenoliths (from the plagioclase stability field, Shimizu et al., 2008), erupted on the flanks of the Alboran domain after 6 Ma. These basalts are characterized by nonradiogenic Sr and radiogenic Nd isotopes and ocean island-type trace-element abundance patterns, suggesting a fundamental change in the composition of the mantle source (Duggen et al., 2003, 2004).

It is generally agreed that the above observations are the manifestation of deep lithospheric mantle removal although the exact mechanisms and timing are debated. Details of the debate can be found elsewhere (Duggen et al., 2003, 2004; Platt and Houseman, 2003; Platt and Vissers, 1989; Platt et al., 1998; Turner et al., 1999). In brief, Platt and Vissers (1989) suggest that the Alboran domain underwent contraction >30 Ma, resulting in the formation of a thickened thermal boundary layer, which subsequently foundered via a Rayleigh–Taylor-type instability. The asthenospheric mantle return flow associated with removal of this thickened boundary layer culminated in uplift and magmatism in the Oligocene and Miocene. Platt and Vissers (1989) suggest that the topographically high Alboran domain would have gravitationally collapsed, driving extension in an active orogenic belt. Duggen et al. (2003, 2004, 2005) suggest a slightly different view. They suggest that most of the lavas prior to 5 Ma erupted in a subduction zone related to westward rollback of an east-dipping Tethyan oceanic lithosphere. They suggest a more recent removal of subcontinental lithospheric mantle beneath Spain and Morocco, driven not by orogenic thickening but by edge-driven convection associated with mantle wedge flow in a retrograding subduction zone. Interestingly, slab rollback may have helped to close the western Mediterranean seaway, resulting in the late Miocene desiccation of the Mediterranean ('Messinian crisis') (Duggen et al., 2003). Seismic tomography and seismicity indeed show a deep high-velocity anomaly beneath the region and deep seismicity separated from the crust by a seismicity gap (Calvert et al., 2000; Grimison and Chen, 1986; Gutscher et al., 2002; Seber et al., 1996). Although there are hints that the high-velocity anomaly dips toward the east, and is thus suggestive of a subducting slab, more detailed seismic studies are needed to move forward. In summary, it is reasonably clear that the continental lithospheric mantle was involved in recycling in the Alboran region, but the mechanisms are still debated. There is no evidence, to date, that the LCC was involved in such recycling.

4.12.4.4 North China Craton

Another place where lithospheric recycling has been proposed is the North China Craton (**Figure 18**). The crustal basement is Archean (~2.7 Ga), but the underlying lithospheric mantle, while variable in age, appears to be, in general, post-Archean. Diamond-bearing kimberlites erupted through the eastern part of the craton in the Paleozoic (~460 Ma), indicating the presence of a thick (>150 km) lithospheric keel at that time (Xu, 2001). By contrast, Cenozoic basalts erupted through the same region contain peridotite xenoliths from much shallower depths (spinel peridotites) with Phanerozoic Re–Os model ages (Chu et al., 2009; Gao et al., 2002; Wu et al., 2003, 2006). Thermobarometric constraints from peridotites hosted in the Cenozoic basalts in the eastern part of the craton indicate that, by the Cenozoic, the lithosphere had thinned to <80 km (Fan and Hooper, 1989; Fan et al., 2000; Menzies et al., 2007; Rudnick et al., 2004; Xu, 2001). The eastern craton is also characterized by high surface heat flux (see Menzies et al., 2007), thinner lithosphere (Chen et al., 2008), and anomalously low shear-wave velocities below the seismic lid (Zhang, 1998). Collectively, these observations indicate that cratonic lithosphere was thinned, most likely in the Jurassic or Cretaceous. However, the mechanism remains unclear. Many of the above features are consistent with foundering of lithospheric mantle, but could also be explained by lithospheric extension or small-scale convective thinning at the base of the lithosphere, perhaps in response to flow associated with subduction of the Pacific plate (Menzies et al., 2007; Xu, 2001). However, the complete lack of Archean peridotite xenoliths in the young basalts of the region has been used to argue for wholesale removal of Archean lithospheric mantle, which seems more consistent with thinning by one or more delamination events rather than by extension (Chu et al., 2009; Gao et al., 2002; Wu et al., 2003, 2006).

For the purposes of this review, the question of interest is whether lithospheric thinning was accompanied by lower crustal recycling. Gao et al. (1998a,b) noted that the composition of the crust in the North China Craton is too felsic and depleted in various compatible trace elements to have been derived directly from the mantle, and therefore suggested that a mafic lower crust was missing. Based on mass-balance constraints, they suggested that this missing mafic reservoir was similar in composition to the 'eclogites' of the Dabie–Sulu ultrahigh-pressure terrane and therefore argued that much of the original mafic lower crust beneath the craton foundered. These conclusions, however, provide no direct constraint on when foundering occurred. Gao et al. (2004) reported reverse-zoned phenocrysts and Paleoproterozoic inherited zircon xenocrysts in Ni-rich, high-Mg/(Mg + Fe) Mesozoic magmas with 'adakitic' signatures (e.g., high Sr/Y), and provocatively suggested that such magmas represent partial melts of sinking 'eclogitic' crust. To explain the high Mg# and Ni contents, they suggested that these liquids ascended and reacted through the mantle before erupting. More recently, Gao et al. (2008) report basaltic magmas with major and trace-element signatures suggestive of a hybrid eclogite–peridotite origin, which has been used to corroborate the suggestion of delamination. In any case, because of the fast rates at which garnet-pyroxenite blobs founder, this interpretation requires that foundering of the lower crust was almost contemporaneous with the emplacement of these Mesozoic 'adakitic' magmas at ~160 Ma. It is worth noting that some geochemical features of 'adakitic' rocks, including reverse zonation, can be explained by mixing

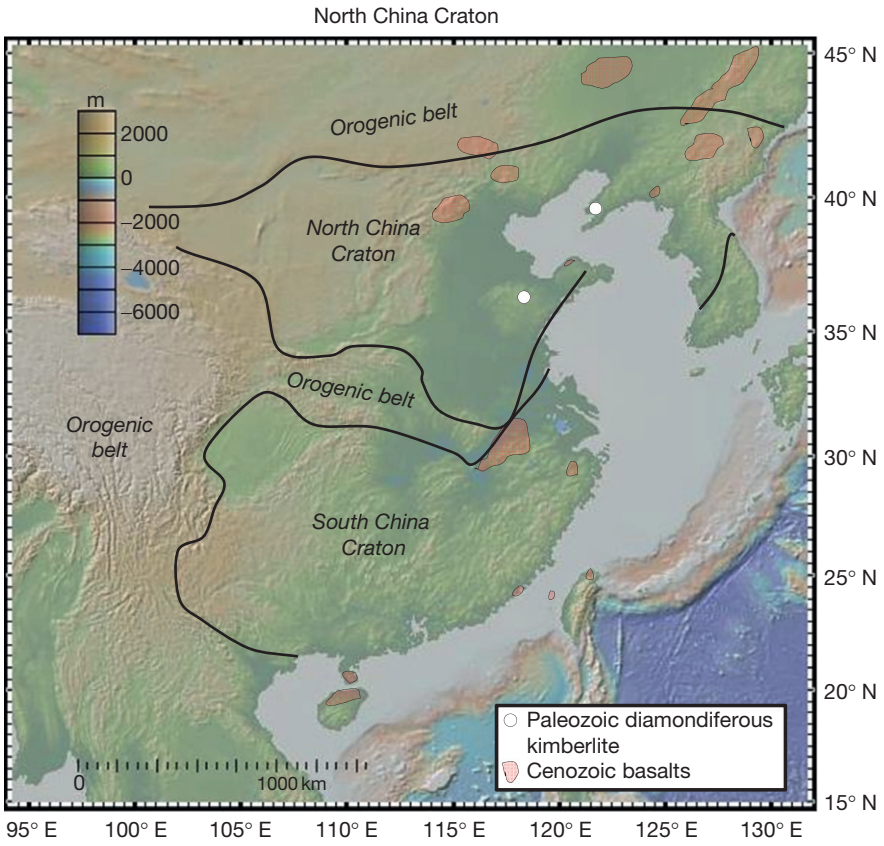

Figure 18 Map of East Asia, showing the Archean boundaries of the North and South China cratons. Intervening orogenic belts are labeled. Late Cenozoic basaltic volcanic fields are denoted by red shapes. White circles represent Paleozoic diamondiferous kimberlites. The Cenozoic volcanic centers do not contain garnet peridotites. This secular change in xenolith demographics has been used to suggest that much of the North China cratonic lithosphere has foundered since the Paleozoic. Map modified from sources in the literature (Gao et al., 2002; Wu et al., 2003, 2006).

of lower crustal melts with recharging basaltic melts (Streck et al., 2007), so not all 'adakitic' magmas should necessarily be interpreted as melts derived from sinking garnet-pyroxenites.

4.12.5 The Composition and Mass Fluxes of Lower Crustal Foundering

4.12.5.1 Where Is Mafic Lower Crust Generated?

Quantifying the time-integrated mass flux of delaminated lower crust is difficult because direct observational constraints are rare or subject to interpretation. One tractable approach is to use mass-balance constraints based on the fact that crustal compositions are felsic and require a missing mafic complement, which presumably foundered. Mass-balance approaches, however, are devoid of geology and therefore do not constrain when or how the mafic complement was removed. What is clear is that only mafic rocks stabilize garnet + pyroxene-rich rocks dense enough to founder, and thus, any estimate of lower crustal foundering rates must first identify when and where such mafic rocks form.

Mafic rocks can be formed by direct magmatic underplating, crystal accumulation, or as the residues of melt depletion. Foundering of magmatically underplated basalts is not particularly interesting from a petrogenetic point of view if the basalt did not undergo differentiation. Crystal accumulation can occur wherever magmas traverse a thermal boundary layer, resulting in cooling and crystallization along vein or dike margins. Such processes should occur in arc and intraplate environments, though the extent of differentiation appears to be much greater in the former as evidenced by the more evolved nature of arc magmas. Formation of restites can also occur in arc and intraplate environments if recently emplaced basalts are remelted by new magmatic additions. Restites can further form during collisional orogeny, where depression of geotherms to greater depths leads to lower crustal heating and partial melting of preexisting crust in the garnet-stability field. These residues would evolve toward mafic bulk compositions if high extents of melt extraction were possible. Of these scenarios, generation of restites and cumulates in arc environments is probably the most important because the trace-element composition of the continental crust is largely dominated by an arc-like signature. This is fortunate because the amount of mafic restites/cumulates generated in arcs is reasonably well-constrained. There are few constraints on the proportions of mafic differentiates in intraplate magmatic systems and collisional orogenies, making it difficult to discuss these scenarios quantitatively. According to Barth et al. (2000), the intraplate contribution to continental crust is <5–20%, so recycling of intraplate-related cumulates is of secondary interest.

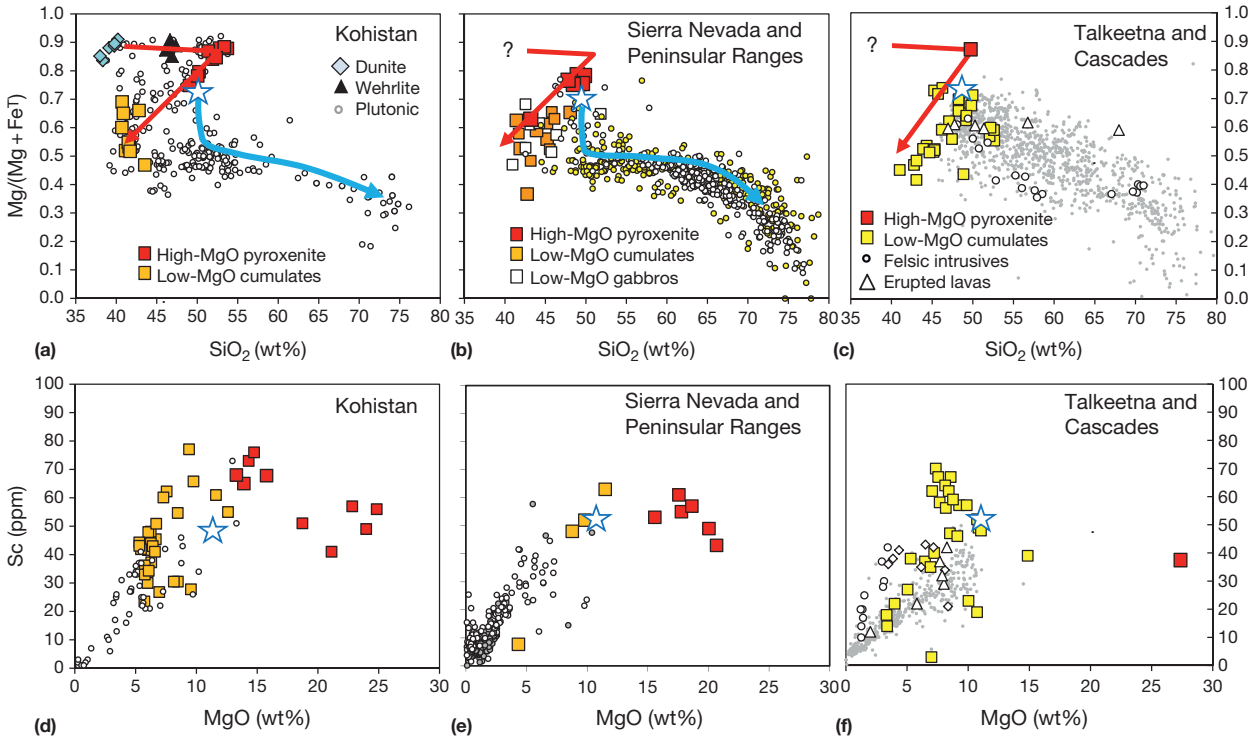

Figure 19 Whole-rock Mg# (atomic $Mg/(Mg+Fe_T)$) versus SiO_2 for rocks from (a) the Cretaceous Kohistan intraoceanic arc, (b) the Cretaceous Sierra Nevada continental arc, and (c) the Jurassic Talkeetna intraoceanic arc. Open circles in (a) and (b) represent plutonic rocks from each of the localities. In (c), the open circles represent intrusive rocks from Talkeetna, and the open triangles represent lavas from Talkeetna. Shown for reference are small gray circles for rocks (dominantly extrusive) from the active Cascades volcanic zone in the northwestern United States (using the GEOROC database; georoc.mpch-mainz.gwdg.de/). In (a–c), large symbols refer to rocks that have a demonstrated petrogenetic origin as cumulates. Star represents a putative primary mantle-derived arc basalt (Kelemen et al., 2003). Blue arrow represents an inferred liquid line of descent from a primary arc basalt. Red arrow shows the crystal line of descent as inferred from the cumulate rocks. (d–f) show whole-rock Sc versus MgO for the same rocks in (a–c). Star shows the Sc and MgO content of primitive arc basalt. Note that evolved liquids mostly have low Sc and Mg contents, which cannot be explained by olivine segregation, but can be explained by segregation of high-MgO and low-MgO garnet-pyroxenites. Datasets are from the literature (Dhuime et al., 2007, 2009; Greene et al., 2006; Jagoutz, 2010; Jagoutz et al., 2009; Kelemen et al., 2003; Lee et al., 2006, 2007).

4.12.5.2 Arc Magmatism as a Case Study of Lower Crustal Recycling

There are three paleo-arc systems where deep crustal and lithospheric mantle sections are accessible in conjunction with their magmatic counterpart (**Figure 19**). These include the Cretaceous Sierra Nevada and Peninsular Ranges continental arc in California and Baja California (Coleman and Glazner, 1997; Coleman et al., 1992; Ducea, 2001, 2002; Ducea and Saleeby, 1998a,b; Lee et al., 2001a, 2006; Saleeby et al., 2003; Sisson et al., 1996), the Cretaceous Kohistan intraoceanic arc in Pakistan (Garrido et al., 2006; Jagoutz, 2010; Jagoutz et al., 2007, 2009), and the Jurassic intraoceanic Talkeetna arc in southcentral Alaska (DeBari and Sleep, 1991; Greene et al., 2006; Kelemen et al., 2003). The deep crust and lithospheric mantle are accessed in the Sierras as xenoliths in late Miocene basalts (see above discussion), whereas in Kohistan and Talkeetna, the deep crust is exposed in exhumed and tilted sections. Relevant geologic background can be found in the above-cited references.

Figure 19(a)–19(c) shows whole-rock Mg# (atomic $Mg/(Mg+Fe_T)$, where Fe_T represents total Fe) versus SiO_2 for magmas and cumulates for the Sierra Nevada, Kohistan, and Talkeetna (Cascades arc lavas are shown in the Talkeetna panel for comparison). A hypothetical primary arc basalt (Kelemen et al., 2003) is shown for reference. Being minimally differentiated, primary arc basalts should have Mg# of ~0.72 as defined by Fe/Mg exchange equilibrium between the liquid and mantle peridotite (Mg# ~0.89) (see Hanson and Langmuir, 1978; Langmuir et al., 1992; Roeder et al., 1979). They have ~50 wt% SiO_2, which reflects the intermediate pressures of melting (1–2 GPa) associated with arc magmatism (Lee et al., 2009). Assuming this primary basalt to be parental to the magmas shown in **Figure 19(a)–19(c)**, the most striking feature is that the majority of magmas in the Sierras and Kohistan have Mg# <0.5, even for gabbros and diorites at 50 wt% SiO_2 (in Talkeetna, the plutonic rocks also have low Mg#). There is thus a distinct Mg# gap early in the differentiation history of these arc magmas, but no such gap is seen with SiO_2. This Mg# gap results from extensive fractionation of ultramafic and mafic cumulates, at sub-Moho depths. The liquid line of descent inferred from the magmatic differentiation series requires early removal of cumulates having high MgO and similar SiO_2 to the parental magma in order to drive the parental magma to low MgO and (Mg#) at constant SiO_2. Next, the liquid line of descent appears to kink in the Mg#–SiO_2 space toward Si enrichment at relatively constant Mg#. This vector requires

another stage of fractionation involving the removal of low-SiO_2 cumulates whose mineral assemblages do not fractionate Mg and Fe.

The cumulates observed in the three arc case studies fit the complementary crystal line of descent required by the kink in the magmatic differentiation series described above (**Figure 19(a)–19(c)**). The early cumulates are defined by high-MgO (>14 wt%) pyroxenites (± garnet) and have SiO_2 similar to the parental basalt as a result of high pyroxene to garnet ratios (**Figure 19**). These cumulates are followed by low-MgO (<14 wt% MgO), low-SiO_2 cumulates represented by garnet-rich (>50% gt) clinopyroxenites and hornblende- and plagioclase-bearing gabbros (**Figures 19**). Their low-Si contents result from the high modal abundance of hornblende or garnet relative to pyroxene. High-MgO pyroxenites are the expected cumulates of primary hydrous basalts at high pressure (>1 GPa) (Müntener et al., 2001), whereas garnet-rich low-MgO pyroxenites are the expected cumulates of more evolved hydrous basaltic and andesitic magmas (Alonso-Perez et al., 2009). Following Lee et al. (2006, 2007), these two cumulate groups are herein referred to as the high-MgO and low-MgO pyroxenite/gabbro cumulates, and collectively they define a vector antithetical to the liquid line of descent in the Mg#–SiO_2 space (**Figure 19(a)–19(c)**). In addition to these pyroxenite/gabbro cumulates, ultramafic cumulates (dunites and wehrlites) are reported in the Kohistan section and represent differentiates even more primitive than the high-MgO pyroxenites. Collectively, these ultramafic and mafic cumulates trace a 'Z-shaped' crystal line of descent in the Mg#–SiO_2 space (**Figure 19(a)–19(c)**; Jagoutz, 2010). However, because of the very high MgO and very low SiO_2 of dunites, significant dunite accumulation would impart a strong negatively sloped vector in the liquid line of descent in the Mg#–SiO_2 space. Early Si enrichment is not seen, which indicates that the proportion of dunite accumulation must be minor relative to that of high-MgO and low-MgO pyroxenite/gabbros.

The major and minor element composition of the high-MgO and low-MgO pyroxenite/gabbro cumulates are given in **Table 1**, based on compilations from the above-cited literature. Also presented are the abundances of trace elements, which behave compatibly (e.g., Ni, Cr, Mg, and Co) or moderately incompatibly (e.g., Y, Yb, Al, Ca, V, Cu, Sc, Zn, Mn, and Fe) during melting of peridotitic mantle. These elements are generally robust to infiltration or retention of small amounts of melts or fluids, and thus their abundances generally preserve the original signatures of their magmagenesis. By contrast, highly incompatible elements are too easily disturbed by melts and fluids, so they are not included in **Table 1**. In **Figure 19(d)–19(f)**, these cumulate compositions are compared to primary arc basalts (Kelemen et al., 2003) and global continental crust models (Rudnick and Fountain, 1995; Rudnick and Gao, 2003) in primitive-mantle (PM) normalized spidergrams using the normalizing values of McDonough and Sun (1995). The plotting order of the elements on these plots was chosen so that the PM-normalized MORB spidergram increases monotonically to the right (**Figure 20**). Elements whose PM-normalized concentrations are <1 are

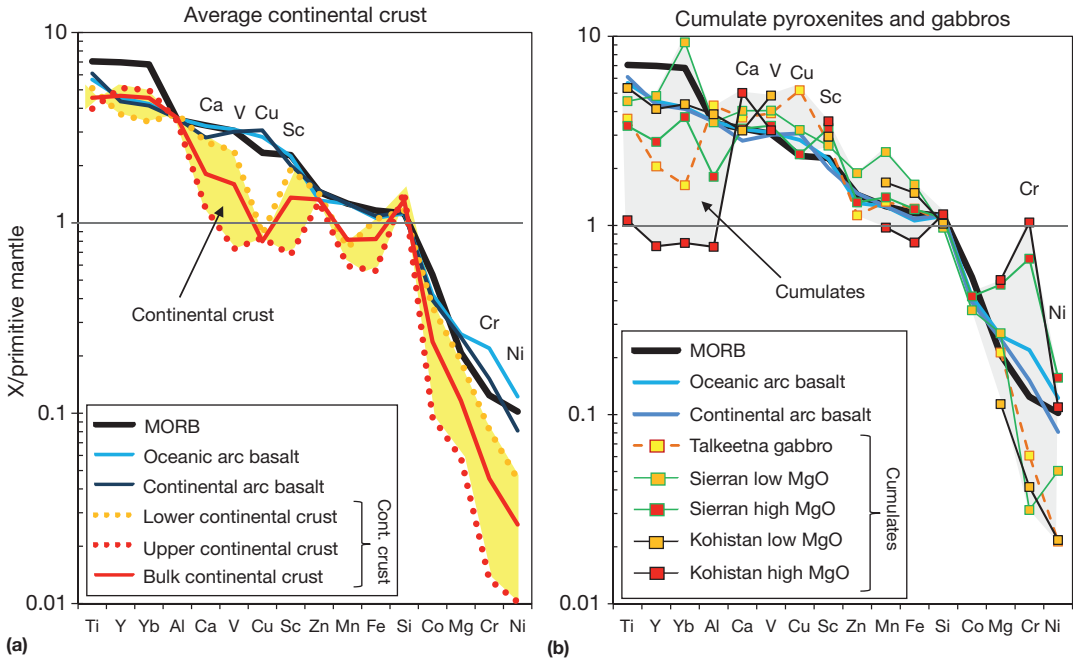

Figure 20 Comparison of pyroxenitic lower crust to average composition of continental crust, mantle and various basalts (primary island arc basalts and MORB). (a) Primitive-mantle (PM) normalized (McDonough and Sun, 1995) compositions for average MORB (Arevalo and McDonough, 2010), primitive arc basalts (Kelemen et al., 2003), and global upper, lower, and bulk continental crusts (Rudnick and Fountain, 1995). (b) Average compositions of high- and low-MgO cumulates from the Sierra Nevada (CA), Kohistan, and Talkeetna paleo-arc systems. Data are from the literature (Dhuime et al., 2007, 2009; Greene et al., 2006; Jagoutz et al., 2009; Kelemen et al., 2003; Lee et al., 2006, 2007). Roughly, elements with PM-normalized abundances <1 are compatible and >1 are incompatible with respect to the solid mantle source during peridotite melting. Elements are plotted so that the MORB abundance pattern decreases smoothly toward the right, corresponding to increasing compatibility toward the right.

compatible and those >1 are incompatible during MORB genesis (mantle melting); thus elements plotting to the right are more compatible than those on the left. Primary island and continental arc basalts show the same overall pattern as MORBs, albeit with slight enrichments in the most incompatible elements, consistent with an origin by partial melting of peridotitic mantle.

By contrast, global continental crust compositions plotted in this ordering do not show smooth, normalized elemental abundance patterns. Al, Y, V, Sc, Cu, Mn, Fe, Co, Cr, and Ni are substantially lower than MORB for both lower and upper continental crust models. Because Al, Y, V, Sc, Cu, Mn, and Fe are moderately incompatible during mantle melting, formation of continental crust requires at least one additional step of differentiation wherein these elements become compatible and fractionate from the system. This in turn implies that there is a complementary cumulate component that is enriched in these same elements relative to the parental arc basalt. High-MgO and low-MgO pyroxenite/gabbro cumulates show the necessary complementary enrichments in these elements, particularly when normalized to a primary arc basalt (**Figure 21**). Importantly, Al, Y, V, Sc, and Cr are compatible in one or more of the mineral phases making up these mafic cumulates (pyroxene, garnet, and amphibole), which explains their depletions in the residual crust (**Figures 20** and **21**). Crustal Mn and Fe depletions can be explained by a combination of garnet and Fe oxide fractionation, whereas Co and Ni depletions can be attributed to pyroxene fractionation or shallow-level olivine fractionation. Cu is incompatible in all silicate minerals and Fe oxides, but highly compatible in sulfides. The coupled depletions in Cu and Sc hint at an intimate connection between pyroxenite fractionation and sulfide segregation (Lee et al., 2012).

4.12.5.3 Estimating the Proportion of Mafic Cumulates Generated during Arc Magmatic Differentiation

One can use mass-balance considerations to estimate the proportions of cumulates and residual crust relative to the parental basalt. This is done by first assuming that a primitive continental arc basalt (Kelemen et al., 2003) differentiates into residual crust and high- and low-MgO pyroxenite cumulates (**Table 1**). The mass-balance equations for all the major and minor element oxides (except for P_2O_5) are then simultaneously inverted. For the Sierra Nevada/Peninsular Ranges batholith, the average composition of the eastern Peninsular Ranges plutons for the residual crust and the average compositions of high-MgO and low-MgO pyroxenites from the Sierra Nevada were used (Lee et al., 2007). The eastern Peninsular Ranges data derive from an equally spaced sampling grid over the batholith, and hence the average composition is an unbiased areal representation of the plutonic part of the batholith. Unbiased estimates of the crust in Talkeetna and Kohistan are not available. Nevertheless, for Talkeetna, the average composition of felsic plutons and high-MgO pyroxenites reported in Kelemen et al. (2003) and the average basal gabbro composition from Greene et al. (2006) for the low-MgO cumulate end member are used (Hacker et al., 2008). For comparison, inversion results using global continental crust for the residual crustal end member are also shown (Rudnick and Fountain, 1995).

The results are shown in **Figure 22** and **Table 2**. For the Sierra Nevada/Peninsular Ranges batholith, the parental basalt differentiates into 16% high-MgO pyroxenites, 50% low-MgO pyroxenites, and 33% residual crust. For Talkeetna, the parental basalt differentiates into 15% high-MgO pyroxenites, 61% gabbros, and 23% residual crust. The greater proportion of cumulates calculated for Talkeetna is due to the higher Si and

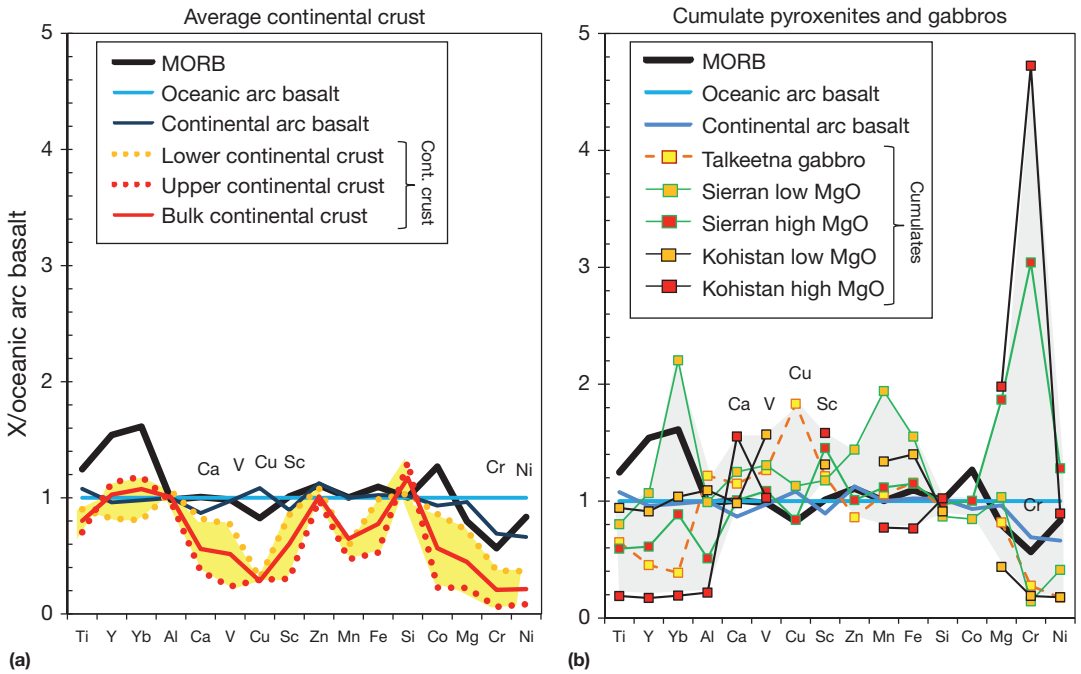

Figure 21 Same as in **Figure 20**, but data are normalized to primitive arc basalt. This figure shows that the cumulate pyroxenites and gabbros in arcs are complementary to the average composition of the continental crust.

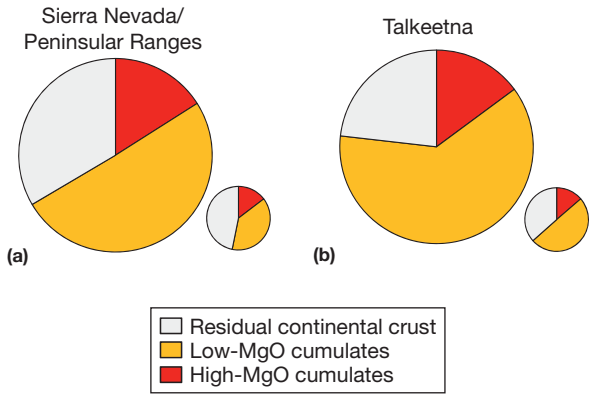

Figure 22 Proportions of high-MgO cumulates, low-MgO cumulates, and residual crust formed by differentiation of primitive arc basalt (**Table 1**). Proportions are calculated by inverting all major and minor element oxides using the compositions shown in **Table 1**. Large circles are calculated using average plutonic rocks for the residual crust (see **Tables 1** and **2**). Small circles show proportions calculated using a global model of bulk continental crust. Reproduced from Rudnick RL and Gao S (2003) Composition of the continental crust. In: Rudnick RL (ed.) *Treatise on Geochemistry*, vol.3, pp. 1–64. Oxford: Elsevier.

Table 2 Results of mass-balance inversions with respect to primary arc basalt

	Sierra Nevada/PRB	*Sierra Nevada/ PRB – BCC*	*Talkeetna*	*Talkeetna – BCC*
Mass balance				
High-MgO pyroxenite	0.17	0.15	0.16	0.15
Low-MgO pyroxenite/ cumulate	0.50	0.38	0.61	0.49
Felsic crust	0.33	0.47	0.24	0.36
Total	1.00	1.00	1.00	1.00
Residuals (wt%)				
SiO_2	0.31	0.29	0.09	0.09
TiO_2	−0.31	−0.28	−0.50	−0.42
Al_2O_3	−1.31	−1.17	−0.15	−0.08
FeO_T	0.76	0.87	−0.61	−0.34
MnO	0.06	0.04	−0.01	−0.02
MgO	−0.93	−0.83	−0.15	−0.12
CaO	0.51	0.23	0.54	0.21
Na_2O	−0.88	−0.65	−0.67	−0.68
K_2O	0.08	0.11	−0.64	−0.14
Sum of squares	2.1	1.9	1.4	0.92

Calculations (given in fractional mass proportions) in the first two columns assume Sierran high-MgO and low-MgO pyroxenites as cumulate end members, but the first column (Sierra Nevada/PRB) assumes average Sierran granitoid as felsic crust end member and the second column (Sierra Nevada/PRB – BCC) assumes global bulk continental crust (BCC) as felsic end member. Calculations in the last two columns use Talkeetna high- and low-MgO cumulates as end members. Left column (Talkeetna) assumes Talkeetna plutons as felsic end member and right column (Talkeetna-BCC) assumes BCC as felsic crustal end member. Residuals for each oxide are given in wt%. Sum of squared residuals ($wt\%^2$) are also shown.

lower Mg of the gabbros compared to the low-MgO pyroxenites in the Sierras, and this may in part be related to differences in average pressures of fractionation (higher in continental arcs, which would favor garnet and lower Si cumulates). In any case, these inversions must be evaluated with caution because uncertainties associated with average cumulate and residual crust compositions are large and unquantifiable because of sampling bias. In addition, erosional removal of much of the volcanic part of the crust is not considered in these calculations. The only robust conclusion that can be made here is that the total proportion of cumulates is likely to be >50%. We can also conclude that low-MgO cumulates dominate, as high-MgO cumulates make up 20–30% of all cumulates. Given that the seismically fast high- and low-MgO cumulates cannot reside above the seismic Moho, considerable differentiation must occur well before arc magmas reach the traditionally defined crust (Moho). Most of these cumulates must be recycled back into the mantle in order to explain the lack of seismic evidence for mafic rocks beneath the continental Moho (Niu and James, 2002) and the low proportions of pyroxenites or cumulate peridotites relative to residual peridotites in many, but not all, continental xenolith suites (cf. Wilshire et al., 1988). The above estimates (>50%) of the amount of mafic cumulates formed and ultimately removed is consistent with similar approaches based on major element mass balance, though the two types of pyroxenites were not considered (Ducea, 2002). In an independent approach based on mass balance using Th and La, Plank (2005) showed that 25–60% of the juvenile crust is differentiated into cumulates/restites that eventually founder. Thus, regardless of the uncertainties in these calculations, a considerable proportion of arc basalts differentiates into mafic cumulates and restites to form the continental crust.

4.12.5.4 Volume Flows

The global recycling rate of mafic lower crust in arcs can be estimated by multiplying the global production rate of primitive arc basalt by the above-estimated cumulate fraction. Taking an arc magmatic production rate per unit arc length of 50–150 $km^3\ km^{-1}\ Ma^{-1}$ (Jicha et al., 2006) and global subduction zone length of 51 310 km (Bird, 2003) yields a global arc magma production rate of 2.6–7.7 $km^3\ year^{-1}$, which translates into 1.5–4.6 $km^3\ year^{-1}$ of mafic lower crustal formation if a cumulate fraction of 60% is assumed (note that density corrections have not been applied). These volume flows can be placed into better context by comparing them with other volume flows (**Table 3** and **Figure 23**). Oceanic crust production rate is ~23 $km^3\ year^{-1}$ assuming a crustal thickness of 7 km and a global areal production rate of oceanic crust of 0.0953 $m^2\ s^{-1}$ (Bird, 2003). Volume flow rates can be expressed relative to the global oceanic crust production rate. Flow rates are shown in **Table 3** for published estimates of global sediment subduction (Clift et al., 2009; Plank and Langmuir, 1998), and subduction erosion (Von Huene and Scholl, 1991) as well as lower crustal foundering associated with continent–continent collision (Clift et al., 2009). Detailed analyses of these mass flows are beyond the scope of this review, but discussions can be found in Plank and Langmuir (1998). In **Figure 23**, these published flow rates are shown

Table 3 Mass flows

	References	*km^3 year^{-1}*	*Oceanic crust normalized*
Production			
Oceanic crust (7 km thickness)	Bird (2003)	22.9	1
Arc magma	Jicha et al. (2006)	2.6–7.7	0.11–0.33
Recycling			
Sediment subduction	Plank and Langmuir (1998)	0.5–0.07	0.02–0.03
Sediment subduction	Clift et al. (2009)	1.65	0.07
Subduction erosion	Von Huene and Scholl (1991)	1.3–1.8	0.06–0.07
Orogenic 'delamination'	Clift et al. (2009)	1.5	0.07
Arc cumulate 'delamination' (Xcum = 0.6)	This study	1.5–4.6	0.07–0.2

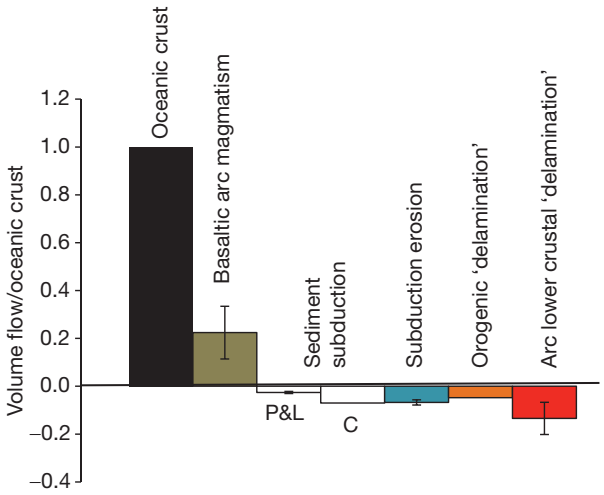

Figure 23 Mass flows normalized to oceanic crust production rate of 23 km^3 year^{-1} based on parameters taken from Bird (2003) and assuming a 7-km-thick crust (oceanic crust = 1). Positive corresponds to production and negative corresponds to recycling. Arc magma production rate is taken from Jicha et al. (2006) and multiplying by the global length of subduction zones (Bird, 2003). This number was multiplied by 0.6 to obtain the arc cumulate mass flow. Sediment recycling rates are taken from Plank and Langmuir (1998) and Clift et al. (2009), the former denoted by 'P&L' and the latter denoted by 'C.' Subduction erosion rate is taken from Von Huene and Scholl (1991). Lower crustal recycling rate during collisional orogeny taken from Clift et al. (2009). 'Error' bars represent minimum and maximum bounds of estimated flows.

normalized to oceanic crust production: magmatic arc production is ~+0.2, sediment recycling is −0.02 to 0.07, subduction erosion is −0.07, orogenic lower crustal foundering is −0.07, and recycling of mafic lower crust beneath arcs (this study) is, on average, −0.13 times that of oceanic crust production (where negative values denote recycling). Although all of these flow rates have large uncertainties, two conclusions can be drawn. First, removal of mafic lower crust in arcs exceeds all other recycling rates, including that estimated for lower crustal recycling during collisional orogenies. Second, the total flow rate of recycling mafic lower crust is comparable to that of arc magma production. Because these flow rates are constrained from <100-Ma geologic processes, extrapolating back in time may be perilous.

4.12.6 Fate of Recycled Mafic Lower Crust

At 20% of the global oceanic crust subduction rate, recycling of mafic lower crust in arc settings will have an important effect on the generation of major-element heterogeneities in the mantle. In terms of trace elements, they are likely to be important for the compatible to moderately incompatible elements only. Because of the strong density jump associated with the γ-olivine to perovskite phase transition at 660 km depth, garnet-pyroxenites without stishovite (some low-MgO cumulates) might be expected to become density-neutral at the bottom of the transition zone (440–660 km) and never sink into the lower mantle. Indeed, a mechanical mixture of garnet-pyroxenite and peridotite seems necessary to explain the anomalously high gradient of seismic velocities with depth in the transition zone (Cammarano and Romanowicz, 2007; Xu et al., 2008). If, however, the pyroxenites contain stishovite, as would be the case for MORB-type eclogites and possibly high-MgO pyroxenites, they may be able to penetrate into the lower mantle, remaining isolated from the upper mantle for long periods. Penetration into the lower mantle can also occur if pyroxenite bodies are dragged down by cold downwellings. These processes could lead to an irreversible chemical stratification of the mantle (Anderson, 2002) and, depending on their compositions, could generate positive or negative seismic velocity anomalies with respect to the peridotitic mantle (Anderson, 2005, 2007). Pyroxenites, however, can rise back to the surface of the Earth by entrainment into thermal upwellings. In addition, it has been suggested that, once these pyroxenites heat up to ambient surroundings, they will undergo significant partial melting because their solidi are lower than that of peridotitic mantle (Pertermann and Hirschmann, 2003a,b). If much of this liquid was retained (as might be expected initially from low-F melts of pyroxenites, which are felsic), a positive compositional buoyancy would be imposed, accelerating the ascent of the pyroxenite blob (Anderson, 2007). In any case, as long as pyroxenite bodies remain in or are returned to the uppermost mantle, their lower solidi render them potential candidates for low-temperature fertile melting anomalies. Because of the thicker lithospheric lid through which intraplate magmas must traverse, the proportional contribution of pyroxenite- to peridotite-derived melts could be far more significant for intraplate magmas than in mid-ocean ridge environments because pyroxenites initiate melting at a greater depth than peridotite during adiabatic decompression (Dasgupta et al., 2010;

Herzberg, 2006; Ito and Mahoney, 2005b; Sobolev et al., 2005, 2007). Are the pyroxenite signatures in many intraplate magmas derived from subducted oceanic crust or from foundered LCC formed in arcs?

A way forward in testing whether recycled arc cumulates are represented in the source regions of intraplate magmatic centers comes from recognizing that such cumulates differ fundamentally from recycled oceanic (MORB) crust. Arc cumulates have higher FeO_T than MORBs, and at least some have higher MgO and Mg#. Some arc cumulates, particularly the low-MgO types, are silica-undersaturated and may give rise to alkali basalts. In terms of trace elements, arc cumulates are probably depleted in the highly incompatible elements, whereas subducted oceanic crust may be enriched in some of these elements as a result of hydrothermal alteration during residence on the seafloor (see Alt and Teagle, 1999; Alt et al., 1986; **Chapter 4.16**). Subducted oceanic crust is likely to have been hydrothermally enriched in CO_2 (in the form of carbonates), H_2O, Li, Rb, Sr, Pb, and U. Perhaps the most diagnostic indicators of arc cumulates in the mantle source region will come from the first-series transition metals, such as V, Sc, Cr, and Co, because they are enriched in cumulate pyroxenites relative to pyroxenites of MORB-protolith.

Additional compositional effects are as follows: Trace-element ratios, such as Nb/U, Nb/La, Nb/Th, and Ce/Pb, are often used as indicators of continental crust contamination in magmas or in their mantle source regions (Hofmann, 1997, 2003; Hofmann et al., 1986). This is because the continental crust is depleted in high-field-strength elements such as Nb relative to U, La, Th, and Pb. The Nb-depleted character of continental crust is generally attributed to the retention in Nb-bearing phases, such as rutile or amphibole, or to the fact that it is not very soluble in the aqueous fluids that occur in subduction zones (Barth et al., 2000; Hofmann, 1988; Hofmann et al., 1986; Kelemen et al., 1993; Klemme et al., 2005; Rudnick et al., 2000). U, La, Ce, and Th are generally considered highly incompatible and less affected by retention in accessory minerals (though monazite could complicate this). Pb is considered to be highly mobile in fluids (Hofmann et al., 1986). Thus, continental crust is generally agreed to be characterized by low Nb/(U,La,Th) and low Ce/Pb compared to MORBs. Cumulate garnet-pyroxenites, however, are not depleted in Nb because many of these pyroxenites have primary rutile and have been shown to have excess Nb contents relative to La, Th, and U (Lee et al., 2006, 2007). Thus, recycling of such pyroxenites is unlikely to be detected by these conventional tracers of continent recycling. As for Ce/Pb, the presence of Cu suggests the presence of sulfide, which, in turn, suggests the presence of Pb. The exact amount of Pb depends on the amount of sulfide, so variable Ce/Pb ratios might be expected.

The compositional effects on the time-integrated isotopic evolution of $^{87}Sr/^{86}Sr$, $^{143}Nd/^{144}Nd$, $^{176}Hf/^{177}Hf$, $^{207}Pb/^{204}Pb$, $^{206}Pb/^{204}Pb$, $^{208}Pb/^{204}Pb$, and $^{187}Os/^{188}Os$ will depend on the nature of parent/daughter elemental fractionation during the genesis of arc cumulates. Detailed discussion of these isotope systems is not of immediate relevance for this review, but some broad predictions can be made. Because garnet is a primary magmatic phase in many of the low-MgO pyroxenites, the cumulates would be expected to have high Lu/Hf ratios for a given Sm/Nd ratio, leading to decoupling of Hf and Nd isotopes from the typical mantle array (Blichert-Toft et al., 1999). Sm/Nd ratios might be expected to be near-chondritic or slightly higher than chondrite depending on the amount of garnet, thus $^{143}Nd/^{144}Nd$ would appear depleted (e.g., radiogenic) or near-chondritic. Rb/Sr ratios are generally low in pyroxenes and garnets, so time-integrated $^{87}Sr/^{86}Sr$ would be expected to be nonradiogenic, though metasomatic effects could complicate Sr isotope systematics. High garnet mode might also be expected to give rise to high Re/Os ratios (Righter and Hauri, 1998) and radiogenic $^{187}Os/^{188}Os$, but as noted above, many of the cumulates are enriched in Cu, which suggests sulfide involvement. In such samples, the predicted effects on Os isotopes could be more complicated. Any samples that contain sulfide, however, will be characterized by low U/Pb ratios (because Pb is compatible in sulfides but incompatible in garnet and pyroxenes), resulting in very low time-integrated Pb isotopic compositions. This may provide a simple explanation for why model estimates of the Pb isotopic composition of the Earth's mantle seem more radiogenic than the model estimates of the bulk Earth (Allegre et al., 1995).

4.12.7 Some Useful Petrologic Approaches in Studying Lower Crustal Recycling

One of the great opportunities of the last decade is the ability to study deep lithospheric processes from geological, geochronological, petrological, geochemical, and geophysical perspectives simultaneously. One of the key constraints in testing whether lower crustal foundering has occurred or is occurring is the spatial and temporal evolution of the LAB. Detailed discussions of what the LAB is and how it can be imaged/inferred by different methods can be found elsewhere (Eaton et al., 2009; Fischer et al., 2010). For the purposes of this review, the LAB represents a rheological transition that limits asthenospheric upwelling and decompression melting. Thermobarometric constraints on mantle and lower crustal xenoliths can be used to track the thermal evolution of the deep lithosphere (Brey and Kohler, 1990). The major element compositions of primitive basalts can be used to estimate last equilibration temperatures (MgO or FeO) and pressures (SiO_2) in the mantle (Lee et al., 2009; Putirka, 2005; Wang et al., 2002). Additionally, first-series transition metals may be able to constrain the major element composition of the source (Humayun et al., 2004; Le Roux et al., 2010; Sobolev et al., 2005, 2007), which may be useful in understanding how different parts of the mantle contribute to melting during or after the foundering process.

As an example, these tools are applied to the alkali and ultrapotassic basalts thought to be associated with lower crustal foundering beneath the Sierra Nevada. Le Roux et al. (2010) showed that Zn/Fe is not fractionated during partial melting of peridotite because Zn/Fe distribution coefficients between olivine, orthopyroxene, and basaltic liquid are 1, and Zn and Fe partitioning between melt and peridotite is largely controlled by these two phases. Melting of garnet- or clinopyroxene-rich rocks, however, yields liquids with high Zn/Fe relative to the source as a result of the low Zn/Fe distribution coefficients between clinopyroxene and garnet relative to olivine, orthopyroxene, and melt. Primitive Sierran

basalts <1 Ma have Zn/Fe identical to that of primitive mantle and evolve along an olivine-controlled fractionation trend (constant Zn/Fe with decreasing MgO). By contrast, older basalts (>3 Ma) have higher Zn/Fe for a given MgO content and also show clinopyroxene-controlled fractionation (Figure 15(b)). These observations indicate that the <1 Ma basalts are melts of peridotite, whereas the older magmas require pyroxenite in the source. One interpretation of these results is that complete removal of the pyroxenite root was not achieved until after 3 Ma even though foundering may have started earlier. Zn/Fe and other first-series transition metal systematics can also be used to guide the application of magma thermobarometry. SiO_2-based basalt barometers rely on the silica-buffering capacity of coexisting olivine and orthopyroxene assemblages, and therefore require a peridotite source for proper application. In addition, estimating the primary magma compositions for thermobarometric analysis requires back-correction for fractionation, and thus knowledge of the source composition is needed so that one knows when to terminate the fractionation corrections. Because the >3-Ma basalts derive from a pyroxenite-bearing source, estimating the exact source composition is difficult, so the SiO_2 barometer cannot be reliably applied. However, the <1-Ma basalts satisfy the conditions for melting of typical peridotitic mantle. Thermobarometric analyses applied to these basalts show that melting initiates at depths of ~75 km, corresponding to a mantle potential temperature of ~1350 °C, and equilibrate to depths of 50 km, overlapping the depth range from which the Cretaceous garnet-pyroxenites resided (Figure 14). These observations are consistent with recent removal of most of the pyroxenite root beneath the Sierras.

4.12.8 Summary and Outlook

In this review, the physics of lower crustal recycling has been summarized and the geologic phenomena predicted in the aftermath of foundering discussed, namely topographic uplift, increased surface heat flux, and small-volume/low-melting-degree basaltic magmatism, followed by a decrease in both topography and heat flux. Care must be taken not to confuse these phenomena with those predicted from active lithospheric extension. Several case studies where lithospheric foundering has been proposed are reviewed, but only in a few places is there direct evidence for lower crustal removal. In most cases, removal of mafic lower crust is hypothesized from mass-balance constraints centered about the felsic nature of the continental crust. Exactly when mafic lower crust is generated and subsequently removed is an open question. One possibility is that mafic lower crust forms from preexisting continental crust by deep crustal anatexis during continent–continent collisions and foundering follows immediately thereafter. Another possibility is that the mafic lower crust is an integral product of magmatic differentiation in arc settings, and is thus formed when juvenile crust itself is formed. In this scenario, foundering occurs during or shortly after the lifespan of the arc. The overall felsic nature of continents today, as constrained by seismic studies, suggests that most of the formation and foundering of mafic lower crust occurs well before continent–continent collisions have a chance to operate. Furthermore, mass-balance constraints based on specific arc sections and extrapolated to arcs globally show that the global mafic crustal recycling in arcs is greater than that inferred for collisional orogens. The estimated lower crust recycling rate of arcs is ~0.2 times that of the oceanic crust production rate, and, therefore, cannot be ignored when discussing the differentiation of the silicate Earth.

Acknowledgments

I thank Peter Luffi and Emily Chin for the discussions and Luffi, in particular, for proofreading. I also thank Stephan Sobolev, Mark Behn, and Roberta Rudnick for their detailed reviews and Gene Humphreys, Peter Molnar, Robert Kay, Sue Kay, Don Anderson, John Platt, and Alan Levander for their discussions on various aspects of this paper at different points in time, but all errors and biases are entirely, and unfortunately, mine. This work was supported by the NSF and the Packard Foundation.

References

Albarède F (1998) The growth of continental crust. *Tectonophysics* 296: 1–14.
Albarède F and Michard A (1986) Transfer of continental Mg, S, O and U to the mantle through hydrothermal alteration of the oceanic-crust. *Chemical Geology* 57: 1–15.
Allegre CJ, Manhes G, and Göpel C (1995) The age of the Earth. *Geochimica et Cosmochimica Acta* 59: 1445–1456.
Alonso-Perez R, Müntener O, and Ulmer P (2009) Igneous garnet and amphibole fractionation in the roots of island arcs: Experimental constraints on andesitic liquids. *Contributions to Mineralogy and Petrology* 157: 541–558.
Alt JC, Honnorez J, Laverne C, and Emmermann R (1986) Hydrothermal alteration of a 1 km section through the upper oceanic crust, Deep Sea Drilling Project Hole 504B: Mineralogy, chemistry, and evolution of seawater–basalt interactions. *Journal of Geophysical Research* 91: 10309–10335.
Alt J and Teagle DAH (1999) The uptake of carbon during alteration of ocean crust. *Geochimica et Cosmochimica Acta* 63: 1527–1535.
Anderson DL (2002) The case for irreversible chemical stratification of the mantle. *International Geology Review* 44: 97–116.
Anderson DL (2005) Large igneous provinces, delamination, and fertile mantle. *Elements* 1: 271–275.
Anderson DL (2007) The eclogite engine: Chemical geodynamics as a Galileo thermometer. In: Foulger GR and Jurdy DM (eds.) *Plates, Plumes, and Planetary Processes, Geological Society of America Special Papers 430*, pp. 47–64. Boulder, CO: The Geological Society of America.
Annen C, Blundy JD, and Sparks RSJ (2006) The genesis of intermediate and silicic magmas in deep crustal hot zones. *Journal of Petrology* 47: 505–539.
Arevalo R and McDonough WF (2010) Chemical variations and regional diversity observed in MORB. *Chemical Geology* 271: 70–85.
Armstrong RL (1991) The persistent myth of crustal growth. *Australian Journal of Earth Sciences* 38: 613–630.
Arndt NT and Goldstein SL (1989) An open boundary between lower continental crust and mantle: Its role in crustal formation and recycling. *Tectonophysics* 161: 201–212.
Barth MG, McDonough WF, and Rudnick RL (2000) Tracking the budget of Nb and Ta in the continental crust. *Chemical Geology* 165: 197–213.
Barth MG, Rudnick RL, Horn I, et al. (2001) Geochemistry of xenolithic eclogites from West Africa, Part I: A link between low MgO eclogites and Archean crust formation. *Geochimica et Cosmochimica Acta* 65: 1499–1527.
Barth MG, Rudnick RL, Horn I, et al. (2002) Geochemistry of xenolithic eclogites from West Africa, Part 2: Origins of the high MgO eclogites. *Geochimica et Cosmochimica Acta* 66: 4325–4345.
Beard BL, Fraracci KN, Taylor LA, et al. (1996) Petrography and geochemistry of eclogites from the Mir kimberlite, Yakutia, Russia. *Contributions to Mineralogy and Petrology* 125: 293–310.
Beard BL and Glazner AF (1995) Trace element and Sr and Nd isotopic composition of mantle xenoliths from the Big Pine volcanic field, California. *Journal of Geophysical Research* 100: 4169–4179.

Beck SL and Zandt G (2002) The nature of orogenic crust in the central Andes. *Journal of Geophysical Research* 107(B10): 2230.

Behn MD, Hirth G, and Kelemen PB (2007) Trench-parallel anisotropy produced by foundering of arc lower crust. *Science* 317: 108–111. http://dx.doi.org/10.1126/science/1141269.

Behn MD and Kelemen PB (2003) Relationship between seismic P-wave velocity and the composition of anhydrous igneous and meta-igneous rocks. *Geochemistry, Geophysics, Geosystems* 4: 1041.

Behn MD and Kelemen PB (2006) Stability of arc lower crust: Insights from the Talkeetna arc section, south central Alaska, and the seismic structure of modern arcs. *Journal of Geophysical Research* 111: B11207.

Bennett VC, Nutman AP, and McCulloch MT (1993) Nd isotopic evidence for transient highly-depleted mantle reservoirs in the early history of the Earth. *Earth and Planetary Science Letters* 119: 299–317.

Bird P (1979) Continental delamination and the Colorado Plateau. *Journal of Geophysical Research* 84: 7561–7571.

Bird P (1988) Formation of the Rocky Mountains, western United States: A continuum computer model. *Science* 239: 1501–1507.

Bird P (2003) An updated digital model of plate boundaries. *Geochemistry, Geophysics, Geosystems* 4: 1027.

Black R and Liegeois J-P (1993) Cratons, mobile belts, alkaline rocks and continental lithospheric mantle: The Pan-African testimony. *Journal of the Geological Society* 150: 89–98.

Blichert-Toft J, Albarède F, and Kornprobst J (1999) Lu–Hf isotope systematics of garnet pyroxenites from Beni Bousera, Morocco: Implications for basalt origin. *Science* 283: 1303–1306.

Bowring SA and Housh T (1995) The Earth's early evolution. *Science* 269: 1535–1540.

Boyd OS, Jones CH, and Sheehan AF (2004) Foundering lithosphere imaged beneath the southern Sierra Nevada, California, USA. *Science* 305: 660–662.

Brey GP and Kohler T (1990) Geothermobarometry in four-phase lherzolites II. New thermobarometers, and practical assessment of existing thermobarometers. *Journal of Petrology* 31: 1353–1378.

Calvert A, Sandvol E, Seber D, et al. (2000) Geodynamic evolution of the lithosphere and upper mantle beneath the Alboran region of the western Mediterranean: Constraints from travel time tomography. *Journal of Geophysical Research* 105: 10871–10898.

Cammarano F and Romanowicz B (2007) Insights into the nature of the transition zone from physically constrained inversion of long-period seismic data. *Proceedings of the National Academy of Sciences of the United States of America* 104: 9139–9144.

Carlier G, Lorand JP, Liegeois JP, et al. (2005) Potassic–ultrapotassic mafic rocks delinate two lithospheric mantle blocks beneath the southern Peruvian Altiplano. *Geology* 33: 601–604.

Carmichael ISE, Nicholls J, and Smith AL (1970) Silica activity in igneous rocks. *American Mineralogist* 55: 246–263.

Chen L, Tao W, Zhao L, and Zheng T (2008) Distinct lateral variation of lithospheric thickness in the northeastern North China craton. *Earth and Planetary Science Letters* 267: 56–68.

Chen W-P and Tseng T-L (2007) Small 660-km seismic discontinuity beneath Tibet implies resting ground for detached lithosphere. *Journal of Geophysical Research* 112: B05309.

Chin EJ, Lee C-TA, Luffi P, and Tice M (2012) Deep lithospheric thickening and refertilization beneath continental arcs: Case study of the P, T and compositional evolution of peridotite xenoliths from the Sierra Nevada, California. *Journal of Petrology* 53: 477–511.

Chu Z-Y, Wu F-Y, Walker RJ, et al. (2009) Temporal evolution of the lithospheric mantle beneath the Eastern North China Craton. *Journal of Petrology* 50: 1857–1898.

Clift PD, Vannucchi P, and Phipps Morgan J (2009) Crustal redistribution, crust–mantle recycling and Phanerozoic evolution of the continental crust. *Earth-Science Reviews* 97: 80–104.

Cloos M, Sapiie B, Van Ufford AQ, Weiland RJ, Warren PQ, and McMahon TP (2005) *Collisional Delamination in New Guinea: The Geotectonics of Subducting Slab Breakoff Geological Society of America Special Papers 400*. Boulder, CO: Geological Society of America.

Coleman DR, Frost TP, and Glazner AF (1992) Evidence from the Lamarck Granodiorite for rapid Late Cretaceous crust formation in California. *Science* 258: 1924–1926.

Coleman DR and Glazner AF (1997) The Sierra crest magmatic event: Rapid formation of juvenile crust during the Late Cretaceous in California. *International Geology Review* 39: 768–787.

Coleman RG, Lee DE, Beatty LB, and Brannock WW (1965) Eclogites and ecogites: Their differences and similarities. *Geological Society of America Bulletin* 76: 483–508.

Conrad CP and Molnar P (1997) The growth of Rayleigh–Taylor-type instabilities in the lithosphere for various rheological and density structures. *Geophysical Journal International* 129: 95–112.

Cunningham WD (2001) Cenozoic normal faulting and regional doming in the southern Hangay region, Central Mongolia: Implications for the origin of the Baikal rift province. *Tectonophysics* 331: 389–411.

Dasgupta R and Hirschmann MM (2006) Melting in the Earth's deep upper mantle caused by carbon dioxide. *Nature* 440: 659–662.

Dasgupta R, Jackson MG, and Lee C-TA (2010) Major element chemistry of ocean island basalts – Conditions of mantle melting and heterogeneity of mantle source. *Earth and Planetary Science Letters* 289: 377–392.

Davies GF (1999) *Dynamic Earth, Plates, Plumes and Mantle Convection*. Cambridge, UK: Cambridge University Press.

De Capitani C and Petrakakis K (2010) The computation of equilibrium assemblage diagrams with Theriak/Domino software. *American Mineralogist* 95: 1006–1016.

DeBari SM and Sleep NH (1991) High-Mg, low-Al bulk composition of the Talkeetna island arc, Alaska: Implications for primary magmas and the nature of arc crust. *Geological Society of America Bulletin* 103: 37–47.

DeCelles PG, Ducea MN, Kapp P, and Zandt G (2009) Cyclicity in Cordilleran orogenic systems. *Nature Geoscience* 2: 251–257.

DePaolo DJ and Daley EE (2000) Neodymium isotopes in basalts of the southwest Basin and Range and lithospheric thinning during continental extension. *Chemical Geology* 169: 157–185.

Dhuime B, Bosch D, Bodinier J-L, et al. (2007) Multistage evolution of the Jijal ultramafic-mafic complex (Kohistan, N Pakistan): Implications for building the roots of island arcs. *Earth and Planetary Science Letters* 261(1–2): 179–200.

Dhuime B, Bosch D, Garrido CJ, et al. (2009) Geochemical architecture of the lower- to middle-crustal section of a paleo-island arc (Kohistan complex, Jijal Kamila area, northern Pakistan): Implications for the evolution of an oceanic subduction zone. *Journal of Petrology* 50: 531–569.

Dodge FCW, Lockwood JP, and Calk LC (1988) Fragments of the mantle and crust beneath the Sierra Nevada batholith: Xenoliths in a volcanic pipe near Big Creek, California. *Geological Society of America Bulletin* 100: 938–947.

Ducea M (2001) The California arc: Thick granitic batholiths, eclogitic residues, lithosphere-scale thrusting, and magmatic flare-ups. *Geological Society of America Today* 11: 4–10.

Ducea MN (2002) Constraints on the bulk composition and root foundering rates of continental arcs: A California arc perspective. *Journal of Geophysical Research* 107(B11): 2304. http://dx.doi.org/10.1029/2001JB000643.

Ducea MN and Saleeby JB (1996) Buoyancy sources for a large, unrooted mountain range, the Sierra Nevada, California: Evidence from xenolith thermobarometry. *Journal of Geophysical Research* 101: 8229–8244.

Ducea M and Saleeby J (1998a) Crustal recycling beneath continental arcs: Silica-rich glass inclusions in ultramafic xenoliths from the Sierra Nevada, California. *Earth and Planetary Science Letters* 156: 101–116.

Ducea MN and Saleeby JB (1998b) The age and origin of a thick mafic-ultramafic keel from beneath the Sierra Nevada batholith. *Contributions to Mineralogy and Petrology* 133: 169–185.

Duggen S, Hoernle K, Van den Bogaard P, and Garbe-Schönberg D (2005) Post-collisional transition from subduction- to intraplate-type magmatism in the westernmost Mediterranean: Evidence for continental-edge delamination of subcontinental lithosphere. *Journal of Petrology* 46: 1155–1201.

Duggen S, Hoernle K, Van den Bogaard P, and Harris C (2004) Magmatic evolution of the Alboran region: The role of subduction in forming the western Mediterranean and causing the Messinian salinity crisis. *Earth and Planetary Science Letters* 218: 91–108.

Duggen S, Hoernle K, Van den Bogaard P, Rupke LH, and Phipps Morgan J (2003) Deep roots of the Messinian salinity crisis. *Nature* 422: 602–606.

Eaton DW, Darbyshire F, Evans RL, Grutter H, Jones AG, and Yuan X (2009) The elusive lithosphere–asthenosphere boundary (LAB) beneath cratons. *Lithos* 109: 1–22.

Elkins-Tanton LT (2007) Continental magmatism, volatile recycling, and a heterogeneous mantle caused by lithospheric gravitational instabilities. *Journal of Geophysical Research* 112: B03405. http://dx.doi.org/10.1029/2005JB004072.

Elkins-Tanton LT, Smrekar SE, Hess PC, and Parmentier EM (2007) Volcanism and volatile recycling on a one-plate planet: Applications to Venus. *Journal of Geophysical Research* 112: E04S06.

English JM, Johnston ST, and Wang K (2003) Thermal modelling of the Laramide orogeny: Testing the flat-slab subduction hypothesis. *Earth and Planetary Science Letters* 214: 619–632.

Esperança S, Carlson RW, Shirey S, and Smith D (1997) Dating crust–mantle separation: Re–Os isotopic study of mafic xenoliths from central Arizona. *Geology* 25: 651–654.

Fan QC and Hooper PR (1989) The mineral chemistry of ultramafic xenoliths of eastern China: Implications for upper mantle composition and the palaeogeotherms. *Journal of Petrology* 30: 1117–1158.
Fan W, Zhang HF, Baker J, Jarvis KE, Mason PRD, and Menzies MA (2000) On and off the North China Craton: Where is the Archean keel? *Journal of Petrology* 41: 933–950.
Farmer GL, Glazner AF, and Manley CR (2002) Did lithospheric delamination trigger late Cenozoic potassic volcanism in the southern Sierra Nevada, California? *Geological Society of America Bulletin* 114: 754–768.
Feldstein SN and Lange RA (1999) Pliocene potassic magmas from the Kings River region, Sierra Nevada, California: Evidence for melting of a subduction-modified mantle. *Journal of Petrology* 40: 1301–1320.
Fischer KM, Ford HA, Abt DL, and Rychert CA (2010) The lithosphere–asthenosphere boundary. *Annual Review of Earth and Planetary Sciences* 38: 551–575.
Forsyth DW and Rau CJ (2009) Isabella anomaly: Lithospheric drip, delamination or fragment of the Farallon plate? *Eos, Transactions, American Geophysical Union* 90: U33C-06.
Fung AT and Haggerty SE (1995) Petrography and mineral composition of eclogites from the Koidu kimberlite complex, Sierra Leone. *Journal of Geophysical Research* 100: 20451–20473.
Gao S, Luo T-C, Zhang B-R, et al. (1998a) Chemical composition of the continental crust as revealed by studies in East China. *Geochimica et Cosmochimica Acta* 62: 1959–1975.
Gao S, Rudnick RL, Carlson RW, McDonough WF, and Liu Y (2002) Re–Os evidence for replacement of ancient mantle lithosphere beneath the North China Craton. *Earth and Planetary Science Letters* 198: 307–322.
Gao S, Rudnick RL, Xu W-L, et al. (2008) Recycling deep cratonic lithosphere and generation of intraplate magmatism in the North China Craton. *Earth and Planetary Science Letters* 270: 41–53.
Gao S, Rudnick RL, Yuan H-L, et al. (2004) Recycling lower continental crust in the North China craton. *Nature* 432: 892–897. http://dx.doi.org/10.1038/nature03162.
Gao S, Zhang B, Jin Z, Kern H, Luo T, and Zhao Z (1998b) How mafic is the lower continental crust? *Earth and Planetary Science Letters* 161: 101–117.
Garrido CJ, Bodinier J-L, Burg JP, et al. (2006) Petrogenesis of mafic garnet granulite in the lower crust of the Kohistan paleo-arc complex (northern Pakistan): Implications for intra-crustal differentiation of island arcs and generation of continental crust. *Journal of Petrology* 47: 1873–1914.
Garzione CN, Hoke GD, Libarkin JC, et al. (2008) Rise of the Andes. *Science* 320: 1304–1307.
Garzione CN, Molnar P, Libarkin JC, and MacFadden BJ (2006) Rapid late Miocene rise of the Bolivian Altiplano: Evidence for removal of mantle lithosphere. *Earth and Planetary Science Letters* 241: 543–556.
Ghosh P, Garzione CN, and Eiler JM (2006) Rapid uplift of the Altiplano revealed through ^{13}C–^{18}O bonds in paleosol carbonates. *Science* 311(5760): 511–515.
Greene AR, DeBari SM, Kelemen PB, Blusztajn J, and Clift PD (2006) A detailed geochemical study of island arc crust: The Talkeetna arc section south-central Alaska. *Journal of Petrology* 47: 1051–1093.
Griffin WL, O'Reilly SY, Abe N, et al. (2003) The origin and evolution of Archean lithospheric mantle. *Precambrian Research* 127: 19–41.
Grimison NL and Chen WP (1986) The Azores–Gibraltar plate boundary: Focal mechanisms, depths of earthquakes, and their tectonic implications. *Journal of Geophysical Research* 92: 2029–2047.
Gutscher M-A, Malod J, Rehault J-P, et al. (2002) Evidence for active subduction beneath Gibraltar. *Geology* 30: 1071–1074.
Haase K (1996) The relationship between the age of the lithosphere and the composition of oceanic magmas: Constraints on partial melting, mantle sources and the thermal structure of the plates. *Earth and Planetary Science Letters* 144: 75–92.
Hacker BR, Mehl L, Kelemen PB, Rioux M, Behn MD, and Luffi P (2008) Reconstruction of the Talkeetna intraoceanic arc of Alaska through thermobarometry. *Journal of Geophysical Research* 113: B03204.
Hales TC, Abt DL, Humphreys ED, and Roering JJ (2005) A lithospheric instability origin for Columbia River flood basalts and Wallowa Mountains uplift in northeast Oregon. *Nature* 438: 842–845.
Hanson GN and Langmuir C (1978) Modelling of major elements in mantle-melt systems using trace element approaches. *Geochimica et Cosmochimica Acta* 42: 725–741.
Harrison TM, Copeland P, Kidd WSF, and Yin A (1992) Raising Tibet. *Science* 255: 1663–1670.
Hawkesworth C and Kemp AIS (2006) Evolution of the continental crust. *Nature* 443: 811–817.
Helmstaedt H and Doig R (1975) Eclogite nodules from kimberlite pipes of the Colorado Plateau – Samples of Franciscan-type oceanic lithosphere. *Physics and Chemistry of the Earth* 9: 91–111.
Helmstaedt H and Schulze DJ (1989) Southern African kimberlites and their mantle sample; implication for Archean tectonics and lithosphere evolution. *Geological Society of Australia Special Publication* 14: 358–368.
Herzberg C (2006) Petrology and thermal structure of the Hawaiian plume from Mauna Kea volcano. *Nature* 444: 605–609.
Herzberg CT, Fyfe WS, and Carr MJ (1983) Density constraints on the formation of the continental Moho and crust. *Contributions to Mineralogy and Petrology* 84: 1–5.
Hirschmann MM (2000) Mantle solidus: Experimental constraints and the effects of peridotite composition. *Geochemistry, Geophysics, Geosystems* 1(10): 1042. http://dx.doi.org/10.1029/2000GC000070.
Hirth G and Kohlstedt DL (1996) Water in the oceanic upper mantle: Implications for rheology, melt extraction and the evolution of the lithosphere. *Earth and Planetary Science Letters* 144: 93–108.
Hofmann AW (1988) Chemical differentiation of the Earth: The relationship between mantle, continental crust, and oceanic crust. *Earth and Planetary Science Letters* 90: 297–314.
Hofmann AW (1997) Mantle geochemistry: The message from oceanic volcanism. *Nature* 385: 219–229.
Hofmann AW (2003) Sampling mantle heterogeneity through oceanic basalts: Isotopes and trace elements. In: Carlson RW (ed.) *Treatise on Geochemistry*, vol. 2, pp. 61–101. Oxford: Elsevier.
Hofmann AW, Jochum KP, Seufert M, and White WM (1986) Nb and Pb in oceanic basalts: New constraints on mantle evolution. *Earth and Planetary Science Letters* 79: 33–45.
Holland TJB and Powell R (1998) An internally consistent thermodynamic data set for phases of petrological interest. *Journal of Metamorphic Geology* 16: 309–343.
Horodyskyj U, Lee C-TA, and Ducea MN (2007) Similarities between Archean high MgO eclogites and Phanerozoic arc-eclogite cumulates and the role of arcs in Archean continent formation. *Earth and Planetary Science Letters* 256: 510–520.
Houseman GA, McKenzie DP, and Molnar P (1981) Convective instability of a thickened boundary layer and its relevance for the thermal evolution of continental convergent belts. *Journal of Geophysical Research* 86: 6115–6132.
Houseman GA and Molnar PA (1997) Gravitational (Rayleigh–Taylor) instability of a layer with non-linear viscosity and convective thinning of continental lithosphere. *Geophysical Journal International* 128: 125–150.
Houseman G, Neil EA, and Kohler MD (2000) Lithospheric instability beneath the Transverse Ranges of California. *Journal of Geophysical Research* 105: 16237–16250.
Huber NK (1981) *Amount and Timing of Late Cenozoic Uplift and Tilt of the Central Sierra Nevada, California – Evidence from the Upper San Joaquin River Basin. US Geological Survey Professional Paper 1197*. Washington, DC: United States Government Printing Office.
Humayun M, Liping Q, and Norman M (2004) Geochemical evidence for excess iron in the Hawaiian mantle: Implications for mantle dynamics. *Science* 306: 92–94.
Humphreys ED and Clayton RW (1990) Tomographic image of the Southern California mantle. *Journal of Geophysical Research* 95: 19725–19746.
Humphreys ED, Hessler E, Dueker KG, Farmer GL, Erslev EA, and Atwater TA (2003) How Laramide-age hydration of North American lithosphere by the Farallon slab controlled subsequent activity in the western United States. *International Geology Review* 45: 575–595.
Ionov DA (2002) Mantle structure and rifting processes in the Baikal–Mongolia region: Geophysical data and evidence from xenoliths in volcanic rocks. *Tectonophysics* 351: 41–60.
Ionov DA, Chanefo I, and Bodinier J-L (2005) Origin of Fe-rich lherzolites and wehrlites from Tok, SE Siberia by reactive melt percolation in refractory mantle peridotites. *Contributions to Mineralogy and Petrology* 150: 335–353.
Ito G and Mahoney JJ (2005a) Flow and melting of a heterogeneous mantle: 1. Method and importance to the geochemistry of ocean island and mid-ocean ridge basalts. *Earth and Planetary Science Letters* 230: 29–46.
Ito G and Mahoney JJ (2005b) Flow and melting of a heterogeneous mantle: 2. Implications for a chemically nonlayered mantle. *Earth and Planetary Science Letters* 230: 47–63.
Jacob DE (2004) Nature and origin of eclogite xenoliths in kimberlites. *Lithos* 77: 295–316.
Jacob DE, Jagoutz E, Lowry D, Mattey D, and Kudrjavtseva G (1994) Diamondiferous eclogites from Siberia: Remnants of Archean oceanic crust. *Geochimica et Cosmochimica Acta* 58: 5191–5207.
Jacobsen SB and Wasserburg GJ (1979) The mean age of mantle and crustal reservoirs. *Journal of Geophysical Research* 84: 7411–7427.
Jagoutz OE (2010) Construction of the granitoid crust of an island arc, Part II: A quantitative petrogenetic model. *Contributions to Mineralogy and Petrology* 160: 359–381.

Jagoutz OE, Burg J-P, Hussain S, et al. (2009) Construction of the granitoid crust of an island arc, Part I: Geochronological and geochemical constraints from the plutonic Kohistant (NW Pakistan). *Contributions to Mineralogy and Petrology* 158: 739–755.

Jagoutz OE, Muntener O, Ulmer P, et al. (2007) Petrology and mineral chemistry of lower crustal intrusions: The Chilas Complex, Kohistan (NW Pakistan). *Journal of Petrology* 48: 1895–1953.

Jicha BR, Scholl DW, Singer BS, Yogodzinski GM, and Kay SM (2006) Revised age of Aleutian island arc formation implies high rate of magma production. *Geology* 34: 661–664.

Jones CH, Farmer GL, and Unruh J (2004) Tectonics of Pliocene removal of lithosphere of the Sierra Nevada, California. *Geological Society of America Bulletin* 116: 1408–1422.

Jordan TH (1978) Composition and development of the continental tectosphere. *Nature* 274: 544–548.

Jull M and Kelemen P (2001) On the conditions for lower crustal convective instability. *Journal of Geophysical Research* 106: 6423–6446.

Kaeser B, Olker B, Kalt A, Altherr R, and Pettke T (2009) Pyroxenite xenoliths from Marsabit (Northern Kenya): Evidence for different magmatic events in the lithospheric mantle and interaction between peridotite and pyroxenite. *Contributions to Mineralogy and Petrology* 157: 453–472.

Katz RF, Spiegelman M, and Langmuir CH (2003) A new parameterization of hydrous mantle melting. *Geochemistry, Geophysics, Geosystems* 4: 1073. http://dx.doi.org/10.1029/2002GC000433.

Kay SM, Coira B, and Viramonte J (1994) Young mafic back arc volcanic rocks as indicators of continental lithospheric delamination beneath the Argentine Puna Plateau, Central Andes. *Journal of Geophysical Research* 99: 24323–24339.

Kay RW and Kay SM (1988) Crustal recycling and the Aleutian arc. *Geochimica et Cosmochimica Acta* 52: 1351–1359.

Kay RW and Kay SM (1993) Delamination and delamination magmatism. *Tectonophysics* 219: 177–189.

Kay SM, Mpodozis C, and Ramos VA (2004) Andes. In: Selley RC, Cocks LR, and Plimer IR (eds.) *Encyclopedia of Geology*, pp. 118–131. Amsterdam: Elsevier.

Kelemen PB (1995) Genesis of high Mg# andesites and the continental crust. *Contributions to Mineralogy and Petrology* 120: 1–19.

Kelemen PB, Hanghoj K, and Greene AR (2003) One view of the geochemistry of subduction-related magmatic arcs, with an emphasis on primitive andesite and lower crust. In: Rudnick RL (ed.) *Treatise on Geochemistry*, vol. 3, pp. 593–659. Oxford: Elsevier.

Kelemen PB, Shimizu N, and Dunn T (1993) Relative depletion of niobium in some arc magmas and the continental crust: Partitioning of K, Nb, La and Ce during melt/rock reaction in the upper mantle. *Earth and Planetary Science Letters* 120: 111–134.

Kelly RK, Kelemen PB, and Jull M (2003) Buoyancy of the continental upper mantle. *Geochemistry, Geophysics, Geosystems* 4: 1017.

Klemme S, Prowatke S, Hametner K, and Günther D (2005) Partitioning of trace elements between rutile and silicate melts: Implications for subduction zones. *Geochimica et Cosmochimica Acta* 69: 2361–2371.

Knapp JH, Knapp CC, Raileanu V, Matenco L, Mocanu V, and Dinu C (2005) Crustal constraints on the origin of mantle seismicity in the Vrancea Zone, Romania: The case for active continental lithospheric delamination. *Tectonophysics* 410: 311–323.

Kohlstedt DL, Evans B, and Mackwell SJ (1995) Strength of the lithosphere: Constraints imposed by laboratory experiments. *Journal of Geophysical Research* 100: 17587–17602.

Langmuir CH, Klein EM, and Plank T (1992) Petrological systematics of mid-ocean ridge basalts: Constraints on melt generation beneath ocean ridges. In: Morgan JP, Blackman DK, and Sinton JM (eds.) *Mantle Flow and Melt Generation at Mid-Ocean Ridges. Geophysical Monograph Series* vol. 71, pp. 183–280. Washington, DC: American Geophysical Union.

Le Bas MJ, Le Maitre RW, Streckeisen A, and Zanettin B (1986) A chemical classification of volcanic rocks based on the total alkali–silica diagram. *Journal of Petrology* 27: 745–750.

Le Pourhiet L, Gurnis M, and Saleeby J (2006) Mantle instability beneath the Sierra Nevada Mountains in California and Death Valley extension. *Earth and Planetary Science Letters* 251: 104–119.

Le Roux V, Bodinier J-L, Tommasi A, et al. (2007) The Lherz spinel lherzolite: Refertilized rather than pristine mantle. *Earth and Planetary Science Letters* 259: 599–612.

Le Roux V, Lee C-TA, and Turner SJ (2010) Zn/Fe systematics in mafic and ultramafic systems: Implications for detecting major element heterogeneities in the Earth's mantle. *Geochimica et Cosmochimica Acta* 74: 2779–2796.

Lee C-TA (2003) Compositional variation of density and seismic velocities in natural peridotites at STP conditions: Implications for seismic imaging of compositional heterogeneities in the upper mantle. *Journal of Geophysical Research* 108: 2441. http://dx.doi.org/10.1029/2003JB002413.

Lee C-TA, Cheng X, and Horodyskyj U (2006) The development and refinement of continental arcs by primary basaltic magmatism, garnet pyroxenite accumulation, basaltic recharge and delamination: Insights from the Sierra Nevada, California. *Contributions to Mineralogy and Petrology* 151: 222–242. http://dx.doi.org/10.1007/s00410-005-0056-1.

Lee C-TA, Luffi P, Chin EJ, et al. (2012) Copper systematics in arc magmas and implications for crust-mantle differentiation. *Science* 336: 64–68.

Lee C-TA, Luffi P, Plank T, Dalton HA, and Leeman WP (2009) Constraints on the depths and temperatures of basaltic magma generation on Earth and other terrestrial planets using new thermobarometers for mafic magmas. *Earth and Planetary Science Letters* 279: 20–33.

Lee C-TA, Morton DM, Kistler RW, and Baird AK (2007) Petrology and tectonics of Phanerozoic continent formation: From island arcs to accretion and continental arc magmatism. *Earth and Planetary Science Letters* 263: 370–387.

Lee C-TA, Morton DM, Little MG, et al. (2008) Regulating continent growth and composition by chemical weathering. *Proceedings of the National Academy of Sciences of the United States of America* 105: 4981–4985.

Lee C-T and Rudnick RL (1999) Compositionally stratified cratonic lithosphere: Petrology and geochemistry of peridotite xenoliths from the Labait Volcano, Tanzania. In: Gurney JJ, Gurney JL, Pascoe MD, and Richardson SR (eds.) *Proceedings of the VIIth International Kimberlite Conference, B. J. Dawson Volume*, pp. 503–521.

Lee C-T, Rudnick RL, and Brimhall GH (2001a) Deep lithospheric dynamics beneath the Sierra Nevada during the Mesozoic and Cenozoic as inferred from xenolith petrology. *Geochemistry, Geophysics, Geosystems* 2(12): 1053. http://dx.doi.org/10.1029/2001GC000152.

Lee C-T, Yin Q, Rudnick RL, and Jacobsen SB (2001b) Preservation of ancient and fertile lithospheric mantle beneath the southwestern United States. *Nature* 411: 69–73.

Lee C-T, Yin Q-Z, Rudnick RL, Chesley JT, and Jacobsen SB (2000) Osmium isotopic evidence for Mesozoic removal of lithospheric mantle beneath the Sierra Nevada, California. *Science* 289: 1912–1916.

Lenardic A, Moresi L-N, Jellinek AM, and Manga M (2005) Continental insulation, mantle cooling, and the surface area of oceans and continents. *Earth and Planetary Science Letters* 234: 317–333.

Li Z-XA, Lee C-TA, Peslier AH, Lenardic A, and Mackwell SJ (2008) Water contents in mantle xenoliths from the Colorado Plateau and vicinity: Implications for the rheology and hydration-induced thinning of continental lithosphere. *Journal of Geophysical Research* 113: B09210.

Liu Y, Shan G, Lee C-TA, Hu S, Liu X, and Yuan H (2005) Melt–peridotite interactions: Links between garnet pyroxenite and high-Mg# signature of continental crust. *Earth and Planetary Science Letters* 234: 39–57.

Livaccari RF and Perry FV (1993) Isotopic evidence for preservation of Cordilleran lithospheric mantle during the Sevier–Laramide orogeny, western United States. *Geology* 21: 719–722.

Luffi P, Saleeby J, Lee C-TA, and Ducea MN (2009) Lithospheric mantle duplex beneath the central Mojave Desert revealed by xenoliths from Dish Hill, California. *Journal of Geophysical Research* 114: B03202.

Maldonado A, Somoza L, and Pallares L (1999) The Betic orogen and the Iberian–African boundary in the Gulf of Cadiz: Geological evolution (central North Atlantic). *Marine Geology* 155: 9–43.

Manley CR, Glazner AF, and Farmer GL (2000) Timing of volcanism in the Sierra Nevada of California: Evidence for Pliocene delamination of the batholithic root? *Geology* 28: 811–814.

McDonough WF and Sun S-S (1995) The composition of the Earth. *Chemical Geology* 120: 223–253.

McQuarrie N (2002) The kinematic history of the Central Andean fold-thrust belt, Bolivia: Implications for building a high plateau. *Geological Society of America Bulletin* 114: 950–963.

Menzies M, Xu Y, Zhang H, and Fan W (2007) Integration of geology, geophysics and geochemistry: A key to understanding the North China craton. *Lithos* 96: 1–21.

Molnar P, England P, and Martinod J (1993) Mantle dynamics, uplift of the Tibetan plateau, and the Indian monsoon. *Reviews of Geophysics* 31: 357–396.

Molnar P, Houseman GA, and Conrad CP (1998) Rayleigh–Taylor instability and convective thinning of mechanically thickened lithosphere: Effects of non-linear viscosity decreasing exponentially with depth and of horizontal shortening of the layer. *Geophysical Journal International* 133: 568–584.

Molnar P and Lyon-Caen H (1988) Some simple physical aspects of the support, structure, and evolution of mountain belts. In: Clark SP, Burchfiel BC, and Suppe J (eds.) *Processes in Continental Lithospheric Deformation, Geological Society of*

America Special Papers 218, pp. 179–207. Boulder, CO: Geological Society of America.
Mordick BE and Glazner AF (2006) Clinopyroxene thermobarometry of basalts from the Coso and Big Pine volcanic fields. *Contributions to Mineralogy and Petrology* 152: 111–124.
Morency C and Doin M-P (2004) Numerical simulations of the mantle lithosphere delamination. *Journal of Geophysical Research* 109: B03410. http://dx.doi.org/10.1029/2003JB002414.
Mosher S, Levine JSF, and Carlson WD (2008) Mesoproterozoic plate tectonics: A collisional model for the Grenville-aged orogenic belt in the Llano uplift, central Texas. *Geology* 36: 55–58.
Mukhopadhyay B and Manton WI (1994) Upper mantle fragments from beneath the Sierra Nevada batholith-partial fusion, fractional crystallization and metasomatism in subduction-related ancient lithosphere. *Journal of Petrology* 35: 1418–1450.
Müntener O, Kelemen PB, and Grove TL (2001) The role of H_2O during crystallization of primitive arc magmas under uppermost mantle conditions and genesis of igneous pyroxenites: An experimental study. *Contributions to Mineralogy and Petrology* 141: 643–658.
Nelson KD (1992) Are crustal thickness variations in old mountain belts like the Appalachians a consequence of lithospheric delamination? *Geology* 20: 498–502.
Niu F and James DE (2002) Fine structure of the lowermost crust beneath the Kaapvaal craton and its implications for crustal formation and evolution. *Earth and Planetary Science Letters* 200: 121–130.
Oncken O, Hindle D, Kley J, Elger K, Victor P, and Schemmann K (2006) Deformation of the Central Andean upper plate system – Facts, fiction, and constraints for plateau models. In: Oncken O, Chong G, and Franz G, et al. (eds.) *The Andes – Active Subduction Orogeny*, pp. 3–27. Heidelberg: Springer.
Pertermann M and Hirschmann MM (2003a) Anhydrous partial melting experiments on MORB-like eclogite: Phase relations, phase compositions and mineral-melt partitioning of major elements at 2–3 GPa. *Journal of Petrology* 44: 2173–2201.
Pertermann M and Hirschmann MM (2003b) Partial melting experiments on a MORB-like pyroxenite between 2 and 3 GPa: Constraints on the presence of pyroxenites in basalt source regions from solidus location and melting rate. *Journal of Geophysical Research* 108: 2125. http://dx.doi.org/10.1029/2000JB000118.
Plank T (2005) Constraints from thorium/lanthanum on sediment recycling at subduction zones and the evolution of continents. *Journal of Petrology* 46: 921–944.
Plank T and Langmuir C (1998) The chemical composition of subducting sediment and its consequences for the crust and mantle. *Chemical Geology* 145: 325–394.
Platt JP and England P (1993) Convective removal of lithosphere beneath mountain belts: Thermal and mechanical consequences. *American Journal of Science* 293: 307–336.
Platt JP and Houseman G (2003) Evidence for active subduction beneath Gibraltar: Comment and reply. *Geology* 31: 322.
Platt JP, Soto J-I, Whitehouse MJ, Hurford AJ, and Kelley SP (1998) Thermal evolution, rate of exhumation, and tectonic significance of metamorphic rocks from the floor of the Alboran extensional domain, western Mediterranean. *Tectonics* 17: 671–689.
Platt JP and Vissers RLM (1989) Extensional collapse of thickened continental lithosphere: A working hypothesis for the Alboran Sea and Gibraltar arc. *Geology* 17: 540–543.
Polyak BG, Fernandez M, Khutorskoy MD, et al. (1996) Heat flow in the Alboran Sea, western Mediterranean. *Tectonophysics* 263: 191–218.
Porreca C, Selverstone J, and Samuels K (2006) Pyroxenite xenoliths from the Rio Puerco volcanic field, New Mexico: Melt metasomatism at the margin of the Rio Grande rift. *Geosphere* 2: 333–351.
Putirka KD (2005) Mantle potential temperatures at Hawaii, Iceland, and the mid-ocean ridge system, as inferred from olivine phenocrysts: Evidence for thermally driven mantle plumes. *Geochemistry, Geophysics, Geosystems* 6: Q05L08. http://dx.doi.org/10.1029/2005GC000915.
Pyle JM and Haggerty SE (1998) Eclogites and the metasomatism of eclogites from the Jagersfontein kimberlite: Punctuated transport and implications for alkali magmatism. *Geochimica et Cosmochimica Acta* 62: 1207–1231.
Ranalli G and Murphy DC (1987) Rheological stratification of the lithosphere. *Tectonophysics* 132: 281–295.
Righter K and Hauri EH (1998) Compatibility of rhenium in garnet during mantle melting and magma genesis. *Science* 280: 1737–1741.
Rodriguez-Vargas A, Koester E, Mallmann G, Conceicao RV, Kawashita K, and Weber MBI (2005) Mantle diversity beneath the Colombian Andes, Northern Volcanic Zone: Constraints from Sr and Nd isotopes. *Lithos* 82: 471–484.
Roeder PL, Campbell IH, and Jamieson HE (1979) A re-evaluation of the olivine–spinel geothermometer. *Contributions to Mineralogy and Petrology* 68: 325–334.
Rosing MT, Bird DK, Sleep NH, and Bjerrum CJ (2010) No climate paradox under the faint early Sun. *Nature* 464: 744–747.
Rosing MT, Bird DK, Sleep NH, Glassley W, and Albarède F (2006) The rise of continents – An essay on the geologic consequences of photosynthesis. *Palaeogeography, Palaeoclimatology, Palaeoecology* 232: 99–113.
Rudnick RL (1995) Making continental crust. *Nature* 378: 571–578.
Rudnick RL, Barth MG, Horn I, and McDonough WF (2000) Rutile-bearing refractory eclogites: A missing link between continents and depleted mantle. *Science* 287: 278–281.
Rudnick RL and Fountain DM (1995) Nature and composition of the continental crust: A lower crustal perspective. *Reviews of Geophysics* 33: 267–309.
Rudnick RL and Gao S (2003) Composition of the continental crust. In: Rudnick RL (ed.) *Treatise on Geochemistry*, vol. 3, pp. 1–64. Oxford: Elsevier.
Rudnick RL, Gao S, Ling W-L, Liu Y-S, and McDonough WF (2004) Petrology and geochemistry of spinel peridotite xenoliths from Hannuoba and Qixia, North China craton. *Lithos* 77: 609–637.
Rudnick RL, McDonough WF, and O'Connell RJ (1998) Thermal structure, thickness and composition of continental lithosphere. *Chemical Geology* 145: 395–411.
Ruppert S, Fliedner MM, and Zandt G (1998) Thin crust and active upper mantle beneath the southern Sierra Nevada in the western United States. *Tectonophysics* 286: 237–252.
Saleeby J (2003) Segmentation of the Laramide Slab – Evidence from the southern Sierra Nevada region. *Geological Society of America Bulletin* 115: 655–668.
Saleeby J, Ducea M, and Clemens-Knott D (2003) Production and loss of high-density batholithic root, southern Sierra Nevada, California. *Tectonics* 22: 1064. http://dx.doi.org/10.1029/2002TC001374.
Schmandt B and Humphreys ED (2011) Seismically imaged relict slab from the 55 Ma Siletzia accretion to the northwest United States. *Geology* 39: 175–178.
Schott B and Schmeling H (1998) Delamination and detachment of a lithospheric root. *Tectonophysics* 296: 225–247.
Schubert G and Reymer APS (1985) Continental volume and freeboard through geological time. *Nature* 316: 336–339.
Schulze DJ (1989) Constraints on the abundance of eclogite in the upper mantle. *Journal of Geophysical Research* 94: 4205–4212.
Schurr B, Rietbrock A, Asch G, Kind R, and Oncken O (2006) Evidence for lithospheric detachment in the central Andes from local earthquake tomography. *Tectonophysics* 415: 203–223.
Schutt DL and Lesher CE (2006) Effects of melt depletion on the density and seismic velocity of garnet and spinel lherzolite. *Journal of Geophysical Research* 111: B05401.
Seber D, Barazangi M, Ibenbrahim A, and Demnati A (1996) Geophysical evidence for lithospheric delamination beneath the Alboran Sea and Rif-Betic Mountains. *Nature* 379: 785–790.
Selverstone J, Pun A, and Condie KC (1999) Xenolithic evidence for Proterozoic crustal evolution beneath the Colorado Plateau. *Geological Society of America Bulletin* 111: 590–606.
Shen B, Jacobsen B, Lee C-TA, Yin Q-Z, and Morton DM (2009) The Mg isotopic systematics of granitoids in continental arcs and implications for the role of chemical weathering in crust formation. *Proceedings of the National Academy of Sciences of the United States of America* 106: 20652–20657.
Shimizu Y, Arai S, Morishita T, and Ishida Y (2008) Origin and significance of spinel–pyroxene symplectite in lherzolite xenoliths from Tallante, SE Spain. *Mineralogy and Petrology* 94: 27–43.
Simon NSC, Carlson RW, Pearson DG, and Davies GR (2007) The origin and evolution of the Kaapvaal cratonic lithospheric mantle. *Journal of Petrology* 48: 589–625.
Simon NSC, Irvine GJ, Davies GR, Pearson DG, and Carlson RW (2003) The origin of garnet and clinopyroxene in 'depleted' Kaapvaal peridotites. *Lithos* 71: 289–322.
Sisson TW, Grove TL, and Coleman RG (1996) Hornblende gabbro sill complex at Onion valley, California, and a mixing origin for the Sierra Nevada batholith. *Contributions to Mineralogy and Petrology* 126: 81–108.
Smith D (2000) Insights into the evolution of the uppermost continental mantle from xenolith localities on and near the Colorado Plateau and regional comparisons. *Journal of Geophysical Research* 2000: 16769–16781.
Smith D, Connelly JN, Manser K, et al. (2004) Evolution of Navajo eclogites and hydration of the mantle wedge below the Colorado Plateau, southwestern United States. *Geochemistry, Geophysics, Geosystems* 5: Q04005. http://dx.doi.org/10.1029/2003GC000675.
Sobolev SV and Babeyko AY (2005) What drives orogeny in the Andes? *Geology* 33: 617–620.
Sobolev AV, Hofmann AW, Kuzmin DV, et al. (2007) The amount of recycled crust in sources of mantle-derived melts. *Science* 316: 412–417.

Sobolev AV, Hofmann AW, Sobolev SV, and Nikogosian IK (2005) An olivine-free mantle source of Hawaiian shield basalts. *Nature* 434: 590–597.

Song S, Yang J, Liou JG, Wu C, Shi R, and Xu Z (2003) Petrology, geochemistry and isotopic ages of eclogites from the Dulan UHPM Terrane, the North Qaidam, NW China. *Lithos* 70: 195–211.

Stern CR (2004) Active Andean volcanism: Its geologic and tectonic setting. *Revista Geologica de Chile* 31: 161–206.

Streck MJ, Leeman WP, and Chesley J (2007) High-magnesian andesite from Mount Shasta: A product of magma mixing and contamination, not a primitive mantle melt. *Geology* 35: 351–354.

Taylor SR and McLennan SM (1985) *The Continental Crust: Its Composition and Evolution*. Oxford: Blackwell.

Taylor SR and McLennan SM (1995) The geochemical evolution of the continental crust. *Reviews of Geophysics* 33: 241–265.

Taylor LA and Neal CR (1989) Eclogites with oceanic crustal and mantle signatures from the Bellsbank kimberlite, South Africa, Part I: Mineralogy, petrography, and whole rock chemistry. *Journal of Geology* 97: 551–567.

Taylor LA, Snyder GA, Keller R, et al. (2003) Petrogenesis of group A eclogites and websterites: Evidence from the Obnazhennaya kimberlite, Yakutia. *Contributions to Mineralogy and Petrology* 145: 424–443.

Tsenn MC and Carter NL (1987) Upper limits of power law creep of rocks. *Tectonophysics* 136: 1–26.

Turner S, Arnaud N, Liu J, et al. (1996) Post-collision, shoshonitic volcanism on the Tibetan plateau: Implications for convective thinning of the lithosphere and the source of ocean island basalts. *Journal of Petrology* 37: 45–71.

Turner S, Platt JP, George RMM, Kelley SP, Pearson DG, and Nowell GM (1999) Magmatism associated with orogenic collapse of the Betic-Alboran Domain, SE Spain. *Journal of Petrology* 40: 1011–1036.

Unruh JR (1991) The uplift of the Sierra Nevada and implications for late Cenozoic epeirogeny in the western Cordillera. *Geological Society of America Bulletin* 103: 1395–1404.

Van Kooten GK (1980) Mineralogy, petrology, and geochemistry of an ultrapotassic basaltic suite, central Sierra Nevada, California, U.S.A. *Journal of Petrology* 21: 651–684.

Van Kooten GK (1981) Pb and Sr systematics of ultrapotassic and basaltic rocks from the central Sierra Nevada, California. *Contributions to Mineralogy and Petrology* 76: 378–385.

Von Huene R and Scholl D (1991) Observations at convergent margins concerning sediment subduction, subduction erosion, and the growth of continental crust. *Reviews of Geophysics* 29: 279–316.

Wang Y, Forsyth DW, and Savage B (2009) Convective upwelling in the mantle beneath the Gulf of California. *Nature* 462: 499–501.

Wang K, Plank T, Walker JD, and Smith EI (2002) A mantle melting profile across the Basin and Range, SW USA. *Journal of Geophysical Research* 107: 2017.

Weber MBI, Tarney J, Kempton PD, and Kent RW (2002) Crustal make-up of the northern Andes: Evidence based on deep crustal xenolith suites, Mercaderes, SW Colombia. *Tectonophysics* 345: 49–82.

Wernicke B, Clayton R, Ducea M, et al. (1996) Origin of high mountains in the continents: The southern Sierra Nevada. *Science* 271: 190–193.

West JD, Fouch MJ, Roth JB, and Elkins-Tanton LT (2009) Vertical mantle flow associated with a lithospheric drip beneath the Great Basin. *Nature Geoscience* 2: 439–444.

Whitehead JA (1986) Buoyancy-driven instabilities of low-viscosity zones as models of magma-rich zones. *Journal of Geophysical Research* 91: 9303–9314.

Whitehead JA and Luther DS (1975) Dynamics of laboratory diapir and plume models. *Journal of Geophysical Research* 80: 705–717.

Wilshire HG, Meyer CE, Nakata JK, et al. (1988) *Mafic and Ultramafic Xenoliths from Volcanic Rocks of the Western United States*. *US Geological Survey Professional Paper*, vol. 1443. Menlo Park, CA: US Geological Society.

Wu F-Y, Walker RJ, Ren X-W, Sun D-Y, and Zhou X-H (2003) Osmium isotopic constraints on the age of lithospheric mantle beneath northeastern China. *Chemical Geology* 196: 107–129.

Wu F-Y, Walker RJ, Yang Y-H, Yuan H-L, and Yang J-H (2006) The chemical-temporal evolution of lithospheric mantle underlying the North China Craton. *Geochimica et Cosmochimica Acta* 70: 5013–5034.

Xu Y-G (2001) Thermo-tectonic destruction of the Archaean lithospheric keel beneath the Sino-Korean craton in China: Evidence, timing and mechanism. *Physics and Chemistry of the Earth, Part A: Solid Earth and Geodesy* 26: 747–757.

Xu W, Lithgow-Bertelloni C, Stixrude L, and Ritsema J (2008) The effect of bulk composition and temperature on mantle seismic structure. *Earth and Planetary Science Letters* 275: 70–79.

Yang Y and Forsyth DW (2006) Rayleigh wave phase velocities, small-scale convection, and azimuthal anisotropy beneath southern California. *Journal of Geophysical Research* 111: B07306. http://dx.doi.org/10.1029/2005JB004180.

Yuan X, Sobolev SV, and Kind R (2002) Moho topography in the central Andes and its geodynamic implications. *Earth and Planetary Science Letters* 199: 389–402.

Yuan X, Sobolev SV, Kind R, et al. (2000) Subduction and collision processes in the Central Andes constrained by converted seismic phases. *Nature* 408: 958–961.

Zandt G and Carrigan CR (1993) Small-scale convective instability and upper mantle viscosity under California. *Science* 261: 460–463.

Zandt G, Gilbert H, Owens TJ, Ducea M, Saleeby J, and Jones CH (2004) Active foundering of a continental arc root beneath the southern Sierra Nevada in California. *Nature* 431: 41–46.

Zhang YS (1998) Three-dimensional upper mantle structure beneath East Asia and its tectonic implications. In: Flower MFJ, Chung S-L, Lo C-H, and Lee T-Y (eds.) *Mantle Dynamics and Plate Interactions in East Asia*. *Geodynamics Series* vol. 27, pp. 11–23. Washington, DC: American Geophysical Union.